Evolution Timescale of Pre-Main Sequence Stars with a New Age Determination Method by High-Resolution Spectroscopy

高木，悠平

(Degree)
博士（理学）

(Date of Degree)
2011-03-25

(Date of Publication)
2013-07-22

(Resource Type)
doctoral thesis

(Report Number)
甲5178

(URL)
https://hdl.handle.net/20.500.14094/D1005178

博　士　論　文

Evolution Timescale of Pre-Main Sequence Stars with a New Age Determination Method by High-Resolution Spectroscopy

高分散分光観測による新たな年齢決定方法を用いた
前主系列星の進化タイムスケールの解明

平成23年1月

神戸大学大学院理学研究科
髙木 悠平

Abstract

Evolution timescale of pre-main sequence stars and protoplanetary disks are derived with the age determination method based on high-resolution spectroscopy. Estimating the evolution timescale of the pre-main sequence stars and protoplanetary disks play an important role in revealing the formation and the evolution process of the photosphere, disk, and the protoplanets. The formation of the gaseous planets and hot Jupiters is dependent on the gas dissipation timescale in the disk.

The evolution timescale estimated in the previous study is based on ages of pre-main sequence stars estimated from the photometric observations. The ages of the pre-main sequnece stars are able to be determined by comparing the luminosity and the effective temperatures to the stellar evolution model. Since the luminosity of the pre-main sequence stars contains the uncertainty of distance, extinction, and veiling, the age determination based on the photometric observation is difficult.

To estimate the age of the pre-main sequence stars with no contaminations of the uncertainties of distance, extinction, and veiling, the new age determination method based on the high-resolution spectroscopy is presented in this study. The ages of the PMS stars can be calculated from the surface gravity due to the photospheric contraction during the evolution. Equivalent widths of the absorption lines from stellar atmosphere depend on the effective temperature, metallicity and the surface gravity. It is also free from the distance and extinction uncertainties. To estimate the surface gravity with no contamination caused by the veiling, the equivalent width ratios calculated by using the nearby absorption lines were developed as a surface gravity diagnostic.

The equivalent width ratios (EWRs) of the Fe (8186.7$\AA$ and 8204.9$\AA$) and Na (8183,3$\AA$ and 8194.8$\AA$) lines in the optical I-band (Fe/Na) and the Sc (22057.8$\AA$ and 22071.3$\AA$) and Na (22062.4$\AA$ and 22089.7$\AA$) lines in the near-infrared K-band are established as surface gravity diagnostics of the pre-main sequence stars with mass of 0.8 $M_{\odot}$ and 0.6-0.7 $M_{\odot}$, respectively. The relation between the EWRs and the surface gravity were estimated by observing the giants and the main sequence stars. For the Fe/Na, 25 giants and 4 main sequence stars with the effective temperature of $\sim$4200 K were observed with the Okayama Astrophysical Observatory 1.88 m telescope HIDES and the Subaru Telescope HDS. The spectra of 10 giants and 10 dwarfs with the effective temperature of $\sim$3800 K were obtained by the observation using the United Kingdom Infrared Telescope CGS4 and Subaru Telescope HIDES, and the archival data for the Sc/Na. From the estimated EWR - surface

gravity relation, the age determination accuracy were within the factor of 1.5 in both method.

Ages of 9 pre-main sequence stars were determined with the established EWR method, with no contamination of the uncertainty of distance, extinction, and veiling. From the estimated ages, the relation between the age and the disk evolution was found, which did not appear from the result of the age estimated by photometric studies. The dissipation timescale of the protoplanetary disks determined from the age estimated by the EWR method was 4.0 Myr.

Contents

Part I
Age Determination Method of Pre-Main Sequence Stars with High-Resolution Spectroscopy

1 Introduction

1.1 Evolution of Young Stars

Study of young stars plays an important role in revealing the universal formation of stars and planets. Estimating the physical parameters of the photosphere such as masses, temperatures, luminosities, and ages allow us to understand the environment of the star itself, and the detailed direct imaging toward these stars unveil the circumstellar disks (e.g. Itoh et al., 2002; Fukagawa et al., 2004; Hioki et al., 2007) and protoplanets (e.g. Marois et al., 2008; Kalas et al., 2008).

1.1.1 Formation Process of Stars

Protostars

Stars with a mass comparable to Sun (1 $M_{\odot}$) form in the molecular cloud, where the number density of the molecular hydrogen is $\sim 10^3 \mathrm{cm}^{-3}$. When the number density increases to $\sim 10^5 \mathrm{cm}^{-3}$ through the gravitational "first collapse", the gas clump reaches to a state of dynamic equilibrium, creating a core of the protostar which is called "the first core" (Masunaga, Miyama, & Inutsuka, 1998). The central temperature and the mass of the first core is around 1000K and 0.01 $M_{\odot}$, respectively. Since the first core stage ends in 10^4 years, it is yet to be observed. The temperature increases due to the continuing gas accretion. The hydrogen molecules dissociate when the central temperature becomes about 2000K. The pressure of the gas decreases since this dissociation is an endoergic reaction. This leads to a "second collapse", and forms a protostar.

The protostar phase is defined as a period of the significant mass increase due to the accretion (Hanawa et al., 2008). This phase continues for around 10^5-10^6 years. Protostars are surrounded by envelopes and disks. The gas first accrete from the envelope to the disk, and fall to the photosphere. The infall rate from the envelope to the disk is $10^{-5} M_{\odot}$ per year (Shu, Adams, & Lizano, 1987).

Another name it is known by is Class I stars, due to the classification of Lada (1987, figure 1). These stages are distinguished based on the spectral energy distribution (SED) of the star. The SED of a protostar shows a large infrared excess due

to the disk and the envelope. For the classification of the young stars, Lada (1987) made a definition based on the slopes of the SED at 2 - 20 μm. The index α is:

$$\alpha = \frac{d\log(\lambda F_\lambda)}{d\log\lambda}. \tag{1}$$

The class I stars are defined as $\alpha > 0$. The star with $\alpha = 0$ is called a flat spectrum objects, which is the stellar stage between Class I and Class II.

Pre-Main Sequence Stars

After most of the circumstellar materials accreted to the star, the star initiates the pre-main sequence stage. The interior of the low mass stars ($< 2M_\odot$) in this phase are fully convective (Hayashi, 1961). In this stage, the star radiates by releasing the gravitational energy. The relation between the luminosity (L), radius (R), and effective temperature (T) of the star is expressed the following equation

$$L = 4\pi R^2 \sigma T^4, \tag{2}$$

where σ is the Stefan-Boltzmann constant. Since most of the gravitational energies are converted to the radiation, the effective temperature of star in the fully convective phase remains constant. Therefore, pre-main sequence stars contract as they evolve, and become dim. The evolution tracks of the pre-main sequence stars in the Hertzsprung-Russell (H-R) diagram first descend nearly vertically, which is so-called Hayashi Tracks (figure2). The pre-main sequence stars with a solar mass spend several 10^6 to 10^7 years in this phase. The timescale of the gravitational contraction is expressed as the Kelvin-Helmholtz timescale

$$t_{\rm KH} = \frac{GM^2}{RL}, \tag{3}$$

where G is the gravitational constant. The $t_{\rm KH}$ will increase as the star contracts, and therefore the contraction of the star gets slower as the star evolves.

During the contraction of the photosphere, the core temperature keeps increasing. As the inner temperature rises, the convective zone shifts outward, and the radiative core will be created. In this phase, the effective temperature starts increasing and the luminosity stops decreasing. This is called the Henyey phase.

When the central temperature of the star reaches to 1.5×10^7K, nuclear fusion reaction of hydrogen will begin in the core. The star will join the main sequence phase at this point, and the contraction ends due to the pressure of the reaction. The star with 1 $M_\odot$ spends $\sim 10^8$ years in the pre-main sequence phase.

The stars in the pre-main sequence stage are divided into two classes, based on the SED classification (Lada, 1987). Class II stage contains a star with $-2 < \alpha < 0$, as defined in equation (1). Pre-main sequence stars in this stage has an optically thick disk and bipolar outflows. The ages of Class II stars are in the order of 10^6 years. Since the envelope dissipates in this stage, it can be observed in optical and near-infrared wavelengths. These stars are equal to the stars called classical T Tauri stars (CTTSs). CTTSs show strong emission lines, especially Hα. CTTS is defined as a star with equivalent width[1] of the Hα line larger than 10 $\AA$. This emission line arises by the gas accretion from the protoplanetary disk to the photosphere. Some forbidden lines also appear due to the jet and outflow, which play an important role in releasing the angular momentum.

The Class III objects are the evolved pre-main sequence stars, which show a small infrared excess (-3< α <-2). The ages of these stars are $\sim 10^7$ years. An optically thin, evolved disk surrounds the photoshpere. It is also called weak-lined T Tauri star (WTTS), where the EW of the Hα line is smaller than 10$\AA$. The small EW indicates that the accretion from the protoplanetary disk has reduced compared to the CTTS. This also suggests that the disk around the class III objects has an evolved disk.

[1]Equivalent width (EW) is an indicator of the strength of the absorption and emission lines. This is defined as

$$EW = \int (F_c - F_\lambda) d\lambda / F_c, \tag{4}$$

where F_c is the flux of the continuum and the F_λ is the flux of the spectrum(figure3).

1.1.2 The formation and evolution of protoplanets

Protoplanetary disk is the birthplace of planets. The primordial disk is composed mostly of hydrogen and helium gas. It also contains dusts, a few percentage in mass compared to the gas. The size of the dusts are thought to be around 0.1 μm. The dust collide each other when the gas and dust settle to the disk plane, and the size grows to an order of centimeter. The dust collision will create many planetesimals, the seeds of the planets. The size of the planetesimals are 1 - 10 km. The orbits of these objects get messed up due to their gravitational attraction, which invoke the "Runaway growth" (Kokubo & Ida, 1996), and produce protoplanets. When the mass of the protoplanets reaches to 5 - 10 earth mass, which is mostly created beyond the snowline due to the rich icy planetesimals, the gas falls and the gas giant planets are created. Solid, a terrestrial planets form in the inner disk, where the protoplanets will not gain enough mass to create gaseous planets. The gas and the dust evolution process play a key role in the planet formation. Therefore, the gas and dust evolution timescale should be estimated precisely to reveal the planet formation.

1.2 Importance of the Age Determination of Pre-Main Sequence Stars

Many of the formation and evolution processes of the stars and planets are still unrevealed. One of the unveiled processes is the dissipation of the disk. Generally, the disks become optically thin during the evolution, due to the accretion and the dissipation of the gas. However, the disk with an inner hole has been discovered in recent years. These disks are called "Transition disks", which is a state in between the CTTS and WTTS disk (Najita, Strom, & Muzerolle, 2007). The creation process and the evolution timescale of the transition disks are has been estimated (e.g. Bertout, Siess, & Cabrit, 2007), but some confusion remains (see part II). The other process is the rotational spin up of the photosphere. Since the star contracts during the evolution, the rotation velocity of the photosphere increases as the star evolves. However, the rotation velocities of the main sequence stars are slower compared to the WTTSs. Therefore, there should be a mechanism to eject the angular momentum, which is still unknown. Also, the timescale of the angular momentum ejection is not studied. Therefore, it is important to estimate the ages of the pre-main sequence stars to solve these problems.

The age of the pre-main sequence stars are also an excellent tool to study the star formation history. Palla & Stahler (2002) combined the ages and the stellar positions of the pre-main sequence stars in the Taurus-Auriga star forming region. From their study, the young stars in this region first formed at a relatively low level for about 10^7 years, and then the star forming rate increased in the last million years. Consequently, the age of young star is a vital parameter in the star-formation study. The accurate age determination will reveal the detailed star and planet formation mechanism.

1.2.1 The General Age Determination Method of Pre-Main Sequence Stars

As a star evolves, the photosphere contracts and the luminosity and the effective temperature varies (figure 2). Hence, the age of the pre-main sequence star is able to be determined by estimating its luminosity and effective temperature. Strom et al. (1989) observed the optical and near-infrared fluxes of 83 pre-main sequence stars in the Taurus molecular cloud. From the multi-wavelength study, the luminosity and the effective temperature was estimated by fitting the SED. The ages of the stars

were then estimated by comparing this result with the evolution tracks. Kenyon & Hartmann (1995) also estimated the age of the young stars in the Taurus-Auriga.

To estimate the age of the pre-main sequence stars with a high precision, it seems that an observation with accurate luminosity and effective temperature determination is needed. However, the luminosity of the pre-main sequence star is contaminated by several dimming or brightening effects and uncertainties.

(1) Distance

To estimate the luminosity of the star, accurate distance estimation is necessary. The absolute V magnitude M_V is derived from the following equation

$$M_V = m_V - 5\log(r) + 5, \tag{5}$$

where m is the observed magnitude of the star and the r is the distance in parsec(pc). Then, the bolometric magnitude M_{bol} is estimated as

$$M_{bol} = M_V + \mathrm{BC}, \tag{6}$$

where BC is the bolometric correction. The luminosity ($\log(L/L_\odot)$) is finally derived by the equation

$$\log(L/L_\odot) = \frac{4.74 - M_{bol}}{2.5}, \tag{7}$$

where 4.74 is the absolute bolometric magnitude of the Sun.

The most accurate method to determine the distance is to estimate the parallax of the star. Wichmann et al. (1998) estimated the distance of three star-forming regions, Taurus-Auriga, Lupus, and Chamaeleon by observing the parallax of 4-5 pre-main sequence stars in each region. The Hipparcos satellite was used to obtain the parallaxes of the stars. The estimated distance to these regions were 142 ± 14pc, 190 ± 27pc, and 160 ± 17pc, respectively. However, we have to note that these results were derived from the most luminous stars in each region, and some of the stars are multiple (e.g. T Tau).

Since the Hipparcos satellite observation is carried out in V-band and the measurement limit of the distance is $\sim$ 200 pc, the distance estimation by this method are available for the bright, uncovered stars in nearby star-forming regions. Therefore, the distance to the star-forming regions are mainly calculated by an indirect method, such as estimating their distance range by observing how

far the foreground and the background stars are (e.g. Hearty, 2000; Luhman, 2001). Consequently, the distances of the star-forming regions are affected by a systematical error, and has a large error.

(2) Extinction

The circumstellar materials shade the light from the photosphere. This is called the extinction, which makes the star dark, and therefore the pre-main sequence stars are difficult to observe. The flux of the star in each wavelength is dimmed under the extinction law (e.g. Cohen et al., 1982). The extinction magnitude (A_V) of the pre-main sequence star is determined by fitting the SED to the result of multi-wavelength photometric observations. The fitting is conducted by changing the amount of effective temperature and the extinction. A_V also varies from work to work, depending on which wavelength is used as the most unaffected by the veiling (see next paragraph for more details). Previously, the near-infrared J-band (1.1μm) was mainly used. However, Cieza et al. (2005) argued that the more suitable wavelength is the optical I-band. The extinction estimated in each method are not equal, and therefore it makes the luminosity determination difficult. For example, the A_V of V827 Tau, a WTTS in the Taurus-Auriga star-forming region, shows different amounts in the work of Furlan et al. (2006) and Bertout, Siess, & Cabrit (2007). Furlan et al. (2006) assumed the J-band as the most unveiled wavelength, and estimated the A_V as 1.00 mag. On the other hand, Bertout, Siess, & Cabrit (2007) used the I-band, and $A_V = 0.28$ was their result. The age calculated for the V827 Tau from each A_V, comparing the luminosity with the evolution model of Baraffe et al. (1998), will be < 1.0Myr and 2.8Myr, respectively. The extinction uncertainty will make a large difference in the age determination.

(3) Veiling

Pre-main sequence stars show a continuum excess at the wavelength shorter than the ultraviolet and longer than the near-infrared. The ultraviolet excess arises by accreting materials from the disk to the photosphere. Hydrogen surrounding the star radiate by free-bound and free-free emission where the temperature is around 20000K (Rydgren, 1976). The near-infrared excess was first discovered by Mendoza (1966). Myers et al. (1987) suggested that this emission arises from the circumstellar disk. Dust in the disk are heated by the photo-

sphere, and re-radiate in the wavelength longer than near-infrared, due to the temperature of the disk materials.

These excesses are called "veiling", since these are the continuum emission with no absorption or emission features and therefore makes the absorption lines of the stellar atmosphere shallow (Joy, 1945, 1949). The amount of the veiling r is defined as the proportion veiling to the stellar continuum; r=1 means that the star has a veiling equal to the stellar continuum. Basri & Batalha (1990) estimated the optical r of the pre-main sequence stars in the Taurus molecular cloud. They obtained the high-resolution spectra of the stars, and fit the veiling-added dwarf spectra. The typical r of the CTTSs are from 0 to 2-3, and it is said that there is a time variation (Basri & Batalha, 1990). Also, since the standard spectra are those of main sequence, the photospheric absorption features are not equal, due to the surface gravity. Therefore, it is difficult to estimate the value of r precisely. The ages of the pre-main sequence stars in Taurus-Auriga estimated by Bertout, Siess, & Cabrit (2007) was based on an assumption that the excess contribution in I-band is the smallest. However, since the excess in the I-band is not zero, it is impossible to estimate the luminosity without the contamination of veiling.

For these reasons, age determination of pre-main sequence stars with a photometric method includes large systematical errors. Hence, it is difficult to obtain the accurate, correct age from this method. To derive the formation and the evolution of the pre-main sequence stars and planets, it is necessary to estimate the accurate ages of these stars with a new method which is free from the uncertainties of distance, extinction, and veiling.

2 New Age Determination Method

To estimate the age of a pre-main sequence star with no contaminations of the uncertainty of distance, extinction, and veiling, a new age determination method is necessary. Since the luminosity of the stars are influenced by these effects, the new technique needs to use an indicator instead of luminosity. In this study, the surface gravity is used for the age determination.

2.1 The relation between Age and Surface Gravity

The photosphere of a pre-main sequence star contracts during the evolution, due to the gravitational contraction. Hence, the surface gravity increases during the evolution, due to the following equation

$$g = \frac{GM}{R^2} \tag{8}$$

where g is the acceleration of gravity (cm/s^2), G is the gravitational constant, and the M and the R are the mass and the radius of the star, respectively. The relation between the log g and the evolutional track is shown in figure 4. Figure 5 shows the relation between the stellar age and the surface gravity. During the pre-main sequence stage, the surface gravity of a pre-main sequence star becomes 10 times larger, on average, and reaches the main sequence. From this relation, the ages of the pre-main sequence stars are able to be estimated by estimating its surface gravity, instead of luminosity.

2.2 Surface Gravity Estimation with High-Resolution Spectroscopy

To estimate the surface gravity of pre-main sequence stars, high-resolution spectroscopy is suitable. The strength of the atomic absorption lines are sensitive to the metal abundance, effective temperature, and the surface gravity of the star, therefore the equivalent width is a fine diagnostic of these parameters.

2.2.1 Line Absorption Coefficients

The strength of the equivalent width depends on the line profile of the absorption line. The depth of an absorption line r_λ at the wavelength λ is defined as

$$r_\lambda = \frac{F_c - F_\lambda}{F_c}, \tag{9}$$

where F_c is the flux level of the continuum, and F_λ is the flux in the absorption line feature. The strength S of the absorption line is

$$S = \int r_\lambda d\lambda. \tag{10}$$

The continuum flux F_c depends on the continuous absorption coefficient $\kappa(cm^2 \cdot g^{-1})$ and the F_λ is given by the line absorption coefficient $\kappa_\lambda(cm^2 \cdot g^{-1})$. Therefore, r could be written as

$$r_\lambda \sim \frac{\kappa_\lambda}{\kappa}. \tag{11}$$

Continuous Absorption Coefficient

In the stars with the mass nearly equal to sun, the H^- plays a role in the continuous absorption coefficient κ. From the equation of Saha,

$$\log \frac{N_{r+1}}{N_r} \cdot P_e = -\chi_r \cdot \frac{5040}{T} + \frac{5}{2} \log T - 0.48 + \log \frac{u_{r+1} \cdot 2}{u_r}, \tag{12}$$

the κ is able to be expressed as

$$\kappa = C_1 T^{-\frac{5}{2}} P_e \exp(0.75/kT) \quad (C_1 : constant) \tag{13}$$

where N_r、N_{r+1} are the number of atoms which is neutral and one level excited, P_e is the electron pressure, χ_r is the ionization potential, T is the effective temperature, u is the weight, and k is the Boltzmann constant (Gray, 1992).

Line Absorption Coefficient

An absorption line is separated into two parts; the core and the wing. The line absorption coefficient κ_λ is defined in each part. For the core part, the $\kappa_{\lambda core}$ is

$$\kappa_{\lambda core} = \sqrt{\pi} \frac{e^2}{mc^2} \cdot \frac{{\lambda_0}^2 N f}{\Delta\lambda_D} e^{-(\Delta\lambda/\Delta\lambda_D)^2}, \tag{14}$$

where e and m are the electron charge and mass, c is the light speed, λ_0 is the central wavelength of the absorption line, $\Delta\lambda$ is the difference from the λ_0, $\Delta\lambda_D$ is the doppler width, N is the number of the excited element, and f is the weight. The $\kappa_{\lambda wing}$ is defined as

$$\kappa_{\lambda wing} = \frac{1}{4\pi}\frac{e^2}{mc^2} \cdot \frac{{\lambda_0}^4}{c} \cdot \frac{Nf\gamma}{\Delta\lambda^2}, \tag{15}$$

where γ is the damping constant (Unsöld, 1968). The line profile of the core and the wing are able to be approximated by gaussian and lorentzian, respectively. Hence, the full absorption feature can be approximated by the voigt function, which is the convolution of gaussian and Lorentzian.

2.2.2 Relation between the Line Strength and the Stellar Parameters

Effective Temperature

The number of the excited atom N is expressed as

$$N_n = C_2 \cdot g_n \exp(-\chi/kT) \quad (C_2 : constant) \tag{16}$$

where χ is the excitation potential. The N increases with the increasing T, until the element starts ionizing. When the effective temperature reaches to the temperature where the element starts ionizing, the N_n will also depend on equation (12).

Surface Gravity

The wing of the absorption line reflects the surface gravity. In stars with low effective temperature ($\sim T_{\rm eff}$ of Sun), the κ is dominated by negative hydrogen ion. In this situation, the ratio of the line absorption coefficient and the continuous absorption coefficient will be expressed as

$$\frac{\kappa_\lambda}{\kappa} \sim C_3 \cdot \gamma (C_3 : constant). \tag{17}$$

Due to the van der Walls broadening, the γ is proportional to $g^{\frac{2}{3}}$ (Unsöld, 1968). The wing of an absorption line extends as the surface gravity increases, and therefore the equivalent width will also increase. However, this variance occurs when

the absorption line is reached to the limiting depth (Unsöld, 1968). For other lines, the core part of the absorption line becomes shallow with the increasing surface gravity. From the equations (11), (13), (14), and (16), the depth of the core is expressed as

$$\frac{\kappa_\lambda}{\kappa} = \frac{T^{\frac{5}{2}}}{P_e} \exp(-\frac{\chi + 0.75}{kT}). \tag{18}$$

Since the electron pressure P_e is

$$P_e \sim C_4 \cdot g^{\frac{1}{3}} \quad (C_4 : constant), \tag{19}$$

the strength of the absorption lines decreases as the surface gravity increases. This is dependent on the continuous absorption coefficient. When the surface gravity is large, the density of the stellar atmosphere increases and the opacity arises. Hence, the amount of the absorber relatively decreases.

2.2.3 The Advantage of Equivalent Width and Equvalent Width Ratio

One of the best points of the surface gravity estimation from the high-resolution spectroscopy is that the equivalent width is independent of distance and extinction. This is because the equivalent width is derived by dividing the strength of an absorption line by the continuum flux, which means that it is normalized.

However, the equivalent width still depends on the veiling. As mentioned in section 1.2.1, the observed absorption lines of the pre-main sequence stars are relatively weak. This is caused by the added excess from the circumstellar disk to the photosperic radiation (figure 6). The equivalent width of the veiled absorption line becomes smaller than the original amount. The equivalent width (EW) of the absorption line with an area of S in a spectrum with continuum level of I and veiled with r will be expressed as

$$EW = \frac{S}{I + r}. \tag{20}$$

Since this "filling" effect is difficult to remove, the accurate surface gravity estimation from a typical spectral analysis is demanding.

Taking the ratio of the equivalent width (EWR) of the absorption lines is a suitable method to remove the veiling. Meyer et al. (1998) identified the EWR of OH (1.6892μm) and Mg (1.5760μm) as a diagnostic of $T_{\rm eff}$. They also used the EWR of CO (1.6207μm + 1.6617μm) and Mg (1.5760μm) as a luminosity indicator (which reflects the surface gravity). Doppmann & Jaffe (2003, 2005) derived the $T_{\rm eff}$, radial velocity, and the amount of veiling by fitting observational 2.2μm spectra with synthesized spectra. They estimated the surface gravity by calculating the EWR of the Na interval at 2.2μm (including the absorption lines of Na, Sc, Si) and the CO bandhead at 2.3μm. However, when the EWR is calculated by taking the ratio of absorption lines separated, a correction for the amount of veiling is necessary, since it is wavelength dependent.

To derive the photometric EWR directly from observed spectra, without any veiling correction, we calculate EWRs using closely spaced absorption lines. This is practicable because the effects of veiling are nearly constant over small wavelength ranges (figure 7). Considering two nearby absorption lines (l_1, l_2) with the area of S_1 and S_2, in a spectrum with continuum level I and veiled by r, the equivalent width (EW) of each line is expressed as

$$EW_{l_1} = \frac{S_1}{I + r}, EW_{l_2} = \frac{S_2}{I + r}. \tag{21}$$

Then, the ratio of these EWs will be

$$EWR = \frac{EW_1}{EW_2} = \frac{\frac{S_1}{I+r}}{\frac{S_2}{I+r}} = \frac{S_1}{S_2}, \tag{22}$$

which shows that the EWR is free from veiling. In addition, assuming the abundance ratios of the elements are equal, EWR has no dependence on metal abundance. Therefore, the EWR only depends on the effective temperature and the surface gravity of the star. To estimate the age of young stars with completely no contamination of distance, extinction, and veiling, deriving the surface gravity with the EWR calculated with the nearby absorption lines is suitable. To achieve this, it is necessary to create a surface gravity indicator with EWR, by observing the stars with various surface gravities, and fixed temperature.

2.2.4 Line Pair Selection

To create a valuable surface gravity diagnostic with the EWR, the line pair selection is important. The most suitable pair is a combination of a line reached to the limiting depth, and a line close to that which is not reached to the limiting depth. The equivalent width of the former line increases with the increasing surface gravity, since the damping wing broads (equations (12), (14) in 2.2.2). On the other hand, the equivalent width of the latter line decreases in the large surface gravity star, because the continuum opacity increases (equations (15), (16) in 2.2.2). Consequently, the ratio of these two lines is thought to be a sensitive surface gravity diagnostic.

Absorption lines in the optical I-band and the near-infrared K-band was selected for the surface gravity diagnostic creation. Since the pre-main sequence stars are usually embedded in the interstellar materials, it is easier to observe in the long wavelength. The Na lines in both band (I: 8183,3Å, 8194.8Å, K: 22062.4Å, 22089.7Å) are the strong lines reached to the limiting depth, and therefore these lines are suitable for the EWR. In the I-band, the close Fe lines (8186.7Å, 8204.9Å) are selected for the EWR calculation. For K-band, the Sc lines (22057.8Å, 22068.7Å) are selected, since they are close to the Na lines, and are sensitive to the surface gravity (Greene & Lada, 1997). To reveal the EWR - surface gravity relation which is not dependent to the effective temperature, we observed the giants, subgiants, and the main-sequence stars with fixed temperature. The temperature was set to 4200K (late K-type star) and 3800K (early-M type), for the I-band and K-band, respectively.

3 I-band Fe/Na for the late-K type stars

For the accurate age determination of late K-type pre-main sequence stars (0.8 $M_{\odot}$), the establishment of the surface gravity indicator using the ratios of Na (8183,3$\AA$ and 8194.8$\AA$) lines and Fe (8186.7$\AA$ and 8204.9$\AA$) lines (Fe/Na) in I-band is necessary.

3.1 Observations

3.1.1 Object Properties

30 giants (including subgiants) and 6 main-sequence stars were selected in order to estimate the relationship between surface gravity (g) and the Fe/Na. The selected sample objects and their properties are listed in table 1. All targets are single stars. To avoid the absorption line blending of the primary and secondary spectra, the binary stars are not included in the targets. 25 giants and 4 main-sequence stars have $T_{\rm eff}$ of 4200-4300K, since the radiation peak of these stars is in the I-band and they are bright enough to observe. Five giants and two dwarfs with $T_{\rm eff}$ of 4600-4700K were also included to provide an estimate of the dependence of EWRs on $T_{\rm eff}$.

To derive the surface gravity in advance, giants and main-sequence stars of which parallax was measured by the Hipparcos satellite (Perryman et al., 1997) were selected for the target stars. The log g of these objects was calculated as follows:

$$\log g = \log \frac{M}{M_{\odot}} + 4 \log \frac{T}{T_{\odot}} - \log \frac{L}{L_{\odot}} + \log g_{\odot}, \tag{23}$$

where M is the mass, T the effective temperature, and L the luminosity. The luminosity was calculated from the V-band magnitude given in SIMBAD (taken from previous photometric studies), and the parallax. For the effective temperature, the $T_{\rm eff}$-spectral type relationship (Lang, 1992) was used. The error of the effective temperature is not included in the log g estimation and therefore the error of the log g may be underestimated. The relationship of M and spectral type in Drilling & Landolt (2000) was used to derive the masses of the main-sequence stars. The giant star masses were estimated by comparing luminosities and temperatures with

the evolutionary tracks given in Lejeune & Schaerer (2001) (figure 8). Since giants smaller than 2.0 $M_{\odot}$ evolve rapidly after the helium flash, we used the pre-flash evolutionary track, where the giants are in the red giant branch, for these stars. The derived log g of β Gem (2.73±0.01) is consistent with the result of a spectroscopic study (Drake, Smith, 1991), in which it was estimated as 2.75±0.15. The large error in the surface gravity of the giants is attributable to the errors in luminosity (figure 8), which arise from the parallax errors.

Four WTTSs belonging to the Taurus-Auriga star-forming region were also added to our samples to test the effectiveness of the derived EWR-log g relationship. The log g of these WTTSs were also estimated from equation (23). Temperatures were estimated using Lang (1992), following the procedure for the main-sequence stars. We derived luminosities from photometry, including corrections for extinction (A_V), since the excess from the circumstellar disk is small. The A_V for HBC 374 and V827 Tau were taken from Kenyon & Hartmann (1995). For the other objects, RX J0452.5+1730 and RX J0459.7+1430, we estimated the A_V by fitting the SED corrected by an arbitrary A_V to the V, J, H, and K-band magnitudes (figure 9). The V-band magnitude was taken from SIMBAD, and the 2MASS catalog was used for the J, H, and K-band magnitudes. The estimated A_V was 0.69 mag and 0.67 mag for RX J0452.5+1730 and RX J0459.7+1430, respectively. The mass of each star was estimated by using the H-R diagram, comparing the temperature and luminosity with the evolutionary model of Baraffe et al. (1998). The mass of HBC 374 and V827 Tau were 0.8 $M_{\odot}$. On the other hand, the masses of RX J0452.5+1730 and RX J0459.7+1430 were 1.20 $M_{\odot}$ and 1.25 $M_{\odot}$, respectively. The distance to the Taurus-Auriga molecular cloud was fixed at 142±14pc (Wichmann et al., 1998).

3.1.2 Observation details

High-resolution I-band spectroscopy of 30 giants and 6 main-sequence stars was carried out on 2007 January 17 to 24 and 2008 March 24 to 27 using the High Dispersion Echelle Spectrograph (HIDES) on the Okayama Astrophysical Observatory 1.88 m telescope. The slit width was set to 220μm, giving a resolution of ~60000. The angle of the red cross-disperser was selected to center the 69th order of the echelle spectrograph (8165~8300$\AA$) on the 2048×4096 CCD. The integration time range was 90~7200 sec, yielding a S/N of ~100. The maximum integration time was set to 1800 sec to reduce the risk of cosmic rays. Exposures of faint objects were divided into several frames. Flat frame were taken using the flat lamp equipped in

the instrument, and were obtained at the beginning and end of each night's observations. Bias frames and Th-Ar lamp frames for wavelength calibration were taken with the same frequency.

The spectra of the 4 WTTSs were obtained using the Subaru Telescope with High Dispersion Spectrograph (HDS) on 2007 September 18. The slit width was set to 0.6" (R$\sim$60000). The instrument was set to the StdNIRb mode, to obtain the Na and Fe absorption lines in the 73rd order. The integration time for each object was 900 sec. Flat, bias, and Th-Ar frames were also obtained.

3.2 Data Reduction

3.2.1 Extracting the Spectra

The data were reduced using Image Reduction and Analysis Facility (IRAF) software package[2]. The same procedures were applied to both HIDES data and HDS data.

First, the bias was removed for each frame. The average level of the overscan area in each frame was first subtracted. Next, the bias frame, which is a combined bias frame obtained at the beginning and the end of the observation, was subtracted.

Flat fielding was accomplished with the normalized flat frame. Many fringes appear in the wavelength longer than the I-band. The time variability of the fringes was first checked by comparing the flat frames obtained in different time. Since this variance was negligible, the flat frames were combined into a single frame. The scattered light was removed by fitting the non-spectral area of the object frame with a polynomial equation.

Finally, the spectrum was extracted from each object frame by tracing the spectral region with the *apall* task. The extract format was set to "*echelle*". Since the scattered light is already subtracted, the sky was not subtracted in this procedure.

After the spectra are extracted, the wavelength should be determined. The comparison data obtained with the Th-Ar lamp were used for wavelength calibration. By performing the *identify* task to the comparison data, the wavelengths are marked in each echelle order, by identifying the Th-Ar emission. This result was then referred to the stellar spectra data by using the task *refspectra*. Then, by running the *dispcor* task, the wavelength calibrated spectra will be produced.

When the object was taken several times, in order to increase the signal-to-noise ratio (S/N) of the dark stars, the spectra were combined after wavelength calibration. The spectra were normalized at the continuum level and the doppler shift was reduced in the last procedure. All of the obtained spectra of giants, main-sequence stars, and the WTTSs are displayed in figures 10 to 13.

3.2.2 Equivalent Width Mesurement

The SPLOT task was used to measure the equivalent width of each line. The equivalent widths of the lines were measured by fitting each spectrum. The core part

[2]IRAF is distributed by the National Optical Astronomy Observatory.

of an absorption line is able to be approximate by the gaussian. On the other hand, the wing of an absorption line is approximated by lorentzian. Therefore, all of the absorption lines was fit with the Voigt function in this work, which is a convolution of the gaussian and the lorentzian. The fitting of the Na lines and Fe lines were done including the absorption lines, both stellar and telluric, which appear next to these lines, since the edge of the absorptions have no small effect from the neighbors. The telluric lines which appear in this wavelength were de-blended from the photospheric lines during the fitting. The EWs of some Na and Fe lines were difficult to measure because of heavy telluric line blending. The example of the spectrum fitting is shown in figure 14.

The error in the equivalent width was estimated from uncertainty of the continuum level. The wavelength range with no absorption features are selected as the continuum region, which is from 8190-8192$\AA$ in most of the spectra. The calculated root mean square of the continuum level is defined as the error in this study. The upper limit and the lower limit of the equivalent widths are estimated by fitting the absorption lines at the upper level and the lower level of the continuum, respectively. The measured EWs of each object are listed in table 2.

3.3 Results and Disscussions

3.3.1 Relationship between Fe/Na and Surface Gravity

The relationship between log g and the EWR of Fe and Na absorption lines (Fe/Na) are derived from 25 giants and the 4 main-sequence stars of which $T_{\rm eff}$ are around 4200-4300K. The EWRs of four line pairs are calculated: Fe (8186.7Å) / Na (8183.3Å), Fe (8186.7Å) / Na (8194.8Å), Fe (8204.9Å) / Na (8183.3Å), and Fe (8204.9Å) / Na (8194.8Å). Results are shown in figure 15. Filled squares and triangles mark the EWRs of the giants and main-sequence stars, respectively. The solid line in each graph is the best-fit line for these objects. In every case, the line ratios decrease significantly with increasing log g. The averaged slope of the curves in log g = 3.5-4.0 (a typical surface gravity for pre-main sequence stars) are -0.085, -0.067, -0.084, -0.064 in Fe (8186.7Å) / Na (8183.3Å), Fe (8186.7Å) / Na (8194.8Å), Fe (8204.9Å) / Na (8183.3Å), and Fe (8204.9Å) / Na (8194.8Å), respectively. The EWRs falls to 20% on average, when the log g increases from 1.5 to 4.5. These EWRs are considered to be excellent diagnostics for deriving the surface gravity.

Next, we calculated the EWRs of five giants and two main-sequence stars of which $T_{\rm eff}$ is 4600-4700K. The EWRs of these objects are shown as open squares and triangles in figure 15. The best-fit line in each EWR is indicated as a dashed line. The EWRs increase for higher-$T_{\rm eff}$ objects at constant gravity over the range of log g = 3.5-4.0. A comparison of fitted curves indicates that the EWRs of high-$T_{\rm eff}$ objects are 0.007-0.032 larger than the low-$T_{\rm eff}$ EWRs in log g = 3.5. These results indicate that the EWRs have an effective temperature dependency, and therefore, to estimate the surface gravity with a high precision, it is necessary to establish the EWR-log g relationship in each small effective temperature range.

3.3.2 Model Atmospheric Spectra Comparisons

We synthesized spectra using the SPTOOL program (Takeda, 1995), which calculates model spectra based on the ATLAS 9 model (Kurucz, 1993). The model spectra were calculated for $T_{\rm eff}$ of 4200K and 4750K, and a range in log g of 1.0-5.0, and the EWRs were estimated (figure 16). All of the EWRs calculated from the synthesized spectra decreased with increasing log g. This is consistent with the EWRs for the observed spectra.

In addition, although the EWRs of the observed spectra and the data from the

SPTOOL are poorly matched especially in the EWRs from the 4750K model spectra and the Fe (8204.9Å) ratios, the EWRs of the high-$T_{\rm eff}$ objects are larger than those of low-$T_{\rm eff}$ objects with a log g range larger than 3. This occurs because the EW of the Fe lines increases, and the wing of the Na lines decreases in high-$T_{\rm eff}$ spectra.

This discrepancy in the observed spectra and the model spectra could arise from improper values of the excitation potential and the damping constant of the Fe and Na lines. Since the both observed and synthetic EWRs match in the Fe (8186.7Å) / Na (8183.3Å) and Fe (8186.7Å) / Na (8194.8Å) EWRs, the excitation potential and the damping constant of Fe (8186.7Å) line and both Na lines are seem to be estimated correctly. In the Fe (8204.9Å) case, since the observed EWs were weaker than the modeled EWs and has no strong wings, the excitation potential may be underestimated. Further improvements on the line data will increase the utility of this log g diagnostic.

3.3.3 The EWR of WTTSs

We next compared the EWRs of WTTSs with the EWRs of giants and main-sequence stars. Since the Na (8183.3Å) and Fe (8186.7Å) lines of the WTTSs were blended with the telluric lines, only the Fe(8204.9Å) / Na (8194.8Å) was obtained.

As seen in figure 17, the EWRs of two WTTSs (RX J0452.5+1730 and RX J0459.7+1430, marked with open circles) with $T_{\rm eff}$=4590K are larger than the EWR of the WTTS (HBC 374, marked with filled circle) of which $T_{\rm eff}$ is 4060K. This is consistent with results from the fitted curves and the model spectra mentioned in section 3.2.2. The EWRs of high-$T_{\rm eff}$ WTTSs agree closely with the curve from the 4600-4700K objects, and the EWRs of HBC 374 and V827 Tau fits the curve approximated by the 4200-4300K objects. This result indicates that the surface gravity of pre-main sequence stars is able to be determined from this relationship.

By using this relationship, the log g of these two WTTSs are estimated at 3.95, which correspond to the age of 2.8 Myr in the evolution model of Baraffe et al. (1998). This result agrees with the age derived from the photometric observation using the extinction amount of Kenyon & Hartmann (1995) (table 3). However, using the amount of extinction of Furlan et al. (2006) results the log g of HBC 374 and V827 Tau to 3.263 and 3.627, respectively. The ages of these two WTTSs estimated by using this A_V will be less than 1 Myr, which mismatch our result.

3.3.4 Age Determination Accuracy

The age of a pre-main sequence star is able to be estimated by comparing the derived surface gravity with an evolution model. In our method, the accuracy of the calculated ages depends on the precision of the surface gravity value obtained for the pre-main sequence stars. This is dependent on the error in the EWR. We assumed the EWR error of the pre-main sequence star as 7.0×10^{-3}, which nearly corresponds to the error of HBC 374. The log g error calculated from this uncertainty is 0.1-0.2 in the 3.5-4.0 range. Consequently, by comparing with an evolution model of a 0.8 $M_{\odot}$ star in Baraffe et al. (1998), the age of the pre-main sequence star can be determined within a factor of 1.5, in average. This precision will be improved by deriving the general EWR error in the other three EWRs. To adapt this method to pre-main sequence stars of different temperatures, accurate estimations of the relation of EWR-log g relationship for each $T_{\rm eff}$ range are required. In addition, an independent $T_{\rm eff}$ estimation is necessary in order to determine the log g of the pre-main sequence star using this technique.

3.4 Summary

A high-resolution optical spectroscopy was carried out to create a new age determination method for late-K type pre-main sequence stars. The equivalent width ratios were used as the surface gravity indicator, to avoid the problems from veiling contamination and the uncertainties of distance and extinction.

The EW of the Na (8183.3$\AA$ and 8194.8$\AA$) and Fe (8186.7$\AA$ and 8204.9$\AA$) absorption lines in the I-band was used in this work. To derive the relationship between Fe/Na and surface gravity, 25 giant stars, 4 main sequence stars, and 2 WTTSs were observed with the Okayama Astrophysical Observatory 1.88 m telescope and HIDES, and the Subaru Telescope and HDS. $T_{\rm eff}$ of the objects were 4200-4300K and the surface gravity was known from the previous photometric studies. All four EWRs decreased with increasing surface gravity. Therefore, they are efficient diagnostics of surface gravity. Using the Fe (8204.9$\AA$) / Na (8194.8$\AA$) EWR, the log g of pre-main sequence stars with 0.8 $M_{\odot}$ can be estimated with an uncertainty of 0.1-0.2. From comparisons with an evolution model, we concluded that their ages can be determined within a factor of 1.5.

Five giants, two main sequence stars, and two WTTSs with higher-$T_{\rm eff}$ (4600-4700K) were also observed to estimate the temperature dependence of the EWR. The EWRs of the high-$T_{\rm eff}$ objects were larger than those of the low $T_{\rm eff}$ in the typical pre-main sequence star surface gravity range. Therefore, to accurately determine the ages of pre-main sequence stars with masses larger or smaller than 0.8 $M_{\odot}$, new EWR-log g relationship for each $T_{\rm eff}$ range are required.

4 K-band Sc/Na for the early-M type stars

The age determination method mentioned in section 3 was optimized to the pre-main sequence stars with the effective temperature around 4200K. Since the Fe/Na ratios have an effective temperature dependency, it is unacceptable to adapt the derived EWR-log g relation to the young stars with other effective temperature. In order to establish a more universal age determination method using the EWR, the EWR-log g relation in other effective temperature should be estimated. In this section, the EWR age determination method for pre-main sequence stars with 3800K using the Sc (22057.8$\AA$, 22068.7$\AA$) and Na (22062.4$\AA$, 22089.7$\AA$) absorption lines in near-infrared K-band will be presented.

4.1 Observations

4.1.1 Target Selection

In order to reveal the relation between the equivalent width ratios of Sc and Na (Sc/Na) and surface gravity, it is necessary to obtain the spectra of stars with fixed temperature and with different surface gravity. 10 giants, 10 dwarfs of which parallaxes are measured with the Hipparcos satellite (Perryman et al., 1997) are selected as the targets. The surface gravity of these stars are calculated by the equation (23) in section 3.1.1. The effective temperature of the targets were estimated by comparing the spectral type given in SIMBAD and the temperature-spectral type relationship (Lang, 1992). The V-band magnitudes of the targets were also quoted from SIMBAD to calculate the luminosity of the targets. The bolometric corrections for the luminosity calculation were also quoted from Lang (1992). The masses of the main-sequence stars were estimated by comparing the spectral type and the mass-spectral type relation in Drilling & Landolt (2000). For the masses of the giant stars, we used the evolutional tracks of giant stars (Lejeune & Schaerer, 2001) as assuming all the targets are in the red giant branch. The error of the calculated surface gravity is attributed to the error of the parallax, and since the error of the effective temperature is not included, it could be underestimated.

2 CTTSs and 2 WTTSs in the Taurus molecular cloud were also selected as the targets. Since WTTSs have an optical thin disk, its luminosity is less contaminated by veiling. We calculated the surface gravity of the WTTSs using equation 23. The mass, effective temperature, and the luminosity are quoted from Bertout, Siess, &

Cabrit (2007). The 2 CTTSs were selected to determine the ages with the derived Sc/Na - surface gravity relation. The target properties are listed in table 4.

4.1.2 Observations Details

UKIRT/CGS4

8 giants, 6 main-sequence stars, and 4 PMS stars were observed using United Kingdom Infrared Telescope (UKIRT) with Cooled Grating Spectrometer 4 (CGS4) echelle mode, on 17 December, 2008. The resolution power was set to 38000 in order to prevent the blending of the nearby absorption lines. The grating angle was set to 64.7 degree to obtain the Sc and Na absorption lines in the 25th order of the echelle (22000-22125Å). The integration time was 8 seconds to 16 minutes to achieve the S/N of 100. The maximum exposure time of the single exposure was set to 60 seconds, to reduce the risk of cosmic rays and to subtract the sky background accurately. Each frame was obtained by 2x2 exposure pattern, in order to avoid the contamination by the bad pixels. From this observation procedure, a single exposure creates 4 separate frames, and each of the frame is shifted 0.5 pixels in the wavelength direction (figure 18). Therefore, the spectral information of the range which is influenced by the bad pixel will be obtained by other shifted images.

The ABBA exposure pattern was adopted for this observation. This method exposes the star 4 times, and the second and third frame is integrated by nodding the telescope 9 arcseconds along the slit, which is called the B position. The position where the first and the last frame were taken is called the A position. From this procedure, the sky and the dark is able to be subtracted simultaneously (figure 19). The faint objects were integrated several ABBA exposures.

Flat frame were taken by using the flat lamp, and were obtained at the beginning and the end of the observation. The Th-Ar lamp frames were taken with the same frequency, to calibrate the wavelength. We also observed A0 type stars as standard stars for the telluric absorption line correction. These standard stars are selected for each target, to obtain the spectra of the telluric atmosphere in similar airmass of the target stars. The average separation between the targets and the standard stars was 6.8 arcdegree.

Subaru/IRCS

The spectra of 1 giant (HIP 20376) and 1 main-sequence star (GJ 15 A) were observed using the Subaru Telescope with Infrared Camera and Spectrograph (IRCS) on 16-18 September, 2002, which were obtained by K. Sugitani et al., for other purpose. The resolution power of 20000 was selected for this observation. The K filter and the K^- echelle setting was used to obtain the spectra. The Sc and Na lines were placed in the 25th order (22030-22550$\AA$). To achieve the S/N of 100 for each object, HIP 20376 and GL 15 A were integrated 5 and 300 seconds, respectively. The ABBA exposure pattern (figure 19) was also adopted in this observation. Flat frames were obtained at the beginning and the end of the observation, for the flat fielding. The A0 type standard stars were obtained for each target, for the telluric line correction. Since the OH emission lines were used for wavelength calibration, comparison frame was not obtained in this observation.

4.2 Archival data

We obtained the spectra of 1 giant and 3 main-sequence stars from the archival data. The spectra of the giant star and 2 main-sequence stars were obtained from Wallace & Hinkle (1996), and one spectrum of a main-sequence star was taken from the Gemini Science Archive. The spectra from Wallace & Hinkle (1996) were acquired using 4 meter Mayall Telescope with Fourier transform spectrometers, at Kitt Peak observatory. The resolution power was 45000-90000, and the S/N was 90-230. The data taken from the Gemini Science Archive was the data observed on 13 January, 2006 with Phoenix, a high-resolution echelle spectrometer equipped on Gemini South Telescope (P.I. D. Charbonneau). The observed wavelength range was 2.16-2.21 μm. The integration time was 60 sec, and the resolution power was 40000. We also obtained the calibration frames and the data of A0 type standard star.

4.3 Data Reduction

4.3.1 Spectra Extraction

The Image Reduction and Analysis Facility (IRAF) software package was also used for the near-infrared data reduction. The same procedures were applied for all of the observational data. First, the dark and the sky emission (OH lines) were removed by subtracting the B position frame from the A position frame, which are the output frames of the ABBA integration (figure 19). The A frame was subtracted from the B frame for the same purpose. The normalized combined flat frame was used for the flat fielding. The data with several apertures contained in a single frame were divided into a single aperture image, using the *apall* task with the extract format set to "*strip*".

The wavelength calibration and the distortion correction were accomplished concurrently. First, for the data obtained by the Subaru Telescope and the Gemini South Telescope, the OH image was created by adding an object frame to a single frame, in order to gain the count of the OH lines. The location pixels and the wavelength of the Th-Ar and the OH emissions are marked by using the task $identify$. This procedure was done along the spatial direction, once in each 10 pixels. The distortion of the image were next calculated by the task $fitcoords$, by changing the order of the polynomial equation. The average order used for this correction were $xorder =$ and $yorder = 3$. Finally, the distortion of the object frames are reduced by running the task $transform$, by referring the result of the $fitcoords$ task. The wavelength information are also attached to the object frames by the $transform$ task.

The sky was subtracted with the task *background*. The background region is the range where the stellar spectrum does not appear. These regions are fit with a polynomial equation, in each vertically lined (lined along the spatial direction) pixels. The averaged background counts are subtracted from the spectral region.

After these procedures, the spectrum was extracted from each frame. All of the A and B frames were combined into a single spectrum. The targets which were integrated several times were also combined to a single spectrum to increase the S/N.

The absorption lines due to the earth atmosphere should be removed from the stellar spectrum. This could be achieved by dividing the stellar spectra with the spectrum of the A0 type star. Because only few hydrogen absorption lines appear in the A0 star spectra, these stars are fine standard stars for the telluric lines. Finally,

the object spectra are normalized at the continuum level. All of the spectra are displayed in figures 20, 21, and 22.

4.3.2 Measuring the Equvalent Width

The SPLOT task was used to measure the equivalent width of the Sc and the Na lines. Since the Sc and Na lines in the large log g stars are blended due to the strong wing of the Na line, we used the deblending task in the SPLOT package. The Voigt function was used for fitting the Na lines. For the Sc lines, the gaussian function was adopted since the wing of these lines is vanishingly small. Some of the equivalent widths of Sc lines were impossible to measure because of the low S/N and/or the line broadening due to the rapid rotation, especially in the WTTS spectra.

The equivalent width of the Na line in 22062.4$\AA$ was sometime over estimated when the S/N is low, or the absorption lines are boarded. The matter of this problem is the nearby absorption lines such as Sc, Si, and the telluric lines which was not completely reduced by the standard star correction. These lines are able to be fit correctly when the spectrum is obtained with high S/N, however, when the S/N was smaller than the expected amount, or when the lines are spreaded due to the rapid rotation, it becomes difficult to fit. Therefore, the fraction of these lines mix to the Na line, and the Na line will be fit as if it were a line with a large wing. Moreover, the equivalent width of the Sc lines decreases due to the mis-fitting of the Na line.

To avoid this problem, the equivalent width ratio of the Na lines was calculated from the spectra of giant stars and main sequence stars with high S/N (figure 23). The equivalent width ratio is nearly constant with the surface gravity, and the average of the ratio is 1.31. This relation was adopted as a condition for the fitting of the low S/N stars. First, the equivalent width of the Na line in 22089.7$\AA$ was measured, and then that of the Na line in 22062.4$\AA$ was estimated from the Na/Na relation. The fitting of the Sc, Si, and Na lines in the range of 22050-22075$\AA$ was accomplished to agree the estimated equivalent width of Na (22062.4$\AA$), by changing the full-width-half-maximum (FWHM) of the absorption lines. The error in EW was estimated from uncertainty of the continuum level, expressed in section 3.1.3. The measured EWs of each line are listed in table 5.

4.4 Results and Discussions

4.4.1 Sc/Na - surface gravity relation

The relation between surface gravity (g) and the Sc/Na in early-M type stars (effective temperature around 3800K) was derived by using the spectra of 10 giants and 10 main-sequence stars of which spectral types are around M0. The EWRs were calculated using four lines: Sc (22057.8$\AA$) / Na (22062.4$\AA$), Sc (22057.8$\AA$) / Na (22089.7$\AA$), Sc (22071.3$\AA$) / Na (22062.4$\AA$), and Sc (22071.3$\AA$) / Na (22089.7$\AA$). Results are shown in figure 24. The squares and the triangles indicate the EWRs of the giants and main-sequence stars, respectively. The solid line in each EWR graph is the best-fit curve. In every line pair, the EWRs decrease significantly with increasing surface gravity. The EWRs drop to 15% when the log g increases from 1.5 to 4.5. Therefore, these EWRs are considered to be excellent diagnostics for deriving the surface gravity for early M type stars, and the surface gravity of the stars are able to be estimated using this relation.

Next, we calculated the EWRs of 2 WTTSs, and compared with the derived Sc/Na - surface gravity relation (figure 24). Although the EWR of the V827 Tau is slightly larger than the fit curve, which is due to the difficult de-blending to the Si line (22068.7$\AA$), the EWRs of the WTTSs agree with the Sc/Na - surface gravity relation. Hence, these relations are suitable for the surface gravity estimations of PMS stars. As mentioned in section 3.3.1, the EWR - surface gravity relation has an effective temperature dependency. To estimate the age of PMS stars in different temperature range, it is necessary to derive the Sc/Na - surface gravity relation in the particular effective temperature.

4.4.2 Ages of the PMS stars

We estimated the ages of the 2 CTTSs and 2 WTTSs using the Sc line (22057.8$\AA$) and the Na lines (22062.4$\AA$ and 22089.7$\AA$). The Sc line at 22071.3$\AA$ was not used for the age determination due to the blending with the Si line (22068.7$\AA$). First, the surface gravities of the PMS stars were derived by comparing the observed Sc/Na and the Sc/Na - surface gravity relation. The surface gravities of the WTTSs were also re-estimated by this procedure. The error of the surface gravities are calculated from the error of the EWR. Next, the ages of the PMS stars were estimated by comparing the derived surface gravity and the evolution model of the PMS stars

(Baraffe et al., 1998) on the H-R diagram (figure 25). The derived surface gravities and ages of the PMS stars are listed in table 6.

EWR Age vs. Photometric Age

The estimated ages of the PMS stars were compared with the ages derived from photospheric observations. Bertout, Siess, & Cabrit (2007) (hereafter BSC07) deduced the luminosities from the I-band fluxes and the distances. The veiling is considered to be smallest in the I-band (Cieza et al., 2005). The distances are estimated with the kinematic study (Bertout & Genova, 2006). In figure 25, the loci of the PMS stars from BSC07 are also marked.

Although the PMS star ages estimated in our work agree with the age deduced in BSC07, except LkCa 14, all of the ages with the EWR method are older than the photometric method (Figure 25). The luminosity of these stars are estimated to be smaller than the photometric results. We consider that this luminosity discrepancy arises from the inaccurate distance, extinction, or veiling, or the combination of these effects.

We supposed that this difference in CTTSs arises from veiling. For DN Tau, the luminosity ($\log L/L_{\odot}$) of BSC07 is 0.10 dex larger, resulting that the veiling in I-band is r=0.23, where r denotes the proportion of veiling to the stellar continuum. The veiling of DN Tau is measured in Basri & Batalha (1990), by fitting the high-resolution spectrum to the spectral standard star. From their study, the I-band veiling is around 0.2, which is consistent to our result. Also, the veiling of IQ Tau in the I-band is calculated as 0.18. In the study of Basri & Batalha (1990), the I-band veiling of 15 PMS stars are measured as r=0.2-3. Even the veiling of DN Tau and IQ Tau are small compared to the veiling of other PMS stars, the ages from photometric observation conflict with our veiling-free method. Hence, there is a possibility that most of the CTTS ages derived photometrically are younger than the true age.

The ages of the WTTSs are also estimated older by the EWR method, despite the small veiling compared to the CTTSs. The $\log L/L_{\odot}$ of V827 Tau in our result is 0.17 dex smaller than BSC07. This disagreement can be explained by assuming the existence of veiling r=0.47, It can also be described by estimating the distance as 136pc, which is a closer distance compared to result from the kinematic study (Bertout & Genova, 2006), 160pc. Another way is to diminish the extinction. The A_V measured in BSC07 is 0.28 mag. By assuming A_V=0 mag, the luminosity of V827 Tau is reduced to $\log L/L_{\odot}$=-0.17, which is still

slightly brighter (0.06 dex) than estimated luminosity from the EWR method.

For LkCa 14, the age in the EWR method is 3.7 Myr younger than BSC07, which is the largest difference among the 4 PMS stars. Since the A_V of this object is estimated as 0 mag in BSC07, extinction is not the cause. To explain this contrariety, the veiling of this object in the I band should be r=1.48, or the distance to this object has to be 91pc. Both of these amounts are considered unsuitable for a WTTS in Taurus. The Sc line is heavily blended with the Na line (22062.4Å) in the spectrum of LkCa 14 (figure 22), and therefore the Sc/Na could be underestimated. A higher resolution observation is necessary to avoid the blending.

Age Determination Accuracy

The precision of the age determination of this method depends on the accuracy of the surface gravity estimation, which is due to the EWR error. The error of the surface gravity estimation in DN Tau is around 0.1, making the age determination accuracy of DN Tau in a factor of 1.4-1.6. The S/N of the DN Tau spectrum was around 120. Therefore, by observing the PMS star spectrum with S/N=120, the age of the PMS stars are able to be estimated within a factor of 1.5 with the EWR method.

The age of the V827 Tau was also estimated with the optical Fe/Na method described in section 3. The effective temperature of the V827 Tau is 4060K (BSC07). Since the Sc/Na - surface gravity relation is optimized to the effective temperature of 3800K, and the Fe/Na is for the stars with 4200K, the derived age in both methods may include an error of effective temperature dependency of EWR. However, both the Fe/Na and Sc/Na methods conclude that the age of V827 Tau is around 2.8 Myr, which indicates the accuracy of the age determination of the EWR methods.

4.5 Summary

We carried out high-resolution near-infrared spectroscopy to create the age determination method of early-M type pre-main sequence (PMS) stars. Our method is based on the surface gravity estimation using the equivalent width ratio (EWR) of nearby absorption lines, enabling us to estimate the age free from the distance, extinction, and veiling contamination. The Sc (22057.8$\AA$ and 22071.3$\AA$) and Na lines (22062.4$\AA$ and 22089.7$\AA$) were used to establish the surface gravity indicator. The spectra of 10 giants, 10 dwarfs and 4 PMS stars were obtained by observation with Subaru Telescope IRCS and UKIRT CGS4, and from the archive data of Kitt Peak observatory and Gemini South Phoenix. The EWRs of Sc and Na lines decrease with increasing surface gravity. We concluded that these EWRs are fine diagnostics of the surface gravity. By obtaining the spectrum of PMS stars with S/N$\sim$120, the ages of the PMS stars are able to be estimated with a factor of 1.5 on average, by comparing the estimated surface gravity with the evolution model (Baraffe et al., 1998).

The accurate age determination with no contaminations of distance uncertainty, extinction, and veiling allows us to reveal the evolutional process of PMS stars, protoplanetary disks, and planets. All of the estimated ages of the PMS stars observed in our work showed older ages compared to the ages estimated in photometric study (Bertout, Siess, & Cabrit, 2007). We concluded that this discrepancy arises from the uncertainty of distance, extinction and veiling.

Part II
Evolution Timescale of Protoplanetary Disks

5 Introduction

The evolution of the protoplanetary disks is important in understanding the evolution of the planets. The evolution timescale of the disk is one of the most critical part of the planet formation, particularly in the gas giant planets. In the early stage of planet formation, collision and merging of planetesimals encourage the growth of protoplanets. When the mass of a protoplanet reaches to 5 to 10 earth masses, the surrounding gas start to flow in. The mass increase of the planet accelerates the gas accretion, and finally forms a gas giant planets (Ida, 2003). The final mass of the gaseous planets depend on the remained amount of gas when the "core" is formed. Therefore, the dissipation timescale of the gas disk plays an important role in understanding Jovian planets formation.

Also, the gas of the disk triggers the migration of the planets. From the differential rotation of the disk, the disk at the smaller radii than created protoplanet rotates rapidly, and this accelerates the orbital speed of the planet. On the other hand, the outer disk reduces the rotation speed of the planet due to the slower rotation compared to the protoplanet. As calculated by Goldreich et al. (1980), the effect from the outer disk is always stronger than that of the inner disk. Therefore, the protoplanet moves inward, which is called type-I migration.

There is another mechanism which explains the planet migration. When a protoplanet gains the mass and grows into a gas planet, it absorbs the gas from the disk and creates a gas-lacking region, as a "gap" in the disk. This gap shifts inward as the disk materials accrete to the central star. And the planet involved in this gap also shift inward with the disk accretion, due to the gravitational interaction (Lin & Papaloizou, 1993). This is called the type-II migration. This is the most widely accepted theory to explain the formation of the Hot-Jupiters, which are the Jovian Planets orbit at point-blank range from the central star (Lin, Bodenheimer, & Richardson, 1996). For these reasons, estimating the disk dissipation timescale is one of the top priority issues to figure out the universal planet formation.

5.1 Previous Studies

Disk Frequency and the Dissipation Timescale

The timescale of the protoplanetary disk evolution can be estimated by comparing many star-forming regions with different age. Haisch, Lada, & Lada (2000, 2001a,b) estimated the census of the circumstellar disk fractions in the clusters NGC 2024, NGC 2264, NGC 2362, NGC 1960, Trapezium, and IC 348. For these regions, they used the fluxes of the near-infrared $JHKL$ bands, and calculated the colors to identify the pre-main sequence stars with protoplanetary disks. After estimating the fraction of stars with disks in each star-forming regions, Haisch, Lada, & Lada (2001b) compared the disk fraction with the age of the star-forming regions, which were determined from photometric studies (Meyer, 1996; Palla & Stahler, 2000; Balona & Laney, 1996; Barkhatova et al., 1985). As a result, the disk frequency decreases with increasing cluster age, such that half of the pre-main sequence star disks dissipate in $\leq$ 3Myr. This sort of study is updated by many researchers, and recently Mamajek (2009) estimated the average disk lifetime as 2.5 Myr, combining the data of 22 star-forming regions.

Transitional Disk Objects

The disk was thought to be evolved from an optically thick CTTS disk to an optically thin WTTS disk, but in recent years a disk with an inner hole has been discovered. From the multi-wavelength photometric observation (e.g. Strom et al. 1989, Wolk & Walter 1996), some pre-main sequence stars showed a SED with an excess in the wavelength larger the mid-infrared, where there is no near-infrared excess. These SEDs indicate that these pre-main sequence stars has an optically thick outer disk, and an optically thin inner disk. These disks are called Transitional disk, which is considered as an evolution phase between the CTTS disk and WTTS disk.

Najita et al. (2007) derived the mass and the accretion rate of the Transitional disk, and found that these disks have an equal mass to the CTTS disks. However, the accretion rate was 10 times smaller compared to the CTTS disks. This result indicates that the accretion from the Transitional disk is blocked by the protoplanets formed in the optically thin inner hole. Therefore, the Transitional disk object is in an early planet formation phase. A detail study of these objects enables to understand the planet formation in the disk.

Many photometric studies have been conducted to derive the evolution timescale

from CTTSs to WTTSs. For example, Kenyon & Hartmann (1995) obtained the optical, near-infrared, and far-infrared fluxes of the pre-main sequence stars in the Taurus-Auriga star-forming region, and estimated their luminosities. The ages of these stars were estimated by comparing the luminosities with the evolution model of D'Antona & Mazzitelli (1994). Since there was no significant difference between the age of CTTSs and WTTSs, the evolution timescale was difficult to estimate.

Bertout, Siess, & Cabrit (2007) succeeded to estimate this timescale. They determined the ages of 72 pre-main sequence stars in Taurus-Auriga star forming region. They used the effective temperatures, the amount of the extinction, and the fluxes estimated by Kenyon & Hartmann (1995). The difference between these two studies is the distance. The distance of each individual pre-main sequence stars were calculated by Bertout & Genova (2006). From the proper motions and the radial velocities of the pre-main sequence stars, they estimated the distances with the convergent point method and the Monte-Carlo simulations. Figure 27 is the result of the Bertout, Siess, & Cabrit (2007), the H-R diagram with the plots of the pre-main sequence stars. The CTTSs are plotted above the plots of WTTSs, which indicate that CTTSs are relatively younger than WTTSs. They evaluated this difference by the Kolmogorov-Smirnov (K-S) statistics, and confirmed that the parent populations of this two groups are different. This is the first result that the age of CTTSs and WTTSs were distinctly-divided. They concluded that the disk lifetime is $4 \times 10^6 (M/M_\odot)^{0.75}$ years.

All of the results of these studies are derived from the age determination based on the photometric observation. Hence, as mentioned in section 1.2.1, there is a possibility that the estimated age of the pre-main sequence stars includes the uncertainties of distance, extinction, and veiling. The result of Bertout, Siess, & Cabrit (2007) proved that the age of the CTTSs are relatively younger than WTTSs, however there are still some contaminations included in the estimated age (see section 4.4.2). The distance determined in (Bertout & Genova, 2006) could be incorrect if the target star is a binary. To determine the correct disk evolution timescale, with no contamination of these three effects, it is suitable to derive the ages of the CTTSs, Transitional disk objects, and WTTSs using the age determination method created in the part I of this study.

6 Observations and Data Reductions

6.1 Target Selection

To estimate the evolution timescale of Transitional disk objects in the Taurus-Auriga star-forming region, 2 classical T Tauri stars (CTTSs) and 2 Transitional disk objects were selected as the targets. The age of the 2 CTTSs (DN Tau and IQ Tau) and 3 WTTSs (HBC 374, LkCa 14, and V827 Tau) estimated in section 3 and 4 will be combined to the result of this section. The effective temperatures of the newly selected target stars are around 4200K, in order to apply the Fe/Na age determination method described in section 3. These stars are selected from Furlan et al. (2006). The SEDs of the 8 target stars quoted from Furlan et al. (2006) are displayed in figures 28 and 29. The spectral types and the effective temperatures of the 4 targets are listed in the second and the third column of table 7.

LkCa 15 is a well studied pre-main sequence star. Espaillat et al. (2007) proposed that the disk of LkCa 15 is composed of small inner disk (0.12-0.15 AU), a gap, and a disk outward from 46 AU. This was revealed from the observation carried out by Spitzer and Sub-millimeter array. Since the inner disk remains in this star, this star is called pre-Transitional disk object. Thalmann et al. (2010) observed LkCa 15 with the High Contrast Instrument for the Subaru Next Generation Adaptive Optics (HiCIAO) equipped on the Subaru Telescope, and discovered the inner wall of the outer disk. This result supports the shape of the SED and the presence of gap in the disk.

V819 Tau is mostly a WTTS, due to the lacking near-infrared excess, however, the excess in the wavelength longer than 10 μm was discovered by Furlan et al. (2006) (figure 29). Therefore, this star is identified as a Transitional disk in this study. Since the excess is relatively smaller than that of LkCa 15, it could be considered as an evolved Transitional disk object.

6.2 Observation Details

The high-resolution I-band spectroscopy of the 2 CTTSs and 2 Transitional disk objects were carried out on 2010 December 7 using the High Dispersion Spectrograph (HDS) on Subaru Telescope. The slit width of the spectrograph was set to 0.6 arcsecond, in order to achieve the resolution power of 60000. The Cross scan and the Echelle grating was set to 5.69 degree and 0.60 degree, respectively, in order to

observe the 73 order of the echelle, which includes the Na (8183.3$\AA$ and 8194.8$\AA$) lines and Fe (8186.7$\AA$ and 8204.9$\AA$) lines, at the central region of the detector. The integration times of the objects were 1200 sec to 1800 sec, to achieve the S/N of 100. From the previous study in section 3, it was found that the spectrum between 8180-8210$\AA$ contains many telluric absorption features. In order to avoid the blending of these lines, a spectral standard A0 star was also observed. All of the integrations of the target stars were separated into two parts, and the standard star was observed between the divided object exposure. However, since the broad hydrogen absorption line due to the stellar atmosphere appeared in the spectrum of the standard star, it was impossible to remove the telluric lines. The bias frames and the flat frames were obtained at the beginning of the observation. The Th-Ar images for the wavelength calibration were obtained at the beginning and the end of the observation.

6.3 Data Reductions

The procedure used for the data reduction in section 3.1.3 was adopted for the data reduction. The spectra of the 2 CTTSs and 2 Transitional disk objects are shown in figure 30. The measured equivalent width of these objects are listed in table 7.

7 Results and Discussions

7.1 Age of the Pre-Main Sequence Stars

7.1.1 Age Determination

First, the surface gravities of the 2 CTTSs and 2 Transitional disk objects were estimated with the equivalent width ratio (EWR) method calculated by using Na lines (8183.3Å and 8194.8Å) and the Fe line (8204.9Å). The Fe line in 8186.7Å was not used for the surface gravity determination, since there were a large scattering on the EWRs using this line (see figure 15). This uncertainty may arise from the effective temperature dependency of the vanadium line, blended in this Fe absorption. The determined surface gravities are shown in the second column of table 8. The average error of the surface gravity in the 4 pre-main sequence stars are around 0.1 in log g, which is slightly smaller than the amount estimated in section 3.3.4. This higher accuracy was achieved since the EWR calculation using Na line in 8183.3Å was available, where it was unable to use in the previous study due to the telluric line blending.

The ages of these 4 stars were then estimated by comparing the determined surface gravity and the evolution model of Baraffe et al. (1998) (the fourth column in table 8). The age of the LkCa 15, the pre-Transitional disk object, was 1.41 Myr. The age of the V819 Tau, which is considered to be in the later Transitional disk phase due to the small excess, is 2.40 Myr. Hence, the Transitional disk phase lasts more than 1 Myr, by assuming that there is no mass dependency on the evolution timescale of the protoplanetary disk.

7.1.2 EWR Age versus Photometric Age

The ages of the LkCa 15 and the V819 Tau estimated in the photometric study of Bertout, Siess, & Cabrit (2007) (hereafter BSC07) were 5.01 Myr and 6.17 Myr, respectively. The age of these 2 stars are estimated younger in this study, which means that they are more luminous than estimated in BSC07. This difference is able to be explained by assuming that the extinction is larger, or more distant.

From the estimated surface gravity, the luminosity was also estimated by reference to the evolution model of Baraffe et al. (1998). The luminosity of the LkCa 15 from the EWR method was 1.38 $L_{\odot}$. This is 1.62 times larger than the result of BSC07 (0.85 $L_{\odot}$). The photometrically estimated extinction and the distance of

this star is 0.62 mag and 168 pc, respectively (Bertout & Genova (2006), BSC07). To fill this gap, the A_V of LkCa 15 should be 1.14 mag, or the distance is 213 pc. Because this distance is too large for the star in the Taurus-Auriga star forming region (average distance is 142 pc (Wichmann et al., 1998)), the extinction will be the fine explanation.

The luminosity of V819 Tau is calculated as 0.66 $L_\odot$, where the result of BSC07 is 0.43 $L_\odot$. BSC07 also estimated the A_V and the distance as 0.74 mag and 117 pc, respectively. To make up the luminosity difference between the result of our study and BSC07, the extinction magnitude should be 1.82 mag. Since V819 Tau is a nearly-WTTS Transitional disk object, the extinction is considered to be relatively small. Most of the WTTSs has A_V around 1 mag or smaller, by fitting the SED to the result of photometric observation (Kenyon & Hartmann, 1995). Therefore, it is difficult to explain the luminosity difference with the extinction. On the other hand, the estimated distance from the EWR method is 145 pc, which is consistent to the average distance to the Taurus-Auriga star forming region.

7.1.3 The Evolution Model Dependency

Since the ages of the pre-main sequence stars are estimated using the evolution model in either photometric or spectroscopic method, the model dependency is ineffaceable. The ages of the 9 pre-main sequence stars were estimated by using the evolution model of Siess, Dufour, & Forestini (2000), for the purpose of estimating the model dependency of the EWR method. The difference between the models of Baraffe et al. (1998) and the Siess, Dufour, & Forestini (2000) is the constitutive physics such as convection and stellar atmosphere, and the assumed component material such as the metallicity and the deuterium amount. The H-R diagram using the model of Siess, Dufour, & Forestini (2000) was displayed in figure 32. The loci of the pre-main sequence stars in figure 32 differ from that of figure 31, since the luminosity is dependent to the evolution model. The ages estimated from each evolution models is listed in table 8. Although most of the ages of the stars are estimated slightly younger when the model of Baraffe et al. (1998) was used, the age estimated from the surface gravity using two models agree within the margin of error. Hence, there was no obvious difference between the ages determined from two different evolution model.

7.2 Ages of CTTSs, Transitional Disk Objects, and WTTSs

In most of the previous photometric study, there was no significant difference between the ages of CTTSs and WTTSs (e.g. Kenyon & Hartmann, 1995). The loci of the CTTSs and the WTTSs in the H-R diagram were mixed each other (figure 26). BSC07 succeeded to divide the CTTSs and the WTTSs on the H-R diagram (figure 27).

The ages estimated by the EWR method also divided the CTTSs + Transitional disk objects and WTTSs. Figure 31 is the H-R diagram with 4 CTTSs, 2 Transitional disk objects, and 3 WTTSs, with the age estimated by the EWR method in section 3.3.3, 4.4.2, and 7.1.1. Kolmogorov - Smirnov statistics were used to evaluate the age difference between these two groups. From this validation, the age of the CTTSs + Transitional disk objects and WTTSs are different in 95% of the time. Also, by comparing the ages of DL Tau, V819 Tau, HBC 374, and V827 Tau, the ages of the stars increases in the order of the CTTS, the Transitional disk object, and the WTTS. These results denote that the protoplanetary disk evolves from an optically thick disk to an optically thin disk with time.

7.3 The Evolution Timescale of the Protoplanetary Disks

7.3.1 Age versus $K - L$ Color

To estimate the disk evolution level of the 9 pre-main sequence stars, the color of the $K - L$ is used. The $K - L$ colors of the 9 pre-main sequence stars are quoted from the photometric study of Kenyon & Hartmann (1995), which is listed in the column 5 of table 9. The large $K - L$ represent the large near-infrared excess, which indicates the presence of an optically thick, young protoplanetary disk.

First, the relation between the $K - L$ and the age estimated from the luminosity of Kenyon & Hartmann (1995) was revealed. The luminosities of the 9 pre-main sequence stars were determined from the photometric observation. Most of the luminosities of the 9 stars were estimated by defining the J-band flux as the basis wavelength for the SED fitting. For DL Tau, the luminosity was estimated from the optical and far-infrared photometry, since the near-infrared fluxes were not observed. The ages of the stars were then determined by comparing the luminosity and the evolution models of Baraffe et al. (1998). The age of each star estimated from this method is shown in the fourth column of table 9. This is the most common way used

to estimate the age of the pre-main sequence star, however, as mentioned in section 1.2.1, the uncertainties of distance, extinction, and veiling are difficult to remove.

The comparison of $K - L$ and the photometric age is displayed in the bottom panel of figure 33. If the disk gas accretes and dissipates with the increasing age, the $K - L$ color should decrease during the evolution. However, there was no relation between the $K - L$ color and the age estimated from the luminosity of Kenyon & Hartmann (1995).

Next, the age - $K - L$ color relation was derived using the age estimated by BSC07. The age of the BSC07 is thought to be the more accurate than the previous photometric study (table 9, column 3), since the distance to the each star is estimated from the kinematic study (Bertout & Genova, 2006). This result is displayed in the middle panel of the figure 33. There was also no relation between the age and the color, mostly depending on the large estimated Transitional disk object's ages.

The result of the age - $K - L$ color relation using the result of this work (section 3.3.3, 4.4.2, and 7.1.1, summarized in the second column of table 9) is displayed on the top of the figure 33. Since the age estimated with the spectroscopic method is free from the uncertainties of distance, extinction, and veiling, it is considered to be the most accurate age determination method. The linear equation was fit to the plots with the least-square approach. The $K - L$ color decreases with the increasing age, indicating that there is a relationship between the age and the disk evolution.

7.3.2 Dissipation Timescale of the Disk

To estimate the evolution timescale of the protoplanetary disks, the derived age - $K - L$ relation was used. Since the average $K - L$ color of the main sequence stars with the effective temperature of 3800-4350 K is 0.12, it can be considered that the disk dissipates when the $K - L$ color reaches to this amount. From the linear fit derived in the previous section, the disk lifetime in the Taurus-Auriga star forming region is estimated as 4.0 Myr. This is comparable to the result of BSC07, which is estimated as 3.4 Myr for the stars with the mass of 0.8 $M_{\odot}$. This is a smaller result compared to the estimated disk lifetime of Haisch, Lada, & Lada (2001b) which estimated the relation between the disk fraction and the age of several star-forming regions with photometric study (see section 5.1), determined as $\sim$ 6 Myr.

7.3.3 Age versus Equivalent Width of Hα

The estimated ages of the 9 pre-main sequence stars were also compared to the equivalent width of Hα (6562.8$\AA$) emission. This emission feature arises from the active photosphere, due to the gas accretion from the disk. As mentioned in section 1.1.1, a pre-main sequence star with an optically thick disk emits a strong Hα line, and therefore it could be predicted that the younger star has larger equivalent width of Hα. The equivalent width (EW) of the Hα line in each star is quoted from Strom et al. (1989), which is the result of the low to mid-resolution spectroscopy (column 6 of table 9).

The EWs of the Hα were again compared to the ages estimated by Kenyon & Hartmann (1995), Bertout, Siess, & Cabrit (2007), and the EWR method (figure 34). It was difficult to evaluate if there is a relation between the age and the Hα or not, in the result of the photometric studies. There was a poor relation between the Hα and the age determined in this study. To reveal this relationship, the age determination of other pre-main sequence stars is necessary.

8 Conclusion

To derive the evolution timescale of the pre-main sequence stars and the protoplanetary disks, a new age determination method based on high-resolution spectroscopy was established. This method is based on the surface gravity estimation using the equivalent width ratio (EWR) of the nearby absorption lines. Surface gravity is a fine indicator of the age, because the photosphere contracts through the evolution. EWR is free from the uncertainties of distance, extinction, and the veiling of the pre-main sequence stars. The equivalent widths of the absorption lines are independent of distance and extinction. The "filling up" effect due to the veiling is able to be reduced by calculating the ratio of the nearby absorption features. This is a great advantage compared to the general age determination based on the photometric observation, since it is difficult to estimate the correct luminosity due to the distance, extinction, and veiling contaminations.

The EWR has both surface gravity and effective temperature dependency. The relation between the EWR and the surface gravity should be derived to establish the age determination method with EWR. The optical I-band Fe (8186.7$\AA$ and 8204.9$\AA$) and Na (8183.3$\AA$ and 8194.8$\AA$) lines of the 25 giants, 4 main sequence stars, and a WTTS were observed using HIDES mounted on the Okayama Astrophysical Observatory 1.88 m telescope, and HDS equipped on the Subaru Telescope. The effective temperature of the targets were fixed to around 4200K, corresponding to the effective temperature of the pre-main sequence stars with the mass of 0.8 $M_{\odot}$. The surface gravities of these stars were estimated from the previous photometric studies. 4 EWRs were derived by using the Fe and Na lines, and all of the EWRs decreased with increasing surface gravity. Therefore, they are efficient diagnostics of surface gravity. Using the Fe (8204.9$\AA$) / Na (8194.8$\AA$) EWR, the log g of pre-main sequence stars with 0.8 $M_{\odot}$ can be estimated with an uncertainty of 0.1-0.2. From comparisons with an evolution model Baraffe et al. (1998), we concluded that their ages can be determined within a factor of 1.5.

Also, 5 giants, 2 main sequence stars, and 2 WTTSs with higher-$T_{\rm eff}$ (4600-4700K) were also observed to estimate the temperature dependence of the EWR. The EWRs of the high-$T_{\rm eff}$ objects were larger than those of the low $T_{\rm eff}$ in the surface gravity range of a typical pre-main sequence star. Therefore, to accurately determine the ages of PMS stars with masses larger or smaller than 0.8 $M_{\odot}$, new EWR-log g relationship for each $T_{\rm eff}$ range are required.

In order to provide a versatile age determination method using EWR, the EWR

- log g relation in other effective temperature is needed to be estimated. A high-resolution near-infrared K-band spectroscopy was carried out to create the age determination method of early-M type pre-main sequence stars. The Sc (22057.8$\mathring{A}$ and 22071.3$\mathring{A}$) and Na lines (22062.4$\mathring{A}$ and 22089.7$\mathring{A}$) were used to establish the surface gravity indicator for the pre-main sequence stars with the mass of 0.6-0.7 $M_{\odot}$. The spectra of 10 giants, 10 dwarfs and 4 PMS stars were obtained by observation with Subaru Telescope IRCS and UKIRT CGS4, and from the archive data of Kitt Peak observatory and Gemini South Phoenix. The EWRs of Sc and Na lines decrease with increasing surface gravity. It was concluded that these EWRs are fine diagnostics of the surface gravity. By obtaining the K- band spectrum of pre-main sequence stars with S/N$\sim$120, the ages of the PMS stars are able to be estimated with a factor of 1.5 on average, by comparing the estimated surface gravity with the evolution model (Baraffe et al., 1998). All of the estimated ages of the 4 pre-main sequence stars observed in K-band showed older ages compared to the ages estimated in photometric study (Bertout, Siess, & Cabrit, 2007). This discrepancy arises from the uncertainty of distance, extinction and veiling.

By using the EWR age determination method, the age of the 2 Transitional disk objects and 2 CTTSs were estimated. The age of the pre-main sequence stars in the Taurus-Auriga star-forming region estimated by both Fe/Na and Sc/Na were combined in order to derive the evolution timescale of the protoplanetary disk. The color of the $K - L$ was quoted from (Kenyon & Hartmann, 1995) as the indicator of the disk evolution stage. The $K - L$ color decreased with the increasing age, which indicate that the disks evolve with time. This relation was not found when the age estimated by the photometric study was used for the comparison. This result was able to be obtained since the EWR method is free from the uncertainties of distance, extinction, and veiling. From the derived relation, the disk lifetime in the Taurus-Auriga star-forming region is 4.0Myr.

Acknowledgments

First of all, I would like to thank the staff of the Okayama Astrophysical Observatory, the Subaru Telescope, and the Joint Astronomy Centre. Especially, I would like to appreciate Dr. Andy Adamson, for the support he gave me for the observation and the reduction of the UKIRT CGS4 data. Also, I would like to thank Dr. Akito Tajitsu for the service observations of the Subaru Telescope HIDES.

I was supported by the Grant-in-Aid from the Japan Society for the Promotion of Science (JSPS). Also, I was supported by Excellent Young Researchers Overseas Visit Program, and I had a opportunity to work with Professor Michael R. Meyer in the Eidgenössische Technische Hochschule Zürich (ETH), Switzerland. Everything I experienced during the stay at ETH is a valuable asset. I thank Michael and all other people in the Institute of Astronomy, ETH.

I am grateful for the fruitful discussions with emeritus Professor Tadashi Mukai, associate Professor Akiko M. Nakamura. I thank associate Professor Yumiko Oasa and assistant Professor Hideko Nomura for the many advices which moved my research forward successfully. I also thank all of the members of the Laboratory of Solar System Science.

I deeply appreciate all the advice and encouragement which associate Professor Yoichi Itoh gave me during the 6 year research life. I really feel blessed that I had a chance to work on astronomy with him.

Finally, I would like to thank my parents.

References

Baraffe, I., Chabrier, G., Allard, F., & Hauschildt, P. H. 1998, ApJ, 337, 403

Balona, L. A., & Laney, C. D. 1996, MNRAS, 281, 1341

Barkhatova, K. A., Zakharova, P. E., Shashkina, L. P., & Orekhova, L. K. 1985, Soviet Astron., 62, 854

Basri, G. & Batalha, C. 1990, ApJ, 363, 654

Beckwith, S. V. W., Sargent, A. I., Chini, R. S., & Güsten, R. 1990, AJ, 99, 924

Bertout, C. & Genova, F. 2007, A&A, 460, 499

Bertout, C., Siess, L. & Cabrit, S. 2007, A&A, 473, L21

Cieza, L. A., Kessler-Silacci, J. E., Jaffe, D. T., Harvey, P. M., & Evans, II, N. J. 2005, ApJ, 635, 422

Cohen, J. G., Frogel, J. A., Persson, S. E. & Elias, J. H. 1982, ApJ, 249, 481

D'Antona, F. & Mazzitelli, I. 1994, ApJS, 90, 467

Drake, J. J. & Smith, G. 1991, MNRAS, 250, 89

Drilling, J. S. & Landolt, A. U. 2000, in Allen's Astrophysical Quantities, ed. A. N. Cox (New York: Springer-Verlag), 389

Espaillat et al. 2007 ApJ, 670, L135

Fletcher, A. B., & Stahler, S. W. 1994, ApJ, 435, 312

Fukagawa, M. et al. 2004, ApJ, 605, 53

Furlan, E. et al. 2006, ApJS, 165, 568

Goldreich, P. & Tremaine, S. 1980, ApJ, 241, 425

Gray, D. F. 1992, in *The observation and analysis of stellar photospheres*, Ed. J. Wiley & Sons, Canmbridge University Press

Greene, T. P., & Lada, C. J. 1997, AJ, 114, 215

Haisch, K. E., Jr., Lada, E. A., & Lada, C. J. 2000, AJ, 120, 1396

Haisch, K. E., Jr., Lada, E. A., & Lada, C. J. 2001, AJ, 121, 2065

Haisch, K. E., Jr., Lada, E. A., & Lada, C. J. 2001, ApJ, 553, L153

Hanawa, T. et al. 2008, in Modern Astronomy Series, Vol. 6, Part II, Chapter 10, ed. Fukui, Y. et al. (Nippon Hyoronsha CO., LTD.)

Hartmann, L., et al. 2005, ApJ, 629, 881

Hayashi, C. 1961, PASJ, 13, 450

Hearty, T. 2000, A&A, 357, 681

Hioki, T. et al. 2007, AJ, 134, 880

Ida, S. 2003, in 異形の惑星, NHK Books

Itoh, Y. et al. 2002, PASJ, 54, 963

Joy, A. H. 1945, ApJ, 102, 168

Joy, A. H. 1949, ApJ, 110, 424

Kalas, P. et al. 2008, Sci, 322, 1345

Kenyon, S. J. & Hartmann, L. 1995, ApJS, 101, 117

Kokubo, E., & Ida, S. 1996, Icar, 123, 180

Kurucz, R. L. 1993, Kurucz CD-ROM, No.13 (Cambridge: Smithsonian Astrophysical Observatory)

Lada, C. J 1987, IAUS, 115, 1

Lang, K. R. Astrophysical Data: Planets and Stars (New York: Springer-Verlag), ch. 9

Lejeune, T. & Schaerer, D. 2001, A&A, 366, 538

Lin, D. N. C., & Papaloizou, J. C. B. 1993, in Protostars and Planets III, University of Arizona Press, 749

Lin, D. N. C., Bodenheimer, P., & Richardson, D. C. 1996, Nature, 380, 606

Luhman, K. L. 2001, ApJ, 560, 287

Mamajek, E. E. 2009, AIPC, 1158, 3

Marois, C. et al. 2008, Sci, 322, 1348

Masunaga, H., Miyama, S. M., & Inutsuka, S. 1998, ApJ, 495, 369

Meyer, M. R. 1996, Ph.D. thesis, Univ. Massachusetts

Meyer, M. R., Edwards, S., Hinkle, K. H., & Strom, S. E. 1998, ApJ, 508, 397

Mendoza V., E. E. 1966, ApJ, 143, 1010

Myers, P. C. et al. 1987, ApJ, 319, 340

Najita, J. R., Strom, S. E., & Muzerolle, J. 2007, MNRAS, 378, 369

Palla, F., & Stahler, S. W. 2000, ApJ, 540, 255

Palla, F., & Stahler, S. W. 2002, ApJ, 581, 1194

Perryman, M. A. C., et al. 1997, A&A, 323, L49

Rydgren, A. E., Strom, S. E., & Strom, K. H. 1976, ApJS, 30, 307

Shu, F. H., Adams, F. C., & Lizano, S. 1987, ARA&A, 25, 23

Siess, L., Dufour, E., & Forestini, M. 2000, A&A, 358, 593

Strom, K. M., Strom, S. E., Edwards, S., Cabrit, S. & Skrutskie, M. F. 1989, AJ, 97, 1451

Thalmann, C. et al. 2010, ApJ, 718, L87

Takeda, Y. 1995, PASJ, 47, 287

Unsöld, A. 1968, Modern Astronomy, Iwanami Shoten

Wallace, L., & Hinkle, K. ApJS, 107, 312

Wichmann, R., Bastian, U., Krautter, J., Jankovics, I., & Ruciński, S. M. 1998, MNRAS, 301, L39

Weaver, W. B., & Jones, G. 1992, ApJS, 78, 239

Figures

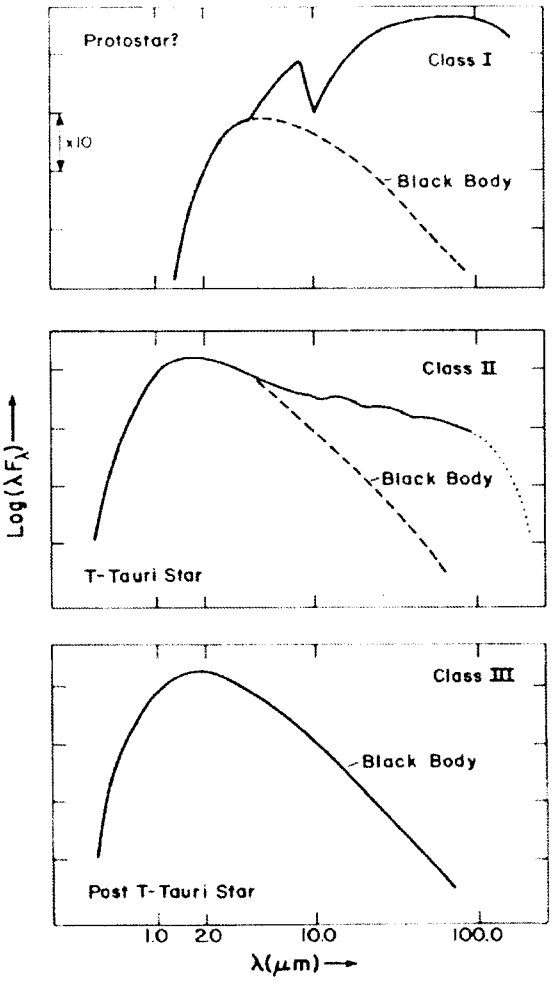

Figure 1: The SED of the pre-main sequence stars (Lada 1987). The top, middle, and the bottom panels show the standard SED of Class I, Class II, and Class III, respectively. The solid lines are the observed flux, and the dashed lines indicate the black body. The excess is large in the Class I star, due to the optically thick disk and envelope. It will decrease with the evolution, because of the accretion and the scattering of the circumstellar material.

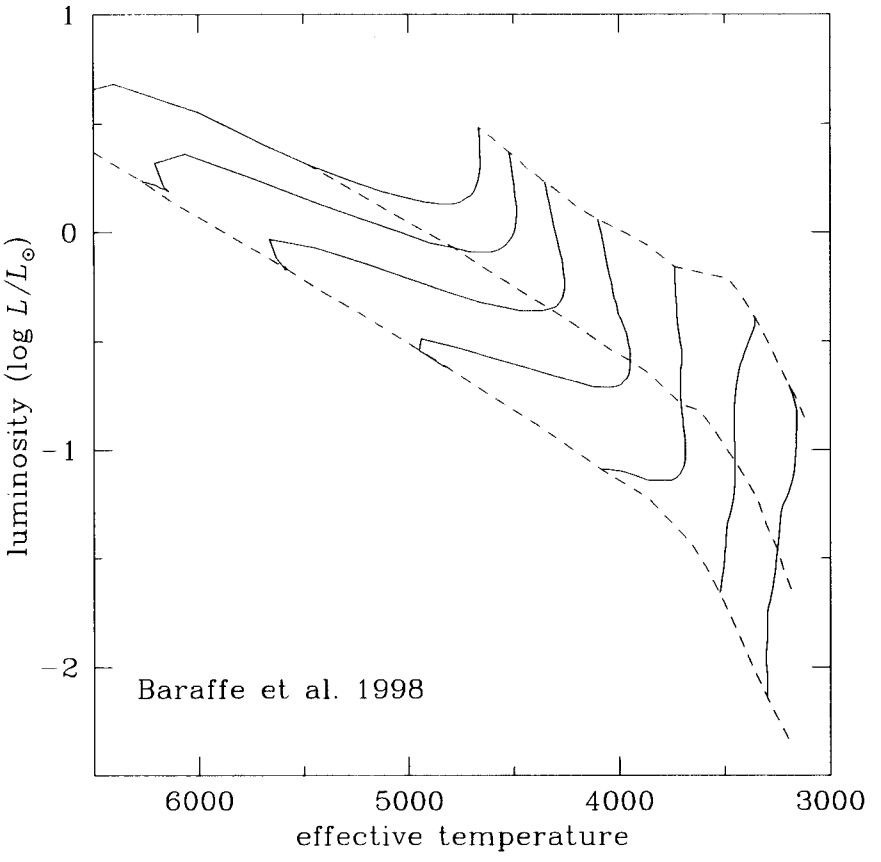

Figure 2: The H-R diagram with the evolution tracks of the pre-main sequence stars (Baraffe et al., 1998). The solid lines indicate the evolution tracks of the stars with the mass of 0.2, 0.4, 0.6, 0.8, 1.0, 1.2, and 1.4 $M_\odot$ from right. The dashed lines denote the isochrones from 1 Myr to 100Myr, from top.

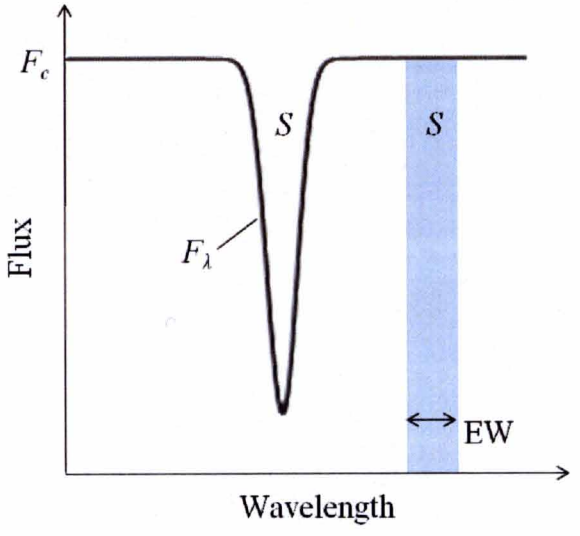

Figure 3: The definition of equivalent width. It is defined as a width of the rectangle, with height and area equal to the continuum level and the area of the spectral feature.

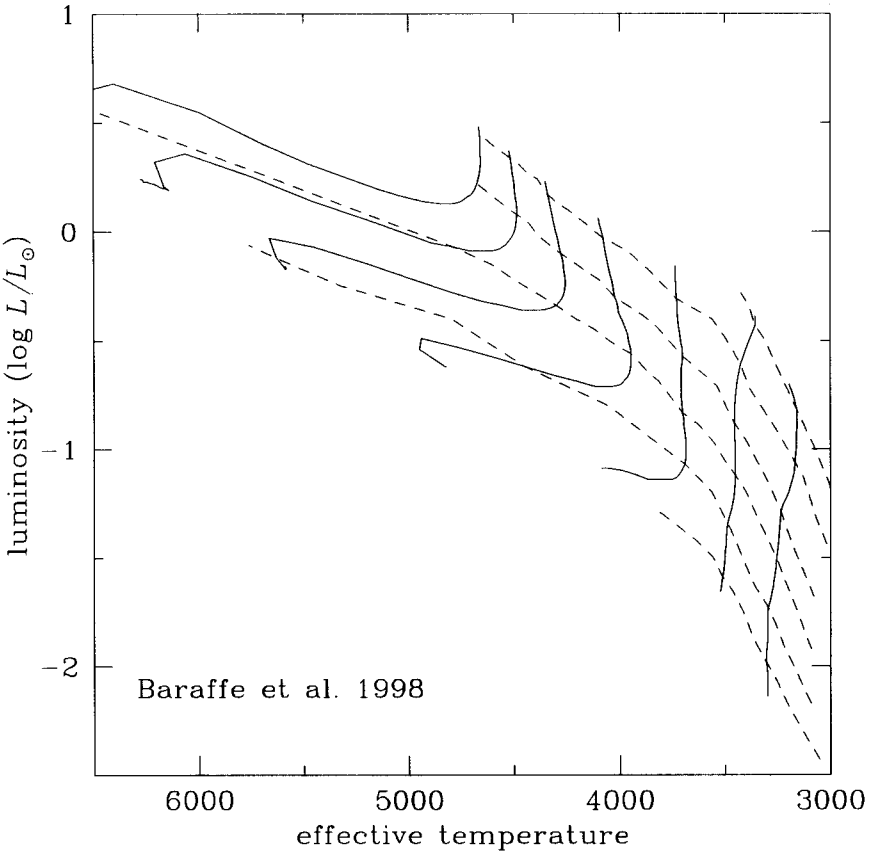

Figure 4: The Heltzsprung-Russel (H-R) diagram with the evolutional track and the constant-surface gravity lines. The solid lines and the dashed lines indicate the evolutional tracks of the stars with the mass of 0.2, 0.4, 0.6, 0.8, 1.0, 1.2, and 1.4 $M_\odot$ from right, and the constant-surface gravity lines with the log g of 3.5, 3.75, 4.0, 4.25, 4.5, and 4.75 from the top, respectively. The surface gravity increases as the pre-main sequence star evolves. These lines are quoted from Baraffe et al. (1998).

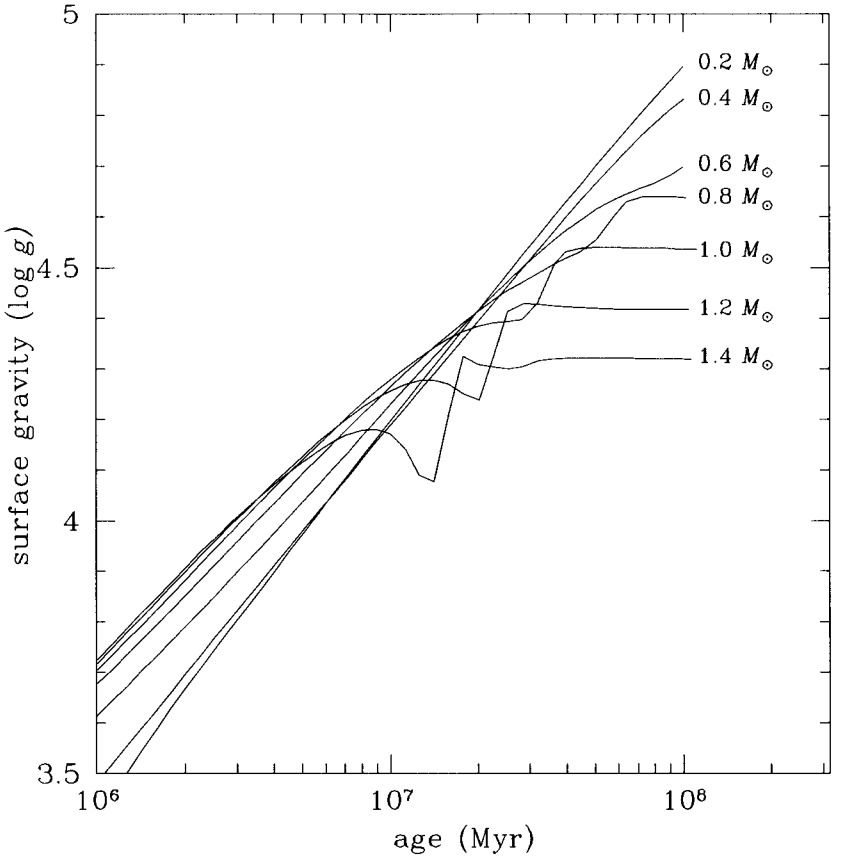

Figure 5: The relation between the age and the surface gravity of pre-main sequence stars Baraffe et al. (1998). The surface gravity increases with the increasing age.

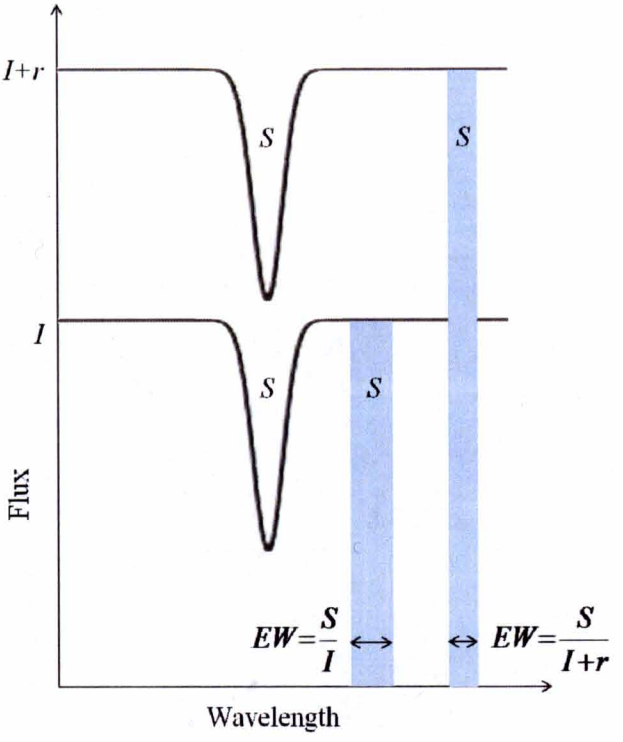

Figure 6: The relation between equivalent width and veiling. When the veiling (r) is added to the stellar continuum (I), the equivalent width (EW) will be underestimated since it will be normalized with $I + r$, where the actual EW is S/I. The veiling "fills up" the absorption lines.

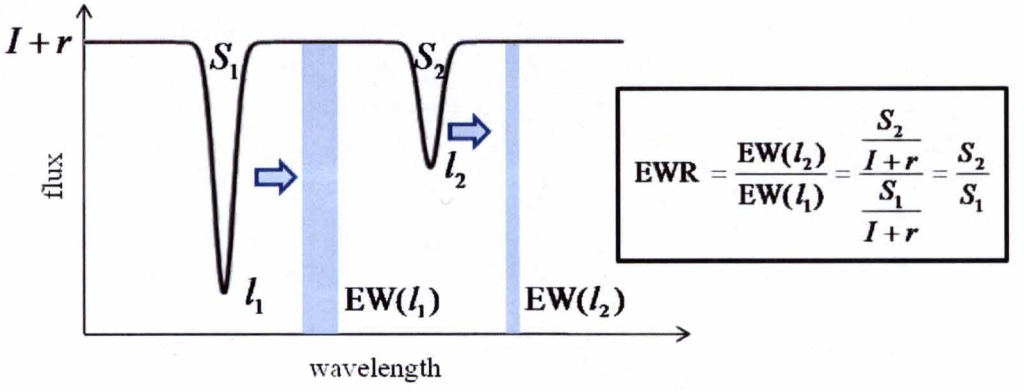

Figure 7: The concept of the equivalent width ratio. By calculating the equivalent width ratio of nearby absorption features, the effect of veiling is able to be eliminated.

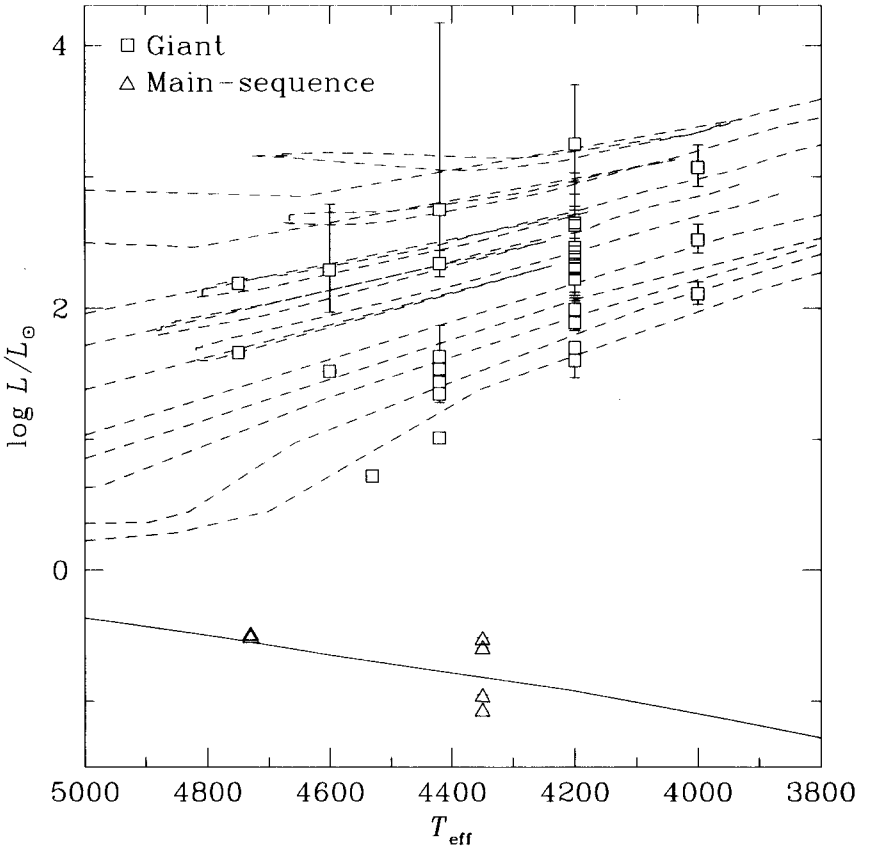

Figure 8: The H-R diagram with the targets. The dashed lines are the evolutionary tracks from Lejeune & Schaerar (2001); M = 0.90, 1.00, 1.25, 1.50, 1.70, 2.00, 2.50, 3.00, 4.00, and 5.00 $M_\odot$ from the bottom. The mass of a giant star was estimated by comparing its locus and the tracks. The solid line indicates the isochrone for 10^9yr (Baraffe et al. 1998).

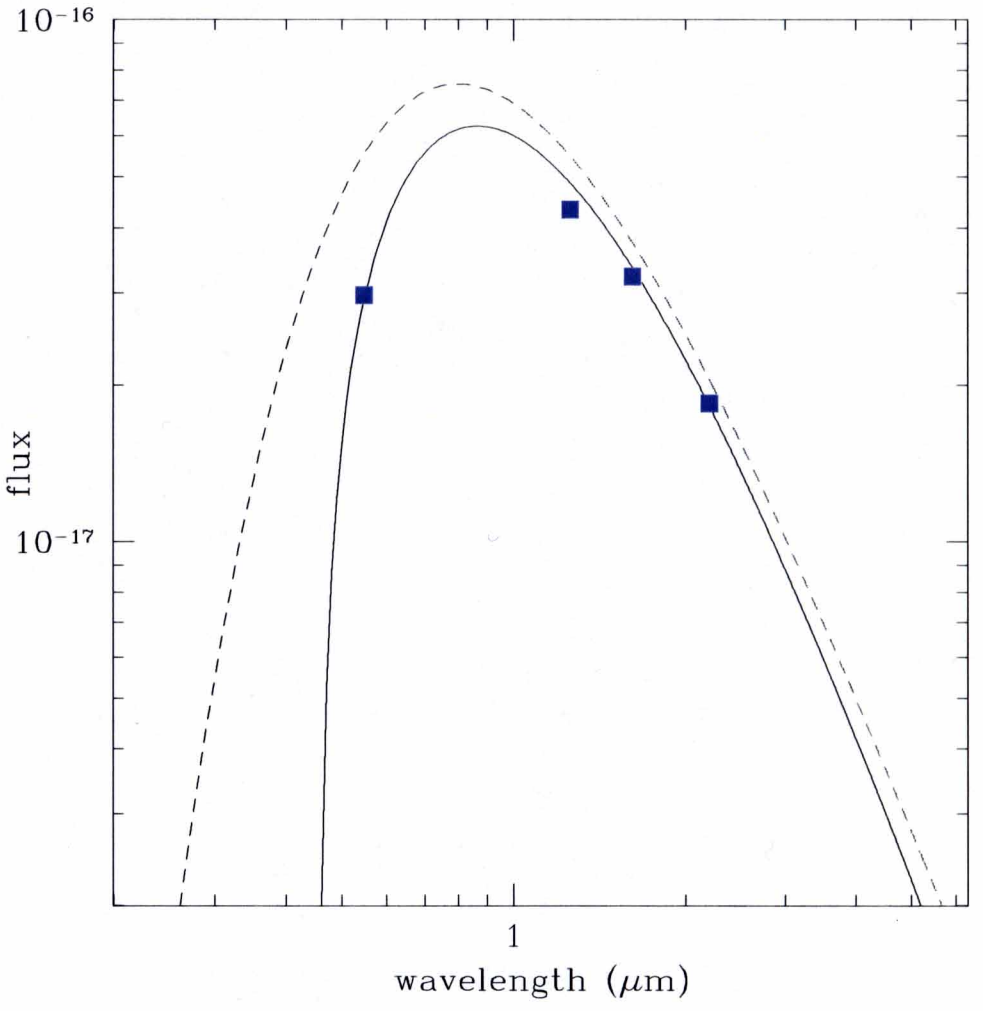

Figure 9: The SED fitting of the RX J0452.5+1730. The dashed line shows the black body with the effective temperature of 4590K. The square plots are the flux of the RX J0452.5+1730 observed by a photometric study. The solid line was derived by subtracting the extinction from the black body until it agrees with the square plots.

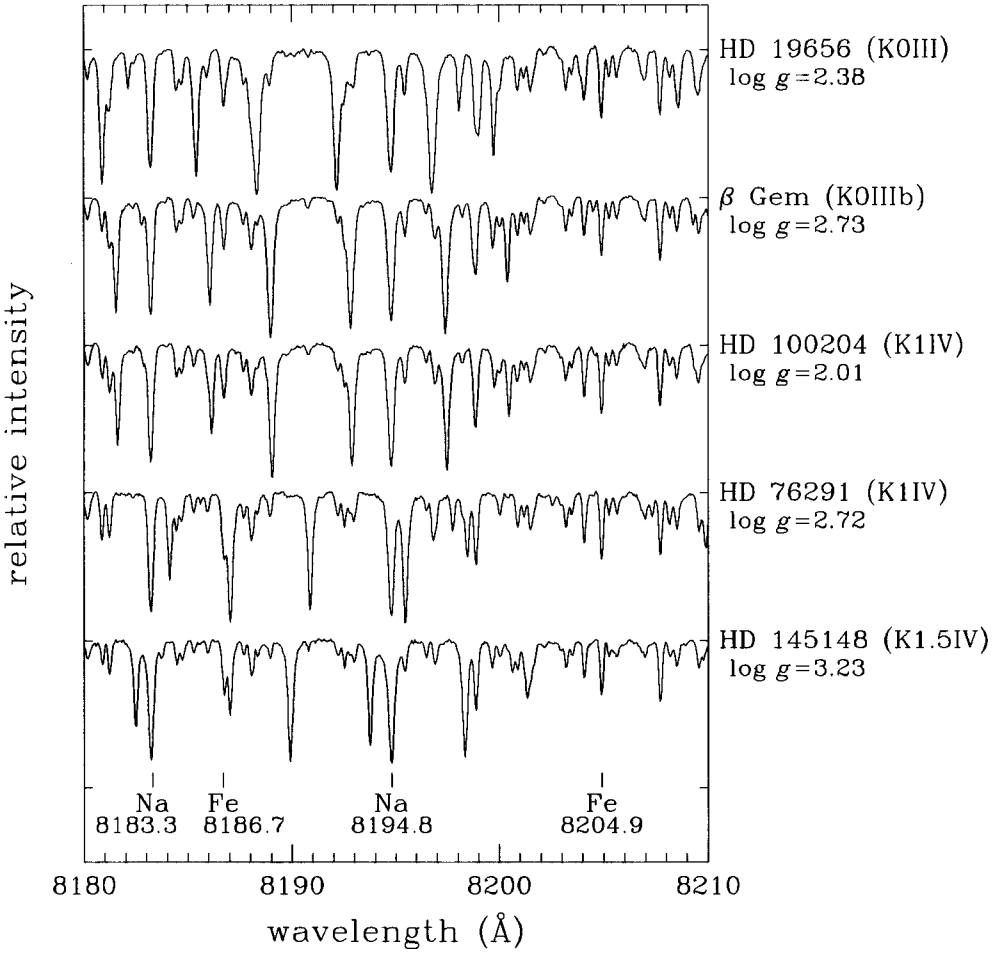

Figure 10: I-band spectra of the giants with effective temperature around 4600-4700K. Doppler shift in each object is corrected. Most of the lines not identified are the telluric lines.

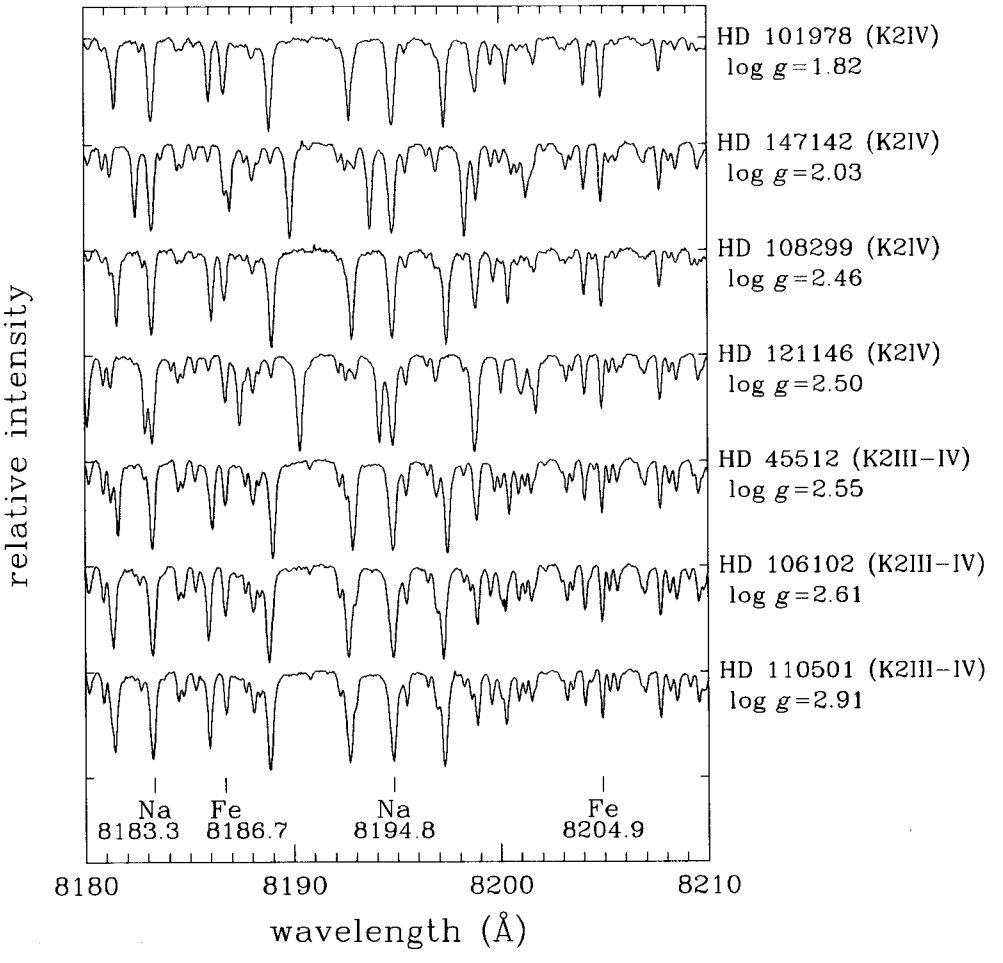

Figure 11: I-band spectra of the giants with the effective temperature around 4200-4300K. Doppler shift in each object is corrected. Most of the lines not identified are the telluric lines.

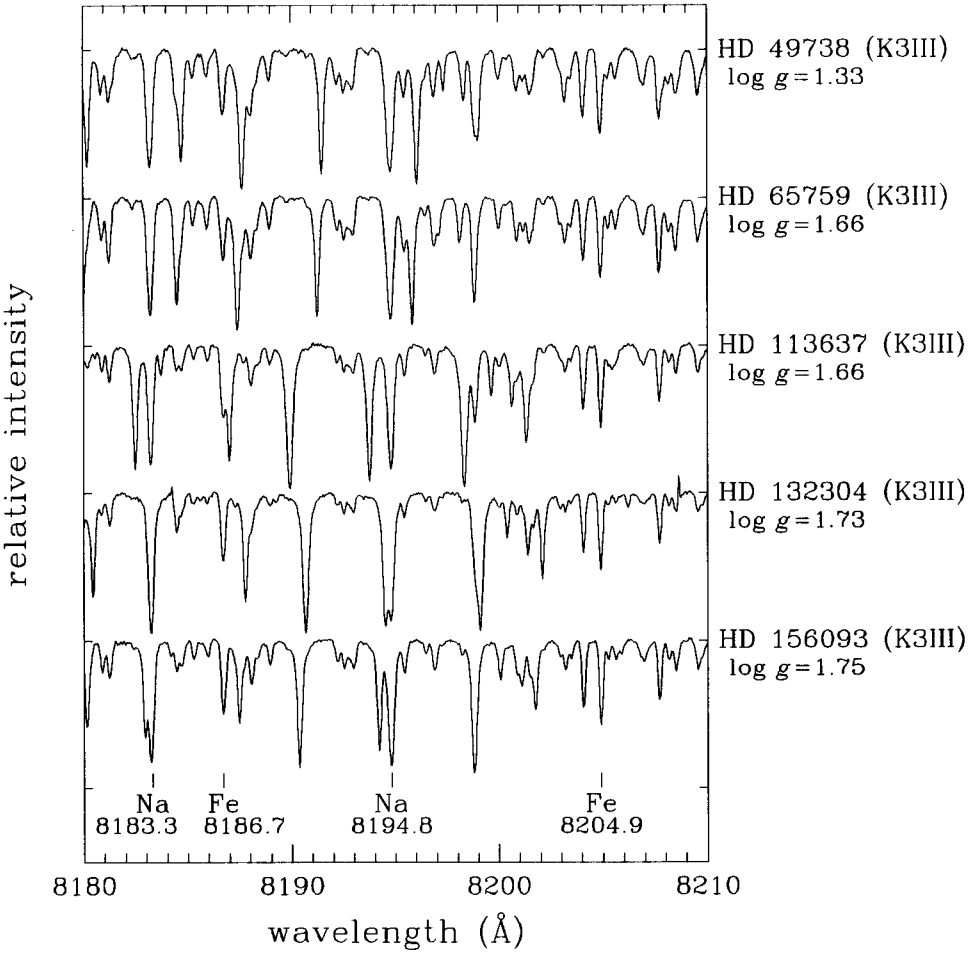

Figure 11: *Continued.*

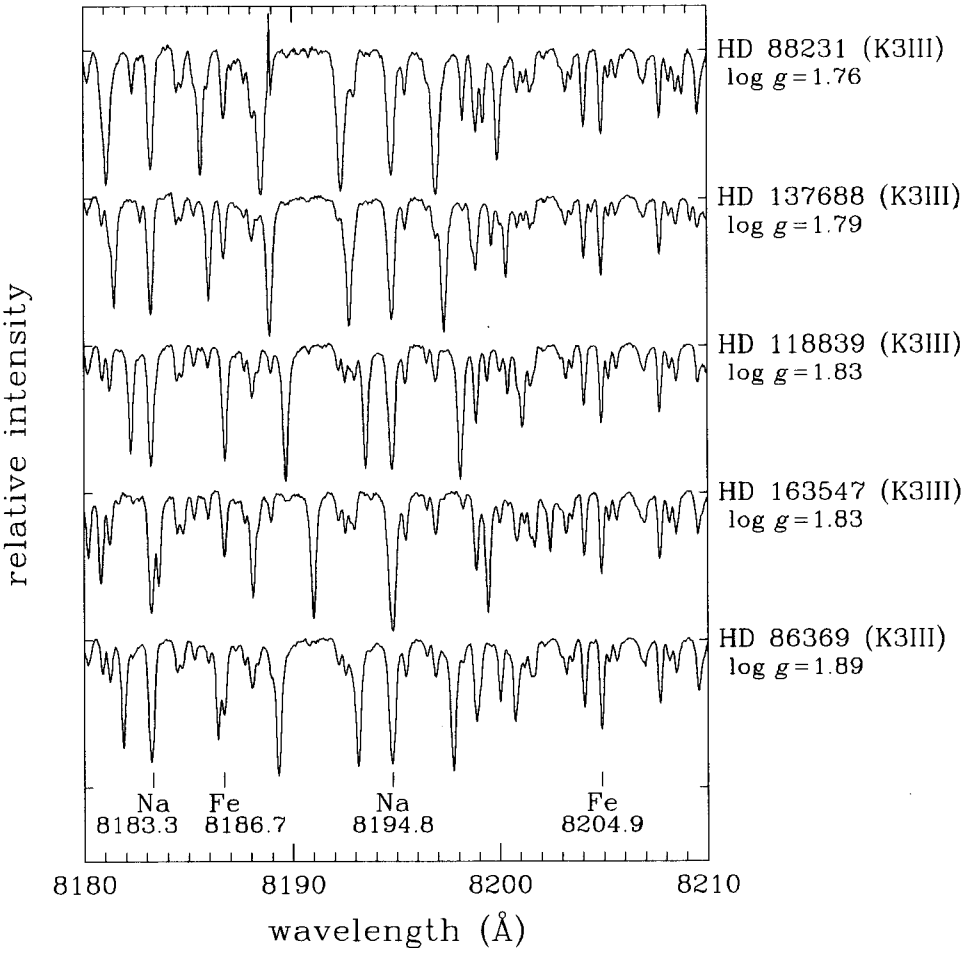

Figure 11: *Continued.*

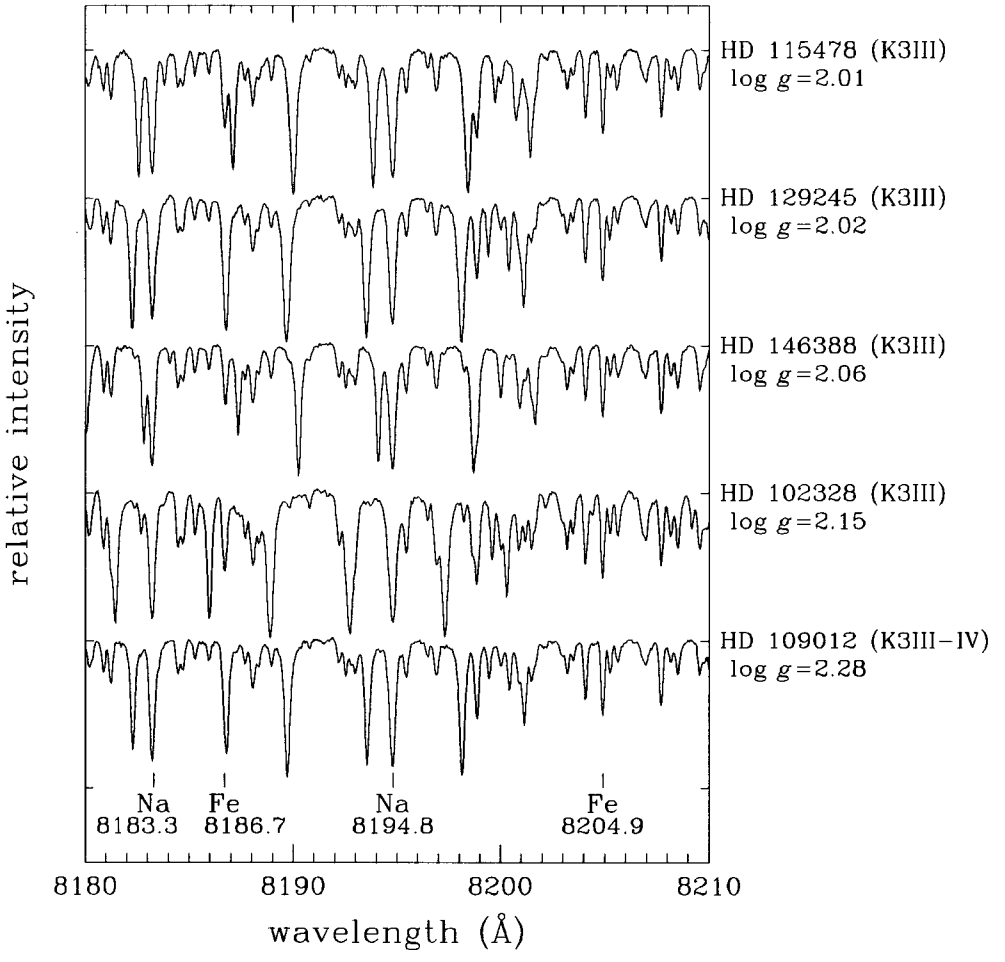

Figure 11: *Continued.*

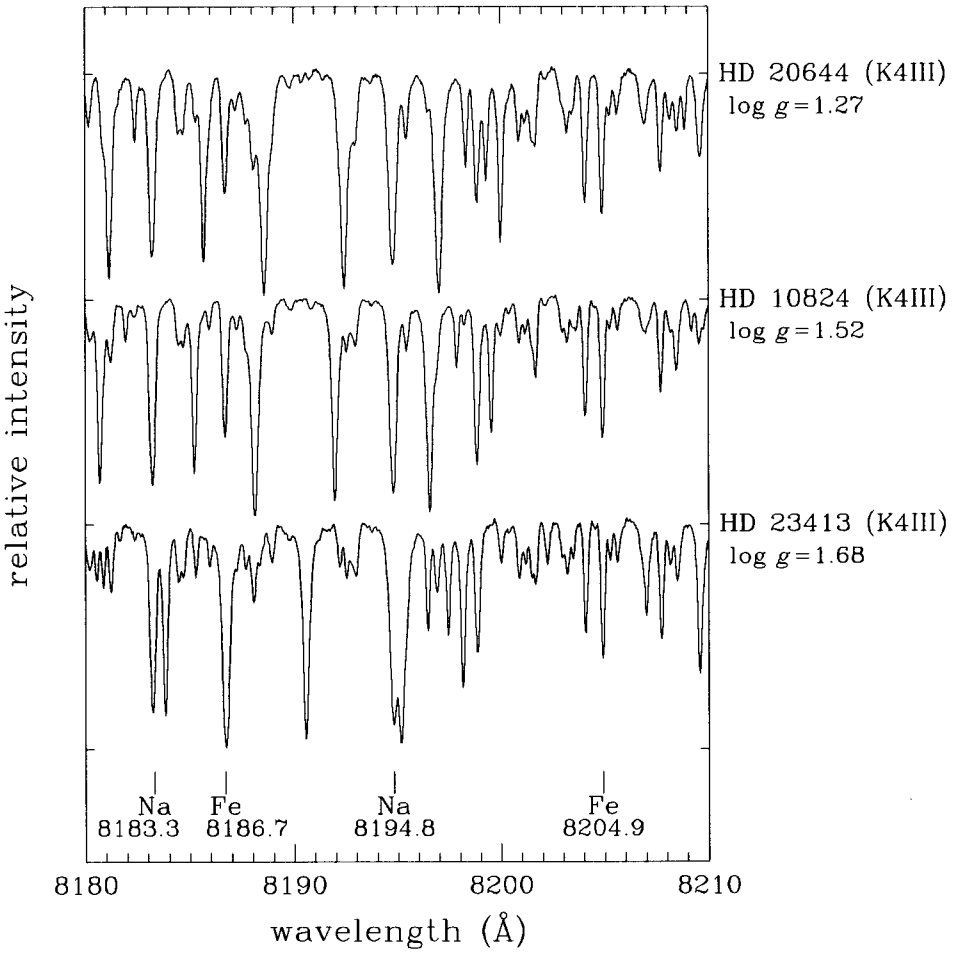

Figure 11: *Continued.*

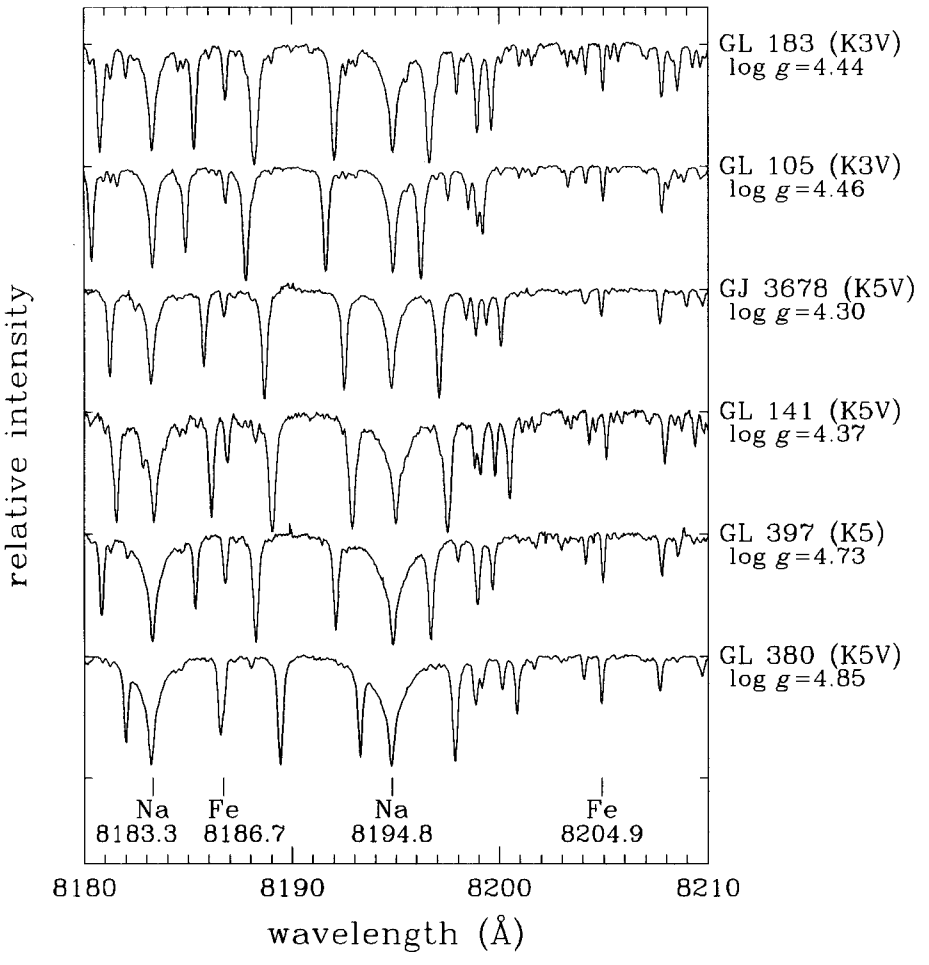

Figure 12: I-band spectra of the main-sequence stars. Doppler shift in each object is corrected. Most of the lines not identified are the telluric lines.

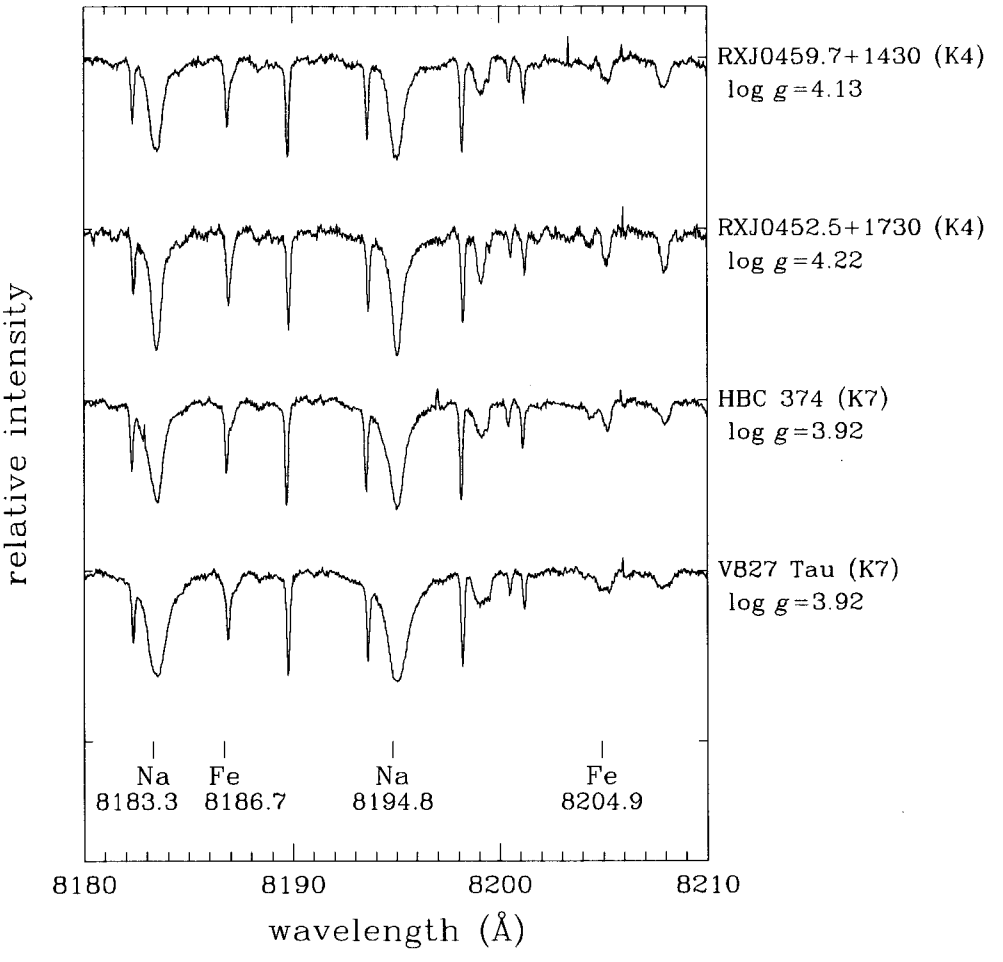

Figure 13: I-band spectra of the WTTSs. Doppler shift in each object is corrected. Most of the lines not identified are the telluric lines.

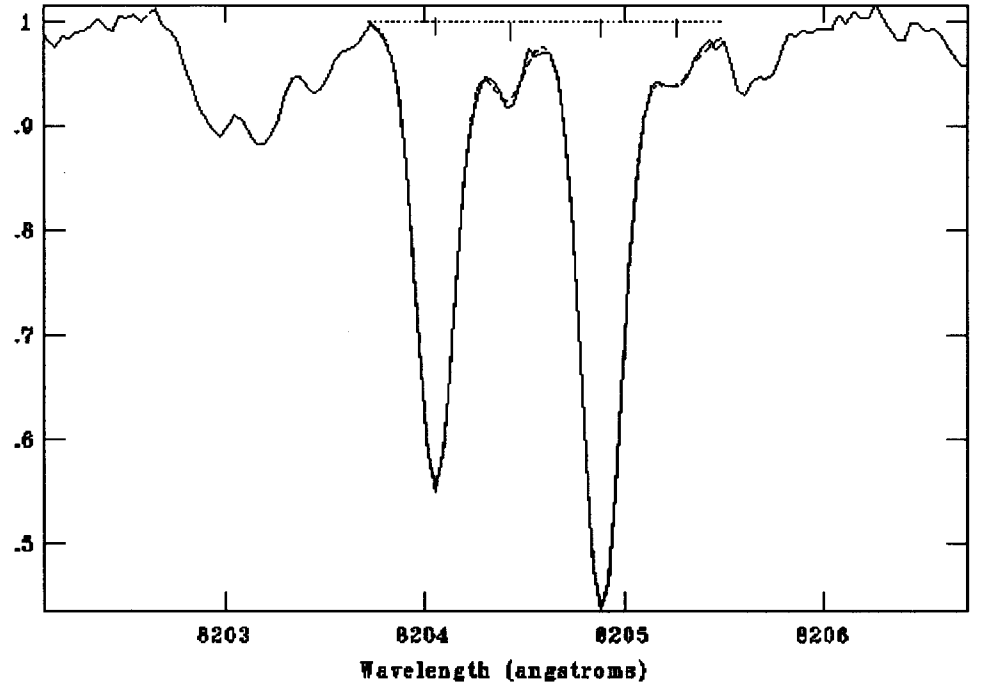

Figure 14: The spectral fitting of the Fe(8204.9$\AA$) of the giant HD 101978. The line in 8204.1$\AA$ is also a Fe absorption. The solid line shows the observed spectra. The horizontal dashed line is the continuum level adopted for the fitting. The fitting result of the 4 absorption features is indicated as a dashed line along the spectra.

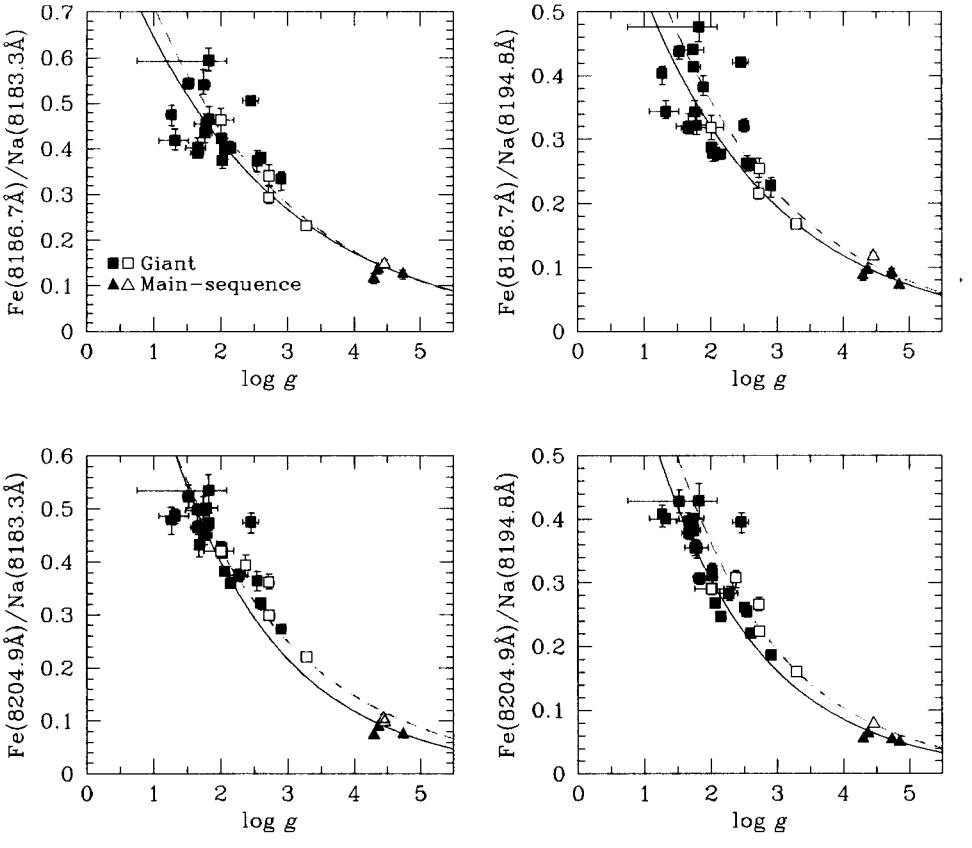

Figure 15: EWR versus log g (g: cm/s^2). The squares mark the EWRs for the giants. The triangles mark the EWRs for main-sequence stars. The filled plots denote the EWRs of objects with $T_{\rm eff}$ around 4200-4300K, and the open plots are for 4600-4700K objects. The solid lines are the fitted curve for the 4200-4300K objects. The lines for the 4600-4700K objects are shown as dashed. Each EWR decreases with the increasing log g, indicating that they are a fine diagnostic of surface gravity.

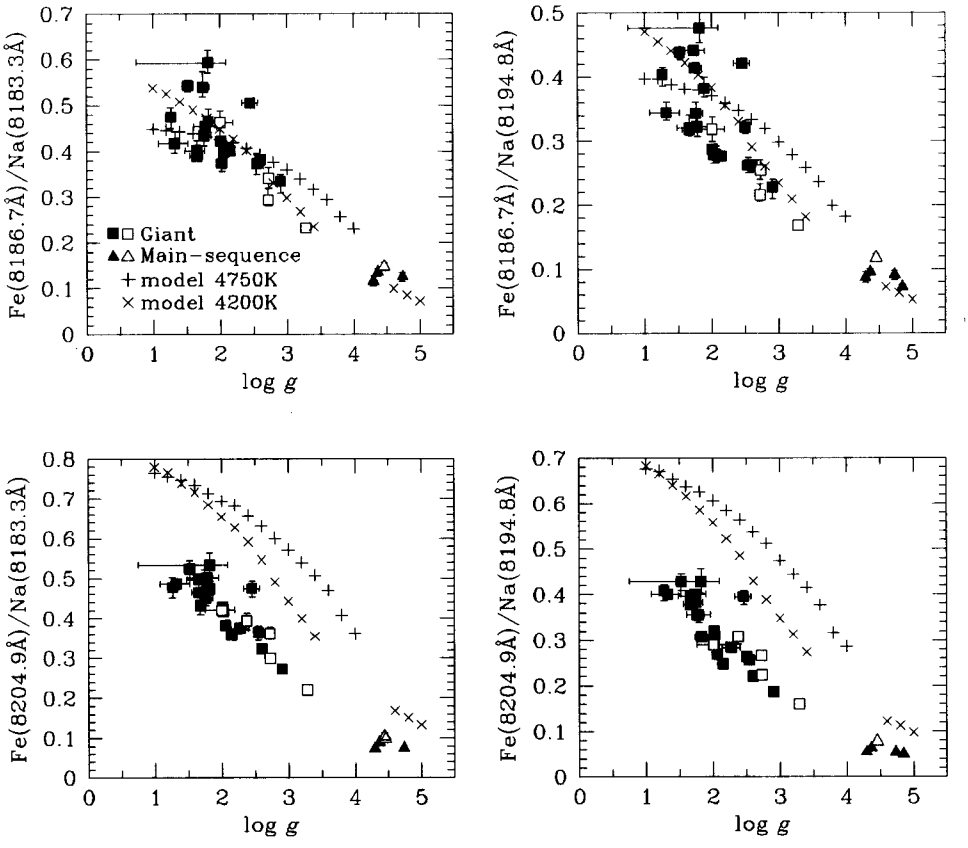

Figure 16: EWR versus log g (g: cm/s^2) with the EWR of the model spectra created by SPTOOL. The squares indicate the EWR of the giants, and the triangles represent the main-sequence stars. The filled plots denote the EWRs of the 4200-4300K objects, and the open plots are for 4600-4700K objects. The plus and cross signs are the EWR from model spectra of $T_{\rm eff}$ = 4750K and $T_{\rm eff}$ = 4250K, respectively. The result from the observation and from the model agree in the EWR using Fe (8186.7$\AA$). On the other hand, in the EWR using the Fe (8204.9$\AA$), the model EWR is larger then that of the observaion. The excitation potential of the Fe (8204.9$\AA$) in the model may be underestimated.

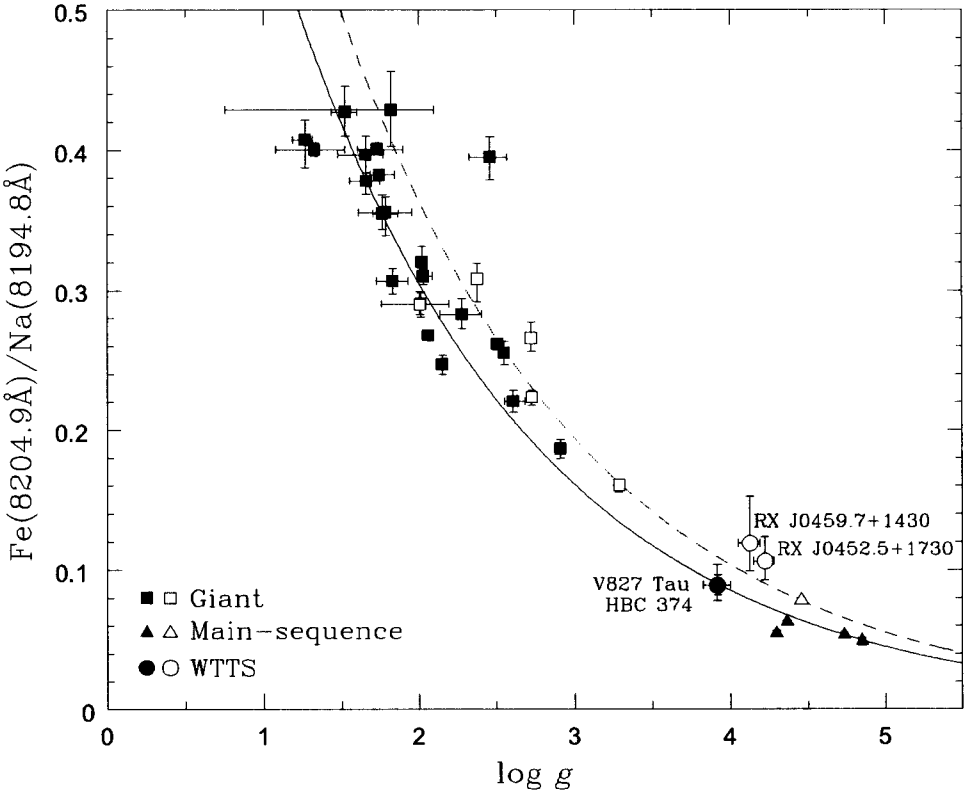

Figure 17: EWR (Fe (8204.9Å) / Na (8194.8Å)) versus log g (g: cm/s^2) for the EWR of WTTSs. The squares, triangles, and the fitted curves are from figure 15. The open and filled circles indicate the EWRs of WTTS of which $T_{\rm eff}$ = 4590K and $T_{\rm eff}$ = 4060K, respectively. The EWRs of the WTTSs match the fit curve, which indicate that the derived EWR-log g relation can be adapted for the surface gravity estimation of pre-main sequence stars.

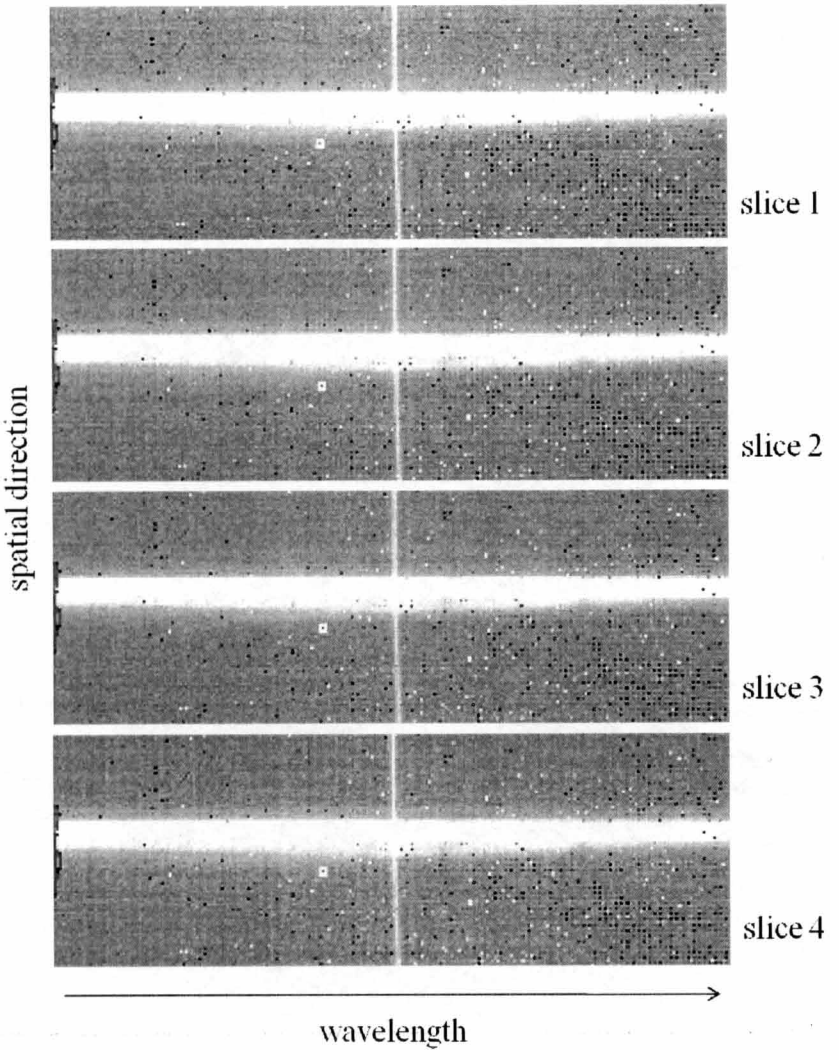

Figure 18: The raw images of the spectra of GJ 14 obtained with a single exposure. The positive part in every image shows the spectrum of GJ 14 in K-band. The single integration creates 4 images, slice 1 to 4. The OH sky emission placed near the center of the images show that each images are shifted toward the shorter wavelength.

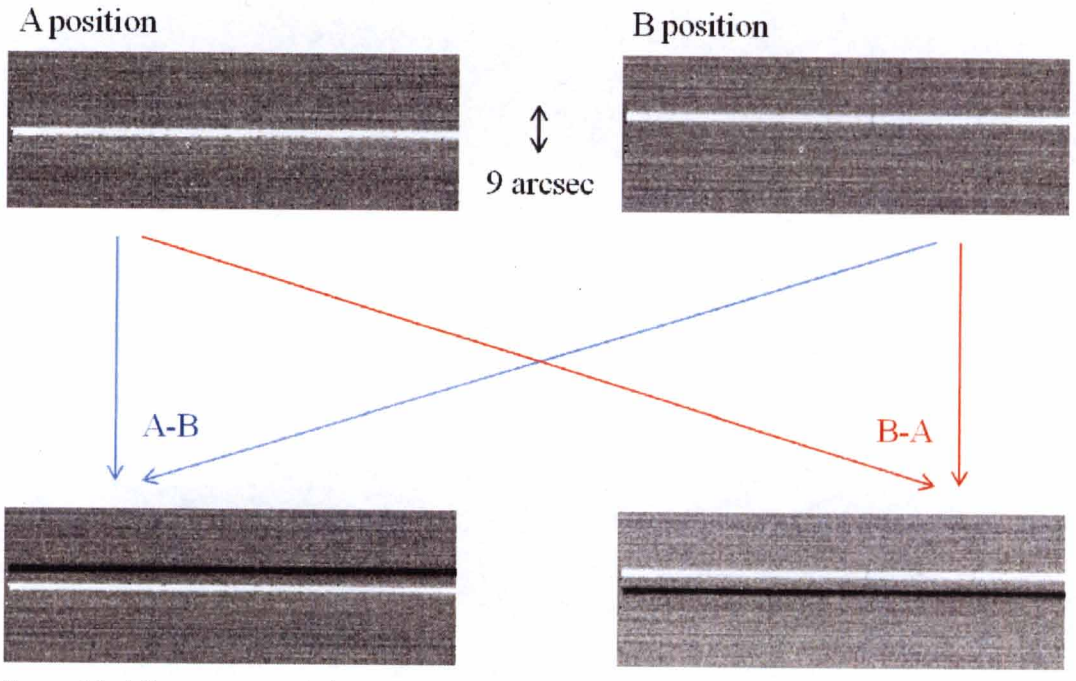

Figure 19: The conceptual diagram of the ABBA integration method. The positive part in each image is the spectrum of HIP 1809. The spectrum in B position is shifted upward, due to the telescope nodding. By subtracting each other frame, the sky and the dark are removed simultaneously. The spectrum of the subtracted frame appears as a negative part in the produced frame.

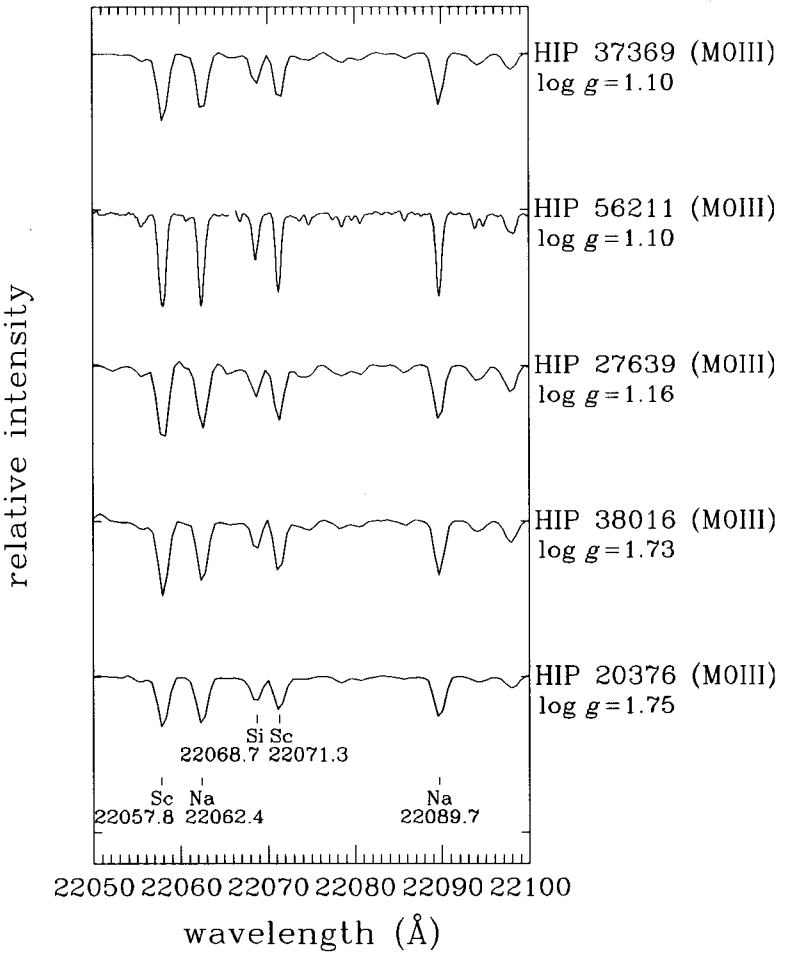

Figure 20: K-band spectra of the giants. Doppler shift in each object is corrected.

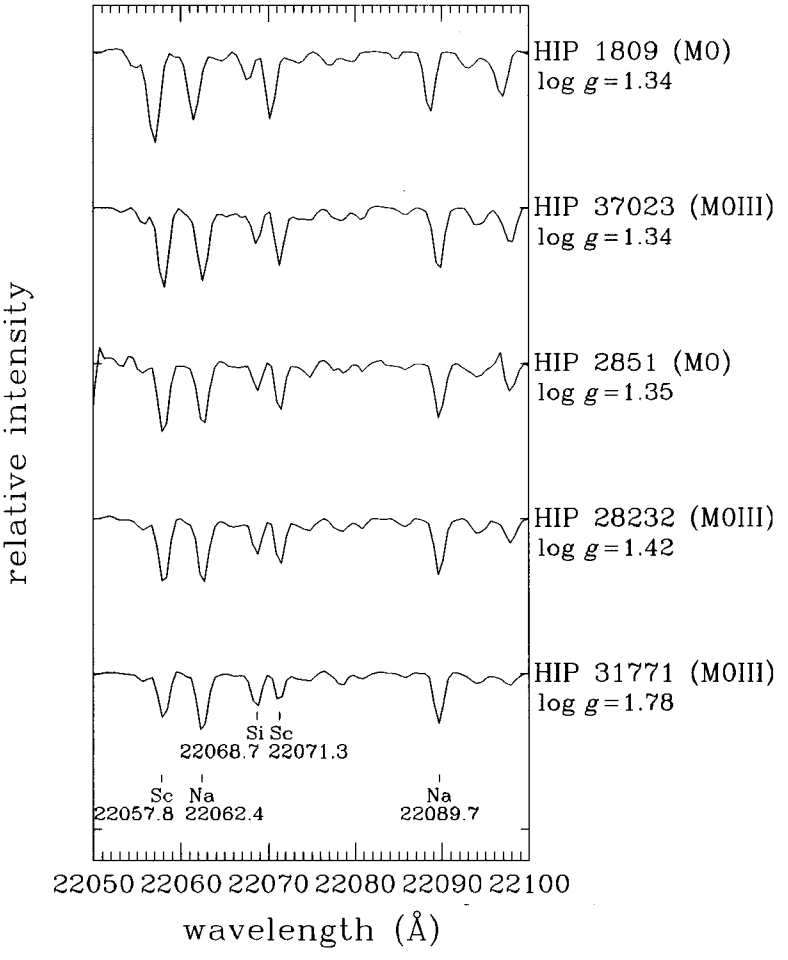

Figure 20: *Continued.*

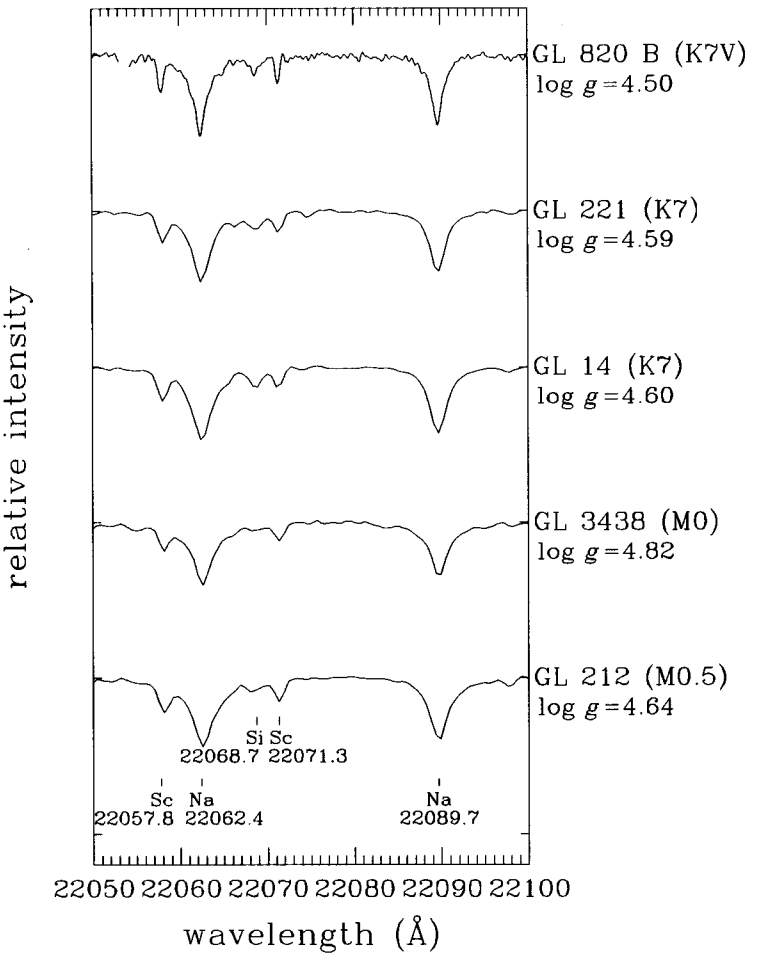

Figure 21: K-band spectra of the main-sequence stars. Doppler shift in each object is corrected.

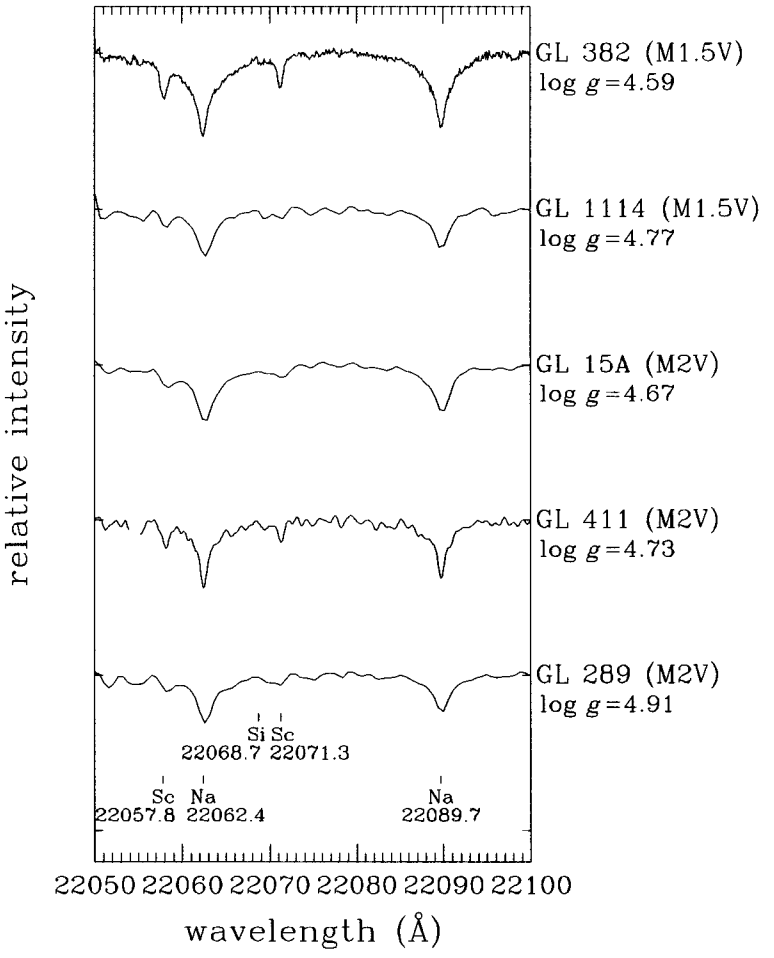

Figure 21: *Continued.*

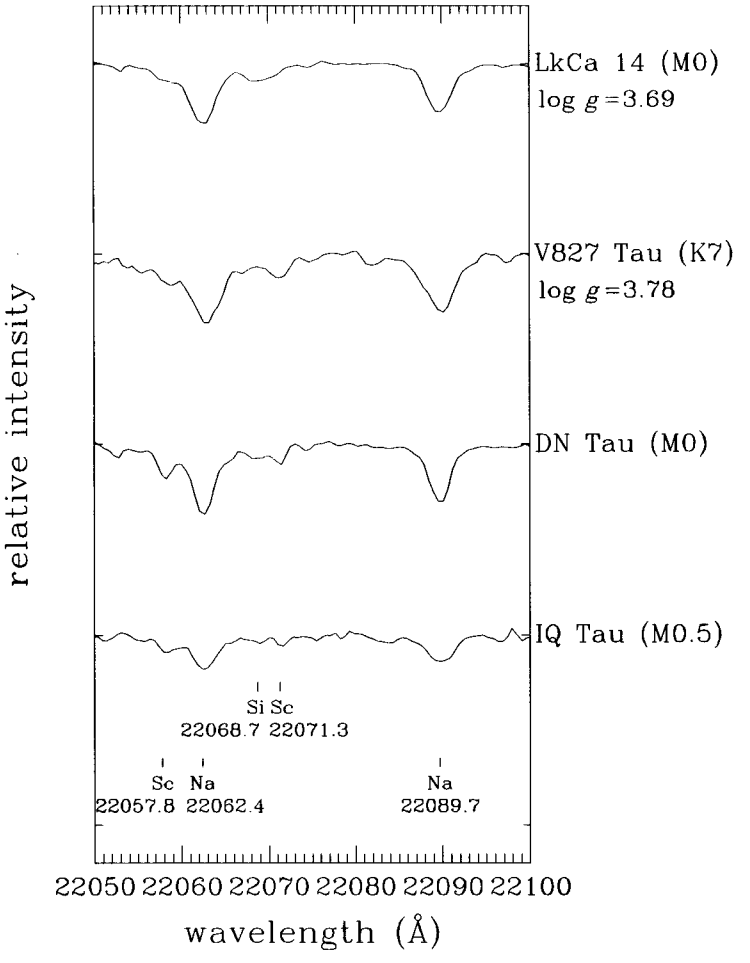

Figure 22: K-band spectra of the pre-main sequence stars. Doppler shift in each object is corrected.

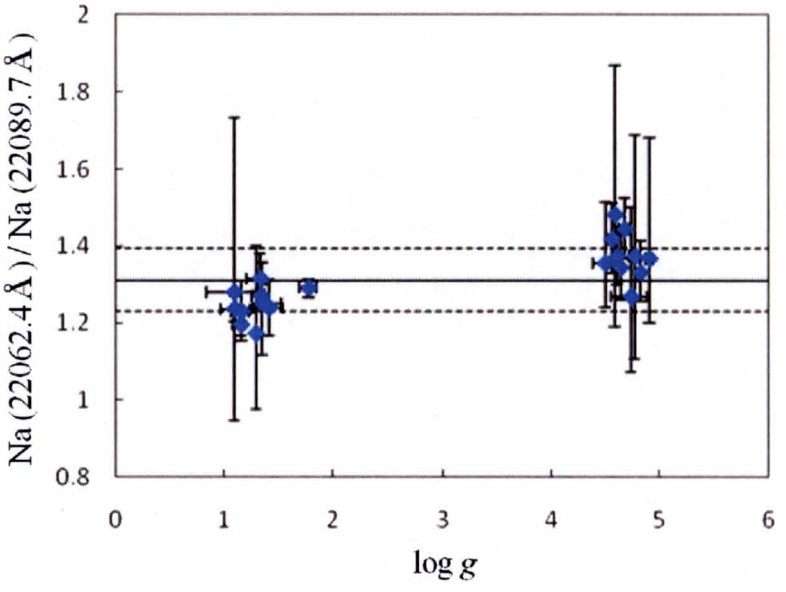

Figure 23: The equivalent width ratio of Na (22062.4Å) and Na (22089.7Å) from the giants and main sequence stars. The blue circles indicate the equivalent width ratios. The solid line shows the average of the Na/Na value, and the dashed lines indicate the 1 sigma of the average. The Na/Na is nearly constant with the surface gravity, where the amount is 1.31.

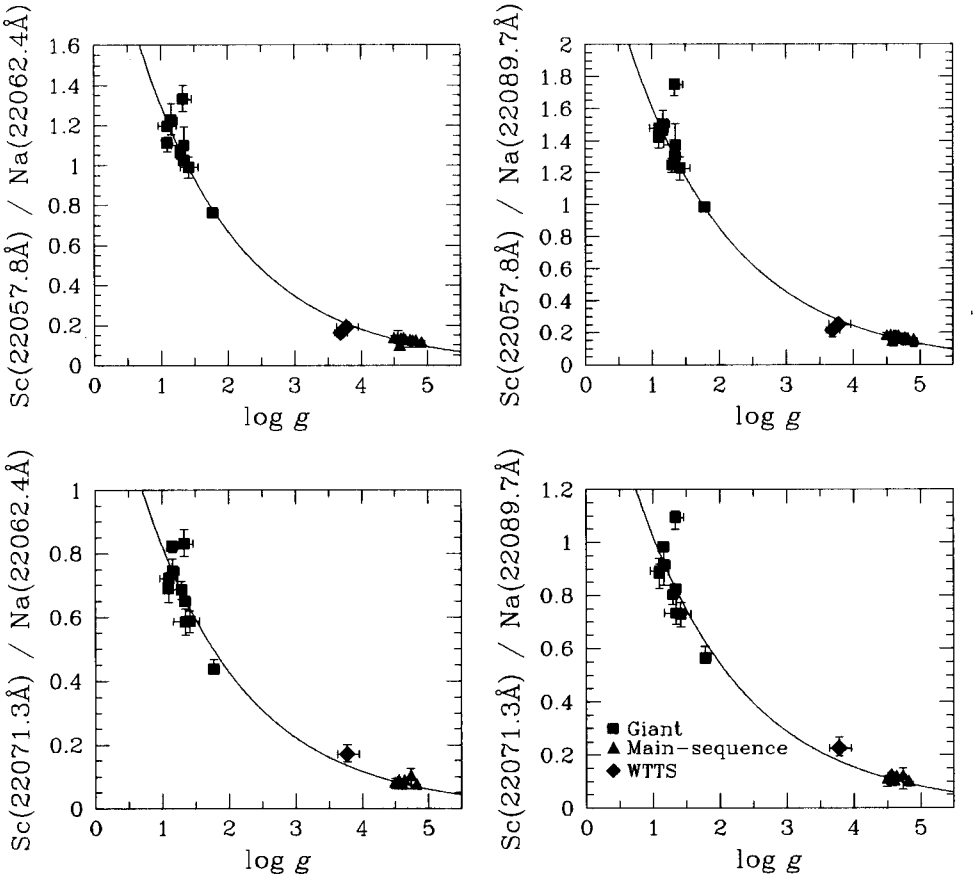

Figure 24: EWR versus log g (g: cm/s^2). The squares, triangles, and the diamonds mark the EWRs for the giants, main-sequence stars, and the WTTSs, respectively. The solid curves are the fit curve created with the plots of giants and main-sequence stars. The EWRs decreases with the increasing surface gravity, indicating that these EWRs are an excellent diagnostic of surface gravity. The EWR of the WTTSs agree the fit curve derived from the giants and main-sequence stars, which denote that the fit curve are suitable for the surface gravity estimation of pre-main sequence stars.

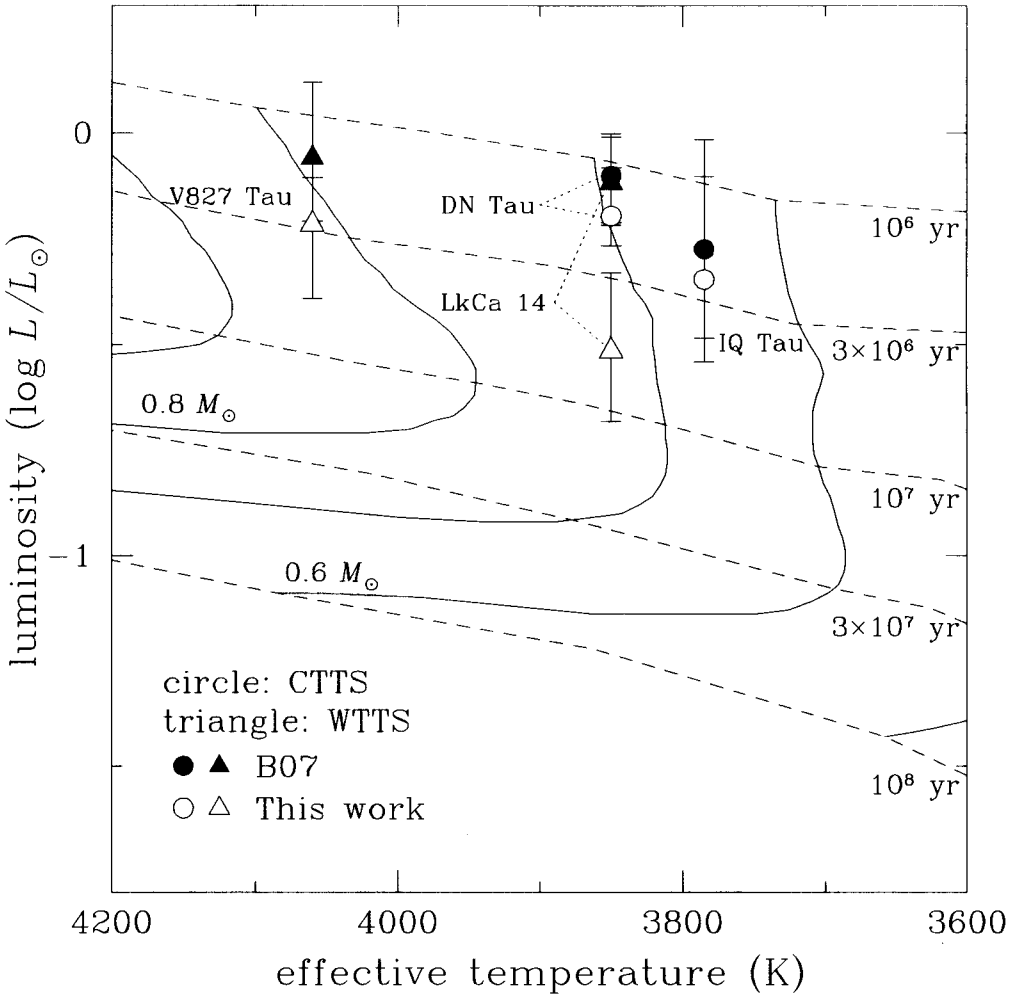

Figure 25: The H-R Diagram with the plots of the 4 PMS stars observed in section 4. The results of this study (open plots) are compared with the result of Bertout, Siess, & Cabrit (2007) (filled plots). The evolutional tracks (solid lines) and the isochrones (dashed lines) are quoted from Baraffe et al. (1998). All of the ages are estimated larger in this study. This difference arises since the age estimated in Bertout, Siess, & Cabrit (2007) is contaminated with the uncertainties of distance, extinction, and veiling.

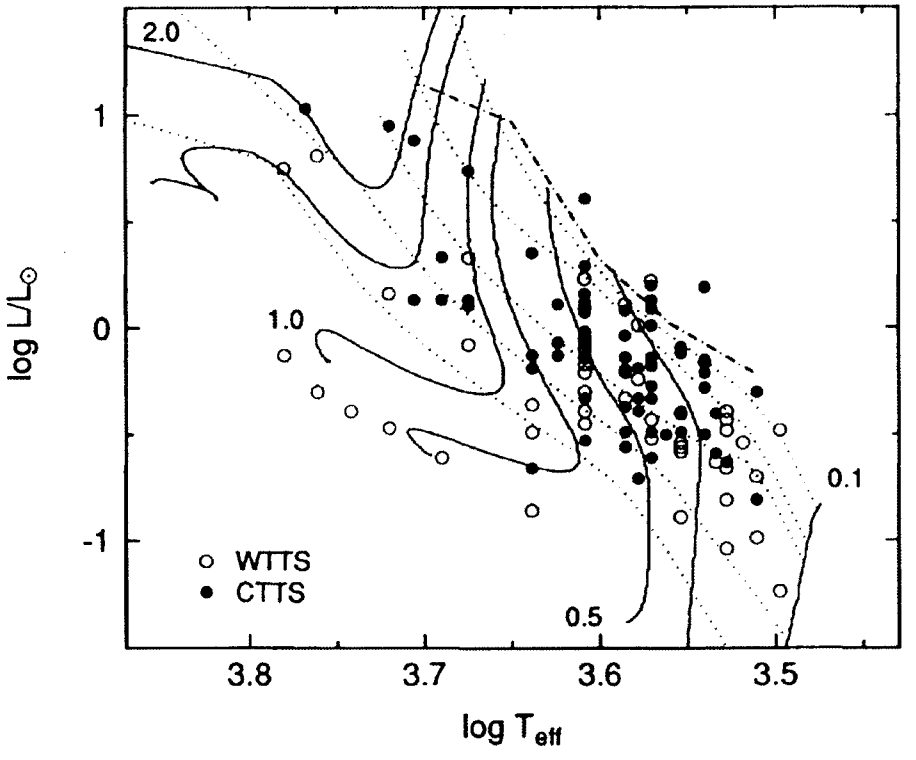

Figure 26: The H-R diagram with the plots of CTTSs and WTTSs quoted from Kenyon & Hartmann (1995). The open circles and the filled circles indicate the plots of WTTSs and CTTSs, respectively. Solid lines and dotted lines show the evolution model tracks and the isochrones, respectively (D'Antona & Mazzitelli, 1994). The dot-dashed line indicates the stellar birth line quoted from Fletcher & Stahler (1994). Since the loci of the CTTSs and the WTTSs are mixed up, it is difficult to estimate the disk evolution timescale from this result.

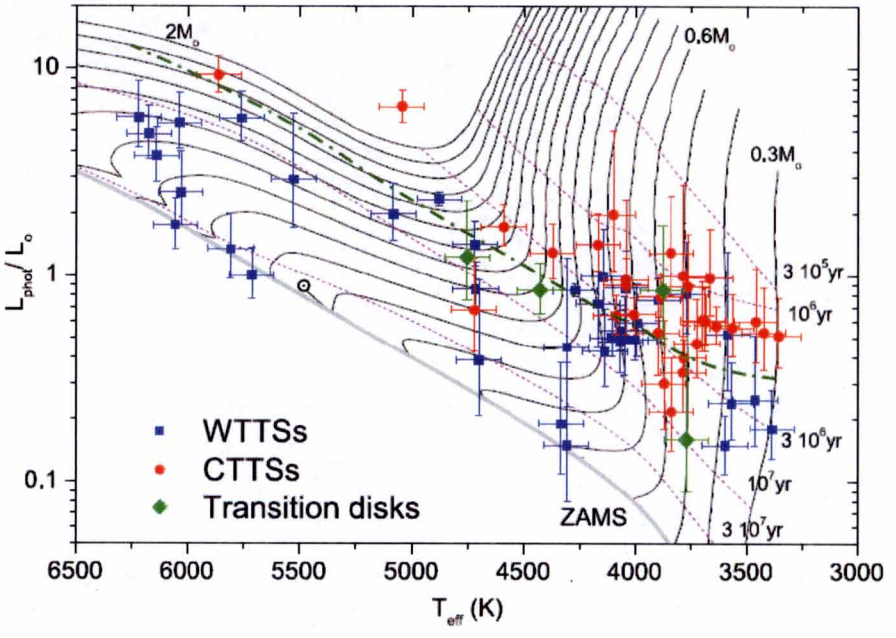

Figure 27: The H-R diagram with the plots of Taurus-Auriga estimated in Bertout, Siess, & Cabrit (2007). The blue squares, red circles, and the green diamonds indicate the loci of WTTSs, CTTSs, and Transitional disk objects, respectively. The evolution tracks and the isochrones are quoted from the evolution model of Siess, Dufour, & Forestini (2000) with solar metallicity. The plots of the CTTSs lie above that of WTTSs, indicating that the CTTSs are relatively younger than the WTTSs. The dark green dash-dotted line shows the disk lifetime estimated in their study, which is estimated as $4.0\times(M/M_{\odot})^{0.75}$ years.

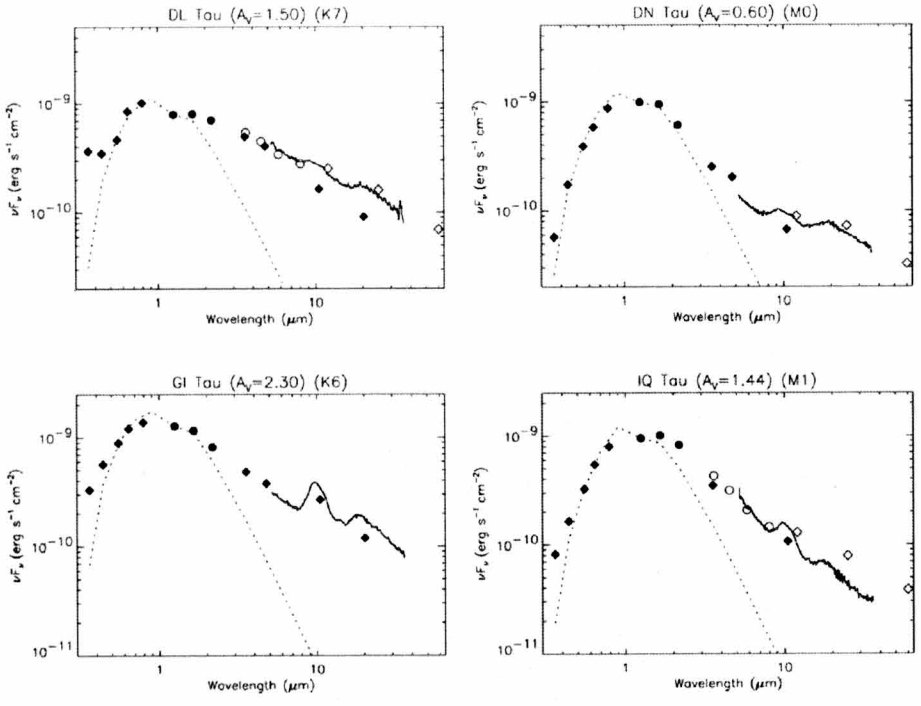

Figure 28: Spectral energy distributions (SEDs) of the CTTSs used for the evolution timescale estimation. These SEDs are quoted from Furlan et al. (2006). The name of the objects, extinctions, and the spectral types are labeled at the top of each frame. The dotted lines show the blackbody of the photosphere. The results of optical to mid-IR photometry (filled diamonds, mostly from Kenyon & Hartmann (1995)), the 2MASS fluxes in J, H, and Ks-bands (filled circles), the *Spitzer*-IRAC 3.6, 4.5, 5.8, and 8.0 μm fluxes from Hartmann et al. (2005) (open circles), and the *IRAS* 12, 25, and 60 μm fluxes (open diamonds) mostly from Weaver et al. (1992) are indicated. The solid spectra are obtaind with the *Spitzer*-IRS. These stars show a significant excess in the wavelenth longer than near-infrared.

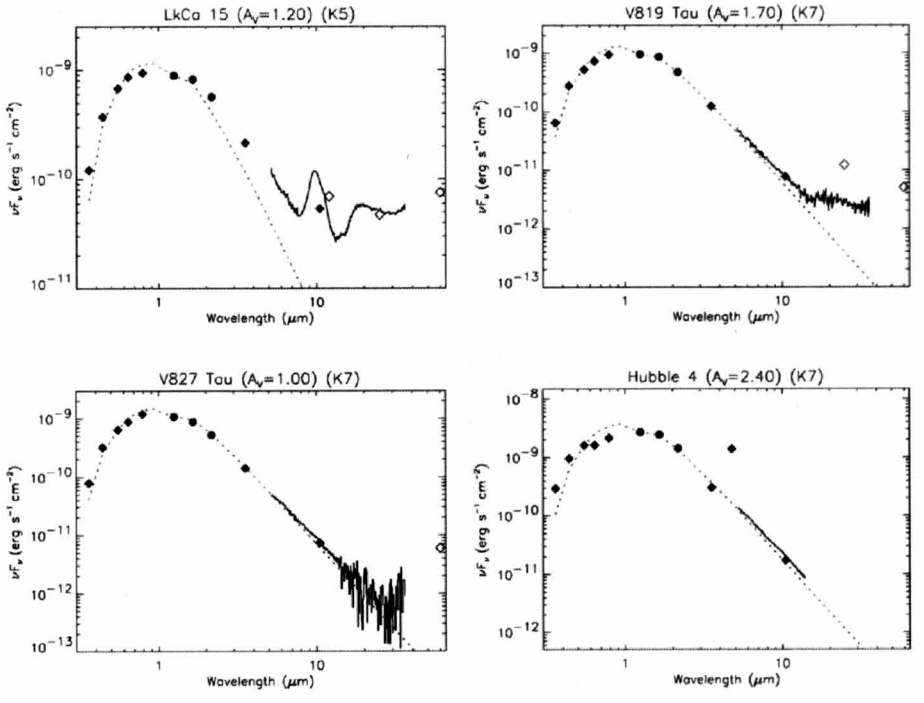

Figure 29: Spectral energy distributions (SEDs) of the Transitional disk object and WTTSs. The top 2 panels represent the SEDs of the transitional disk objects, and the 2 on the bottom are those of the WTTSs. These SEDs are also quoted from Furlan et al. (2006). See the caption of figure 28 legend for a description of the lines and the plots. In the SEDs of the transitional disks, the excess appears in the wavelength longer than $\sim 10\mu$m. On the other hand, the SEDs of the WTTSs show no excess.

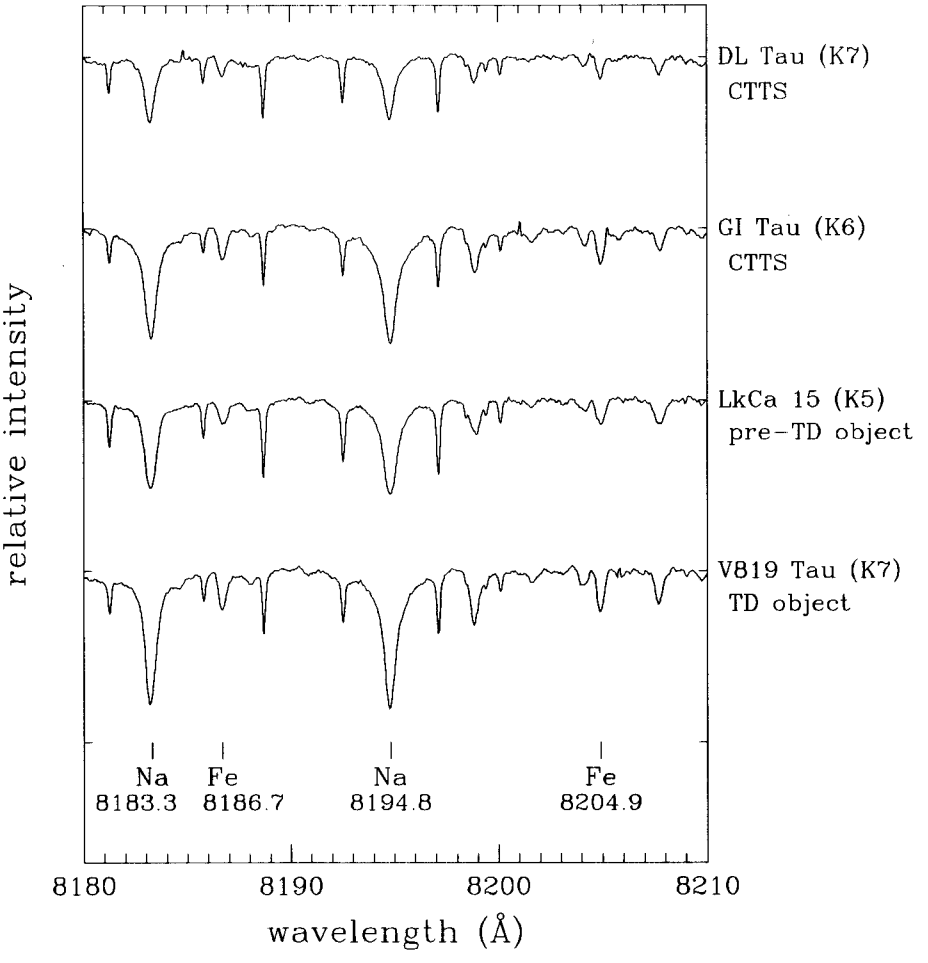

Figure 30: Spectra of observed CTTSs and Transitional disk objects. Doppler shift in each object is corrected. Relatively sharp absorption features are the telluric lines.

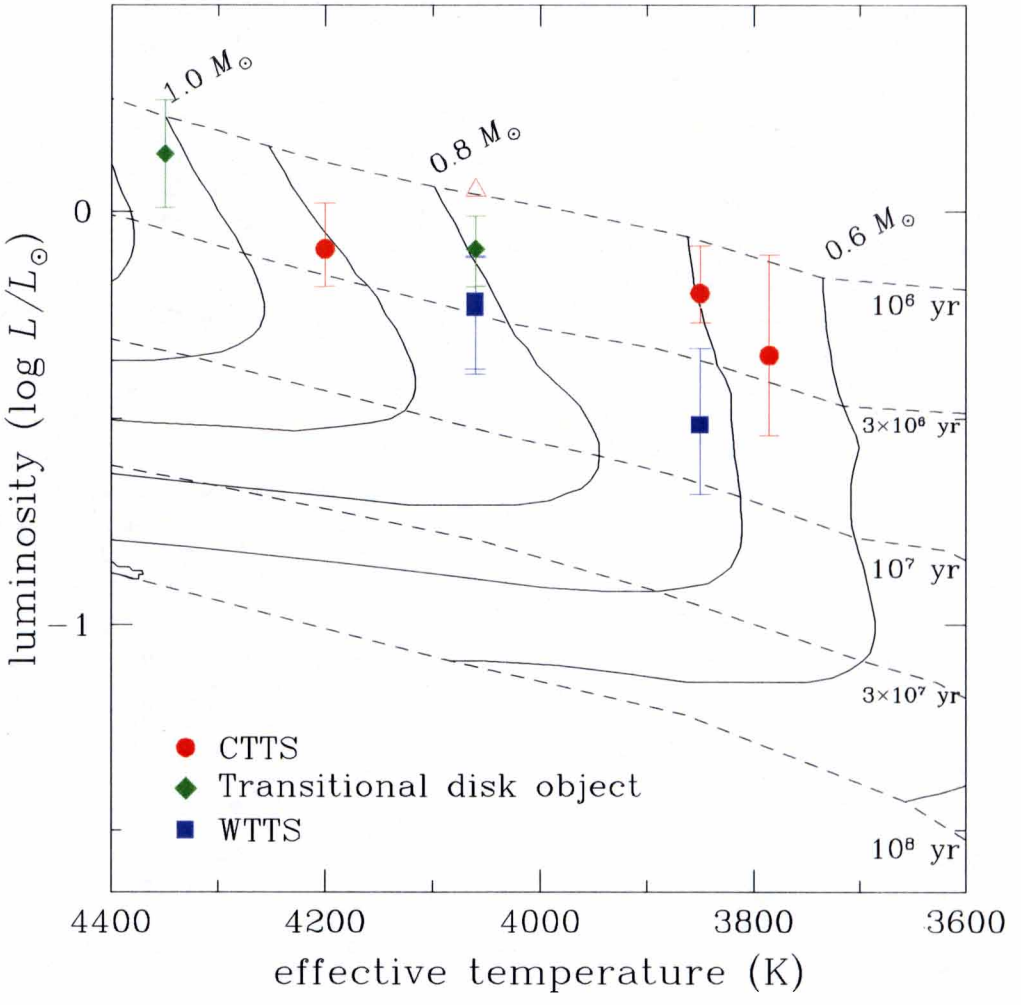

Figure 31: The H-R diagram with the plots of the observed CTTSs, Transitional disk objects, and the WTTSs. The red circles, green diamonds, and the blue squares indicate the CTTSs, Transitional disk objects, and the WTTSs, respectively. The open red triangle is the plot for DL Tau, which is the lower limit in luminosity. The solid lines are the evolution tracks, and the dashed lines are the isochrones quoted from Baraffe et al. (1998).

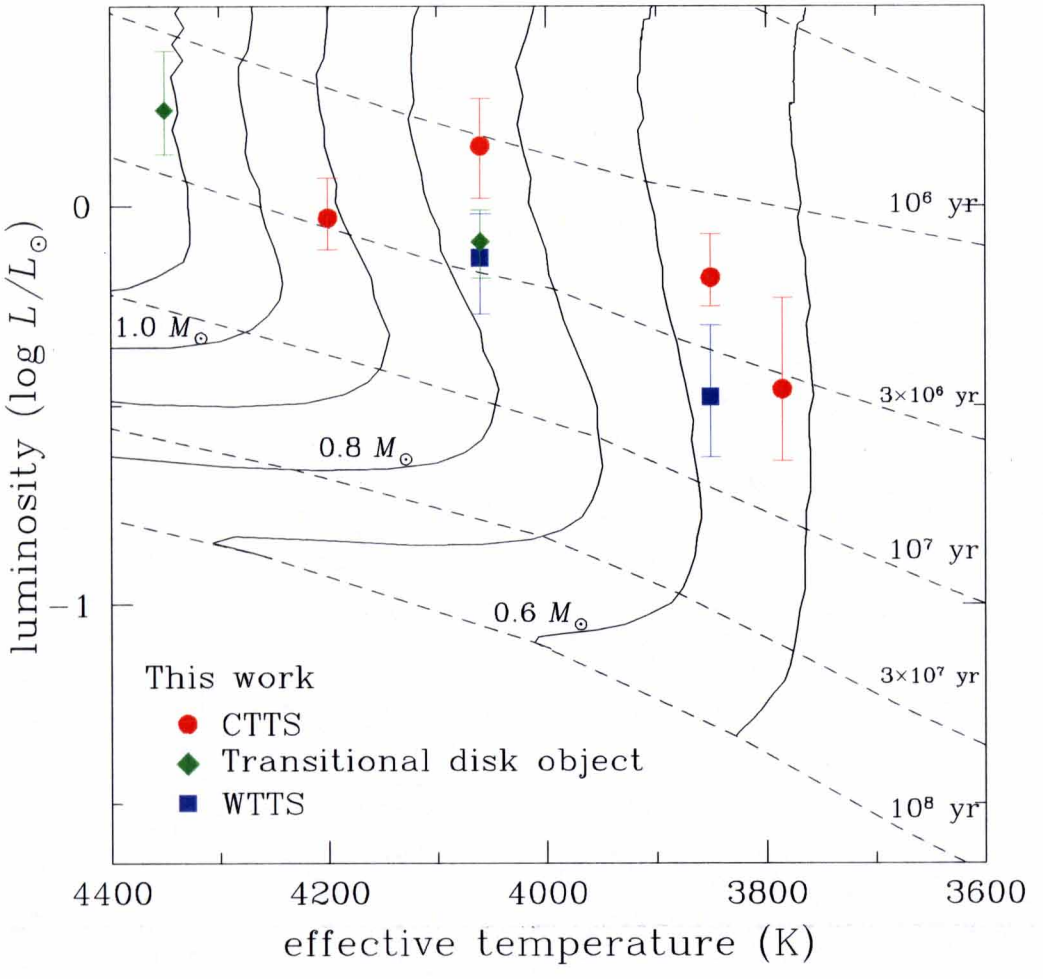

Figure 32: The H-R diagram created from the result and the evolution model of Siess, Dufour, & Forestini (2000).

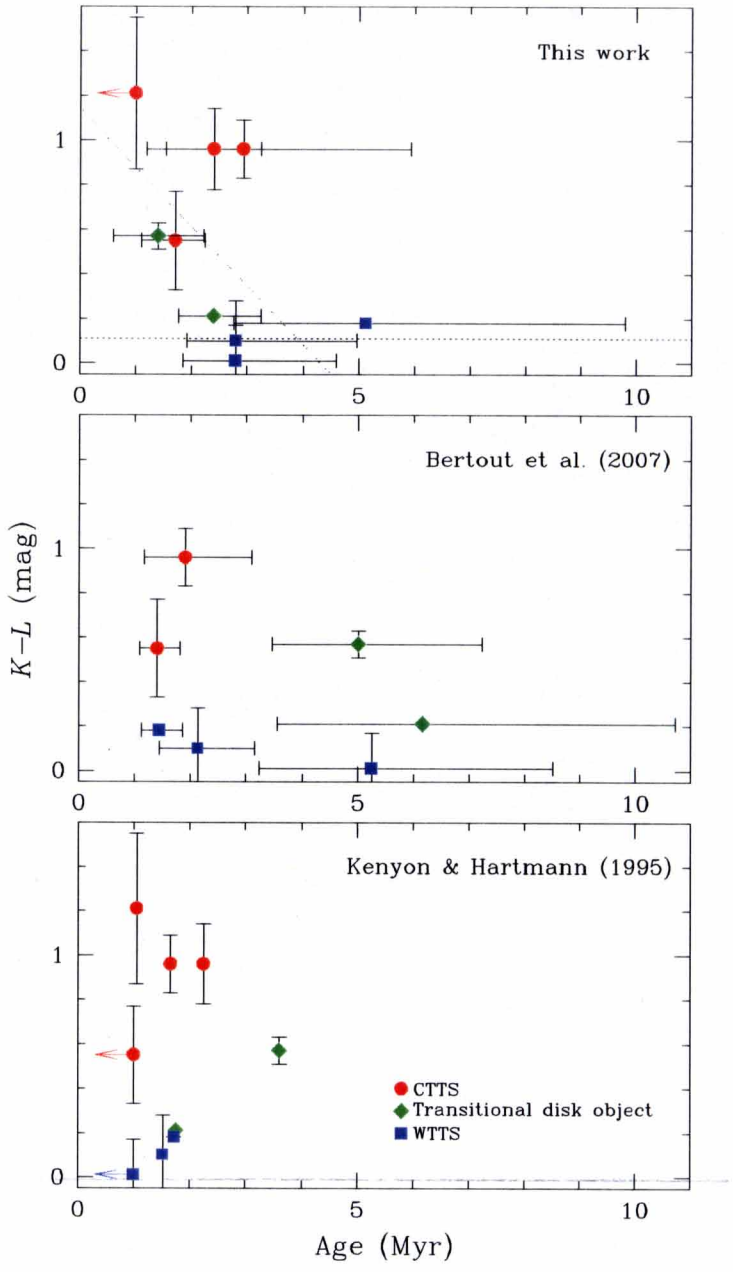

Figure 33: $K - L$ versus the age derived in each study. The top, middle, and the bottom panel show the $K - L$ - age relation with the age estimated by this work, Bertout, Siess, & Cabrit (2007), and Kenyon & Hartmann (1995), respectively. The $K - L$ magnitude were quoted from Kenyon & Hartmann (1995). The arrows are for the plots of which the estimated age is the upper limit. The dashed line and the dotted line in the top panel show the linear fit of the plots and the $K - L$ color of the photosphere with an effective temperature of 4200K, respectively. The result of this work indicates that the near-infrared excess decreases with increasing age, which explains the disk evolution. The disk lifetime estimated from the two lines is 4 Myr.

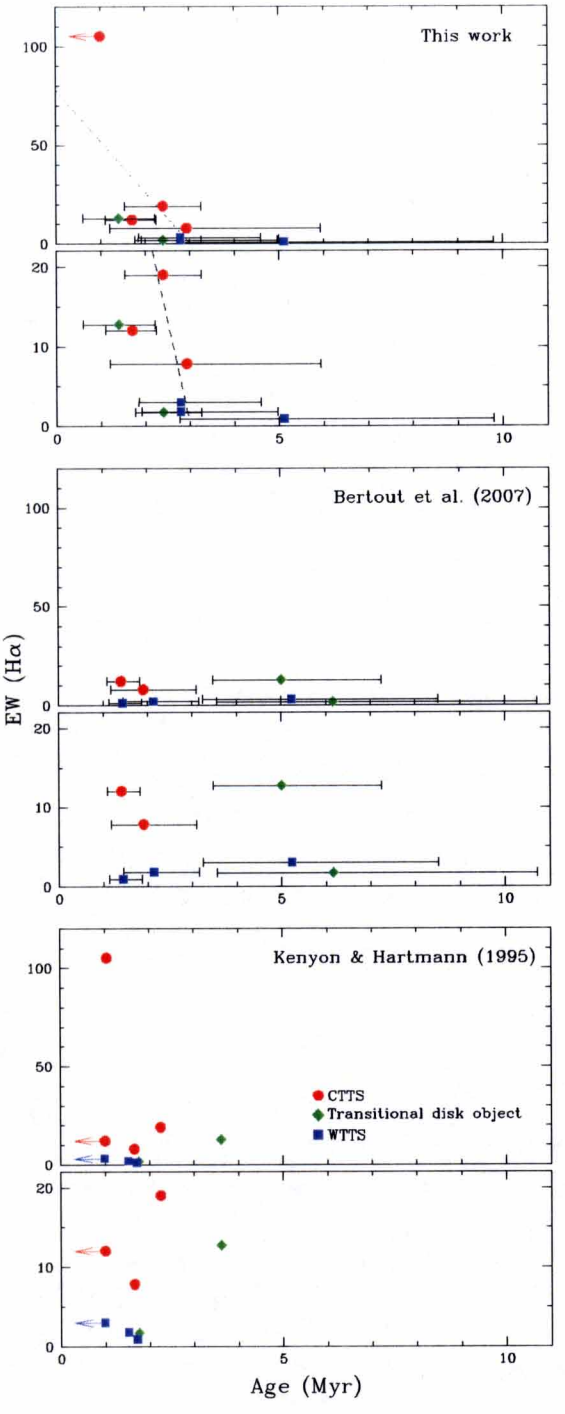

Figure 34: The relation between the equivalent width of Hα (EW(Hα)) and the age derived in each study. Top two panels show the EW(Hα) - age relation, where the age are the results from this study. The lower panel is the close up of the upper panel. The dashed lines indicate the linear fit of the plots, which represent a poor correlation between the age and the EW(Hα). The two panels in the middle and the bottom show the EW(Hα) - age relation by using the result of Bertout, Siess, & Cabrit (2007) and Kenyon & Hartmann (1995), respectively.

Tables

Table 1: The list of the observed stars in I-band and their properties.

Name	Sp. Type	$T_{\rm eff}$ (K)	log g (g: cm s^{-2})	S/N
Giants				
β Gem	K0IIIb	4750	2.73±0.01	160
HD 19656	K0III	4750	2.38±0.02	100
HD 76291	K1IV	4600	$2.72^{+0.02}_{-0.04}$	170
HD 100204	K1IV	4600	$2.01^{+0.19}_{-0.25}$	140
HD 145148	K1.5IV	4530	3.23±0.03	170
HD 45512	K2III-IV	4420	2.55±0.03	130
HD 101978	K2IV	4420	$1.82^{+0.27}_{-1.07}$	160
HD 106102	K2III-IV	4420	$2.61^{+0.08}_{-0.05}$	140
HD 108299	K2IV	4420	$2.46^{+0.11}_{-0.13}$	100
HD 110501	K2III-IV	4420	2.91±0.04	110
HD 121146	K2IV	4420	2.50±0.02	190
HD 147142	K2IV	4420	$2.03^{+0.06}_{-0.03}$	110
HD 49738	K3III	4200	$1.33^{+0.20}_{-0.25}$	110
HD 65759	K3III	4200	$1.66^{+0.09}_{-0.11}$	110
HD 86369	K3III	4200	$1.89^{+0.06}_{-0.09}$	160
HD 88231	K3III	4200	$1.76^{+0.10}_{-0.06}$	80
HD 102328	K3III	4200	2.15±0.02	90
HD 109012	K3III-IV	4200	$2.28^{+0.12}_{-0.14}$	160
HD 113637	K3III	4200	$1.66^{+0.11}_{-0.18}$	120
HD 115478	K3III	4200	2.01±0.03	140
HD 118839	K3III	4200	1.83±0.10	130
HD 129245	K3III	4200	$2.02^{+0.03}_{-0.02}$	90
HD 132304	K3III	4200	$1.73^{+0.16}_{-0.13}$	130
HD 137688	K3III	4200	$1.79^{+0.17}_{-0.18}$	120
HD 146388	K3III	4200	$2.06^{+0.01}_{-0.04}$	140
HD 156093	K3III	4200	$1.75^{+0.10}_{-0.06}$	170
HD 163547	K3III	4200	$1.83^{+0.05}_{-0.06}$	190
HD 10824	K4III	4000	$1.52^{+0.08}_{-0.09}$	150
HD 20644	K4III	4000	$1.27^{+0.04}_{-0.08}$	100

Table 1: The list of the observed stars in I-band and their properties.

Name	Sp. Type	$T_{\rm eff}$ (K)	log g (g: cm s^{-2})	S/N
HD 23413	K4III	4000	$1.68^{+0.08}_{-0.00}$	120
Main-sequence stars				
GL 105	K3V	4730	4.46±0.01	270
GL 183	K3V	4730	4.44±0.01	110
GL 141	K5V	4350	4.37±0.01	120
GL 380	K5V	4350	4.85±0.00	220
GL 397	K5	4350	4.73±0.02	130
GJ 3678	K5V	4350	4.30±0.02	150
WTTS				
RX J0452.5+1730	K4	4590	$4.22^{+0.05}_{-0.07}$	60
RX J0459.7+1430	K4	4590	$4.13^{+0.07}_{-0.08}$	60
HBC 374	K7	4060	$3.92^{+0.08}_{-0.09}$	70
V827 Tau	K7	4060	$3.92^{+0.08}_{-0.10}$	70

Table 2: The list of the measured EW for each object observed in I-band.

Name	EW ($\AA$)			
	Na (8183.3$\AA$)	Fe (8186.7$\AA$)	Na (8194.8$\AA$)	Fe (8204.9$\AA$)
Giants				
β Gem	$0.280^{+0.009}_{-0.011}$	0.100±0.006	$0.374^{+0.008}_{-0.009}$	0.084±0.001
HD 19656	$0.264^{+0.014}_{-0.010}$	—	$0.337^{+0.016}_{-0.007}$	0.104±0.003
HD 76291	0.251±0.006	$0.074^{+0.007}_{-0.003}$	0.342±0.008	$0.091^{+0.003}_{-0.002}$
HD 100204	$0.247^{+0.007}_{-0.005}$	$0.114^{+0.007}_{-0.008}$	$0.359^{+0.007}_{-0.009}$	0.104±0.002
HD 145148	$0.313^{+0.006}_{-0.005}$	0.072±0.001	0.431±0.006	0.069±0.002
HD 45512	$0.304^{+0.014}_{-0.011}$	$0.113^{+0.006}_{-0.005}$	0.434±0.008	0.111±0.003
HD 101978	$0.279^{+0.006}_{-0.008}$	$0.165^{+0.006}_{-0.005}$	$0.347^{+0.012}_{-0.013}$	0.149±0.008
HD 106102	$0.341^{+0.011}_{-0.006}$	$0.130^{+0.001}_{-0.003}$	$0.496^{+0.017}_{-0.019}$	$0.109^{+0.001}_{-0.002}$
HD 108299	$0.274^{+0.007}_{-0.006}$	0.138±0.001	$0.329^{+0.007}_{-0.006}$	$0.130^{+0.004}_{-0.005}$
HD 110501	0.315±0.006	$0.105^{+0.005}_{-0.009}$	$0.460^{+0.013}_{-0.012}$	0.086±0.002
HD 121146	—	$0.126^{+0.006}_{-0.005}$	$0.393^{+0.002}_{-0.001}$	$0.103^{+0.001}_{-0.002}$
HD 147142	$0.293^{+0.006}_{-0.005}$	0.109±0.005	0.393±0.008	$0.122^{+0.000}_{-0.001}$
HD 49738	0.309±0.011	$0.129^{+0.007}_{-0.005}$	$0.375^{+0.004}_{-0.005}$	0.150±0.001
HD 65759	$0.293^{+0.009}_{-0.008}$	0.114±0.001	$0.360^{+0.010}_{-0.007}$	$0.136^{+0.000}_{-0.001}$
HD 86369	—	$0.145^{+0.006}_{-0.005}$	$0.381^{+0.007}_{-0.008}$	—
HD 88231	0.291±0.013	0.126±0.004	$0.368^{+0.014}_{-0.015}$	0.131±0.001
HD 102328	$0.374^{+0.005}_{-0.012}$	0.150±0.003	0.542±0.012	$0.134^{+0.002}_{-0.003}$
HD 109012	0.289±0.006	—	$0.383^{+0.010}_{-0.012}$	0.108±0.003
HD 113637	$0.286^{+0.003}_{-0.002}$	$0.115^{+0.008}_{-0.004}$	$0.358^{+0.004}_{-0.007}$	$0.142^{+0.004}_{-0.006}$
HD 115478	$0.294^{+0.002}_{-0.001}$	$0.124^{+0.003}_{-0.002}$	$0.432^{+0.004}_{-0.002}$	$0.125^{+0.004}_{-0.005}$
HD 118839	—	—	$0.377^{+0.009}_{-0.010}$	0.112±0.002
HD 129245	—	—	0.398±0.006	0.127±0.004
HD 132304	—	0.132±0.002	$0.300^{+0.003}_{-0.004}$	0.120±0.003
HD 137688	$0.248^{+0.002}_{-0.003}$	$0.113^{+0.007}_{-0.003}$	$0.350^{+0.013}_{-0.010}$	$0.124^{+0.002}_{-0.004}$
HD 146388	$0.277^{+0.004}_{-0.005}$	0.110±0.007	0.394±0.001	0.106±0.001
HD 156093	$0.263^{+0.012}_{-0.016}$	$0.142^{+0.003}_{-0.002}$	0.343±0.001	0.131±0.001
HD 163547	$0.264^{+0.006}_{-0.008}$	$0.122^{+0.007}_{-0.005}$	—	$0.124^{+0.004}_{-0.002}$
HD 10824	$0.320^{+0.009}_{-0.008}$	$0.174^{+0.001}_{-0.002}$	0.398±0.011	$0.167^{+0.006}_{-0.005}$
HD 20644	$0.347^{+0.016}_{-0.014}$	0.164±0.004	$0.407^{+0.016}_{-0.007}$	0.166±0.005

Table 2: The list of the measured EW for each object observed in I-band.

Name	EW ($\AA$)			
	Na (8183.3$\AA$)	Fe (8186.7$\AA$)	Na (8194.8$\AA$)	Fe (8204.9$\AA$)
HD 23413	$0.322^{+0.010}_{-0.006}$	—	—	$0.139^{+0.009}_{-0.006}$
Main-sequence stars				
GL 105	$0.478^{+0.013}_{-0.014}$	$0.070^{+0.005}_{-0.004}$	0.596±0.004	0.046±0.001
GL 183	$0.629^{+0.008}_{-0.010}$	—	—	$0.065^{+0.007}_{-0.006}$
GL 141	$0.826^{+0.031}_{-0.015}$	$0.111^{+0.007}_{-0.006}$	$1.171^{+0.020}_{-0.023}$	$0.073^{+0.001}_{-0.002}$
GL 380	—	$0.097^{+0.003}_{-0.004}$	$1.345^{+0.048}_{-0.052}$	$0.066^{+0.004}_{-0.002}$
GL 397	$0.940^{+0.017}_{-0.015}$	0.117±0.011	$1.297^{+0.035}_{-0.028}$	0.069±0.002
GJ 3678	$0.506^{+0.009}_{-0.007}$	$0.058^{+0.008}_{-0.006}$	$0.671^{+0.012}_{-0.006}$	$0.036^{+0.002}_{-0.001}$
WTTS				
RX J0452.5+1730	—	—	$0.772^{+0.026}_{-0.033}$	$0.082^{+0.015}_{-0.013}$
RX J0459.7+1430	—	—	$0.720^{+0.033}_{-0.065}$	$0.086^{+0.024}_{-0.017}$
HBC 374	—	—	$0.963^{+0.037}_{-0.026}$	0.085±0.007
V827 Tau	—	—	$1.223^{+0.021}_{-0.053}$	$0.109^{+0.020}_{-0.017}$

The lines heavily blended with telluric lines were unmeasured (expressed "—").

Table 3: The age of the WTTSs estimated from EWR and photometric method.

Name	Method				
	EWR	Photometric			
		KH95[1]		F06[2]	
	Age (Myr)	A_V	Age (Myr)	A_V	Age (Myr)
HBC 374	2.8	0.76	2.5	2.40	<1.0
V827 Tau	2.8	0.28	2.5	1.00	<1.0

[1]Kenyon & Hartmann (1995)

[2]Furlan et al. (2006)

Table 4: The list of the observed stars in K-band and their properties.

Name	Sp. Type	$T_{\rm eff}$ (K)	log g (g: cm s^{-2})	Telescope / Instrument
Giants				
HIP 1809	M0	3800	$1.34^{+0.00}_{-0.14}$	UKIRT/CGS4
HIP 2851	M0	3800	$1.35^{+0.18}_{-0.02}$	UKIRT/CGS4
HIP 27639	M0III	3800	$1.16^{+0.04}_{-0.08}$	UKIRT/CGS4
HIP 28232	M0III	3800	$1.42^{+0.13}_{-0.15}$	UKIRT/CGS4
HIP 31771	K5III	3950	1.78±0.08	UKIRT/CGS4
HIP 37023	M0III	3800	$1.34^{+0.00}_{-0.08}$	UKIRT/CGS4
HIP 37369	M0III	3800	$1.10^{+0.14}_{-0.13}$	UKIRT/CGS4
HIP 38016	M0III	3800	$1.16^{+0.07}_{-0.10}$	UKIRT/CGS4
HIP 20376	M0III	3800	$1.29^{+0.04}_{-0.00}$	Subaru/IRCS
HIP 56211	M0III	3800	1.10±0.05	Kitt Peak (WH 96)
Main-sequence stars				
GL 14	K7	4060	$4.60^{+0.01}_{-0.02}$	UKIRT/CGS4
GL 212	M0.5	3785	4.64±0.02	UKIRT/CGS4
GL 221	K7	4060	4.59±0.03	UKIRT/CGS4
GL 289	M2V	3580	4.91±0.03	UKIRT/CGS4
GL 1114	M1.5	3650	$4.77^{+0.05}_{-0.06}$	UKIRT/CGS4
GL 3438	M0	3850	4.82±0.03	UKIRT/CGS4
GL 15 A	M2V	3580	4.67±0.00	Subaru/IRCS
GL 382	M1.5V	3650	4.59±0.01	Gemini/Phoenix (Archive)
GL 411	M2V	3580	4.73±0.00	Kitt Peak (WH 96)
GL 820 B	K7V	4060	4.50±0.00	Kitt Peak (WH 96)
WTTSs				
LkCa 14	M0	3850	$3.69^{+0.09}_{-0.11}$	UKIRT/CGS4
V827 Tau	K7	4060	$3.78^{+0.15}_{-0.18}$	UKIRT/CGS4
CTTSs				
DN Tau	M0	3850		UKIRT/CGS4
IQ Tau	M0.5	3785		UKIRT/CGS4

Table 5: Measured EWs of Sc and Na lines for each object observed in K-band.

Name	EW ($\AA$)			
	Sc (22057.8$\AA$)	Na (22062.4$\AA$)	Sc (22071.3$\AA$)	Na (22089.7$\AA$)
Giants				
HIP 1809	$0.970^{+0.032}_{-0.027}$	$0.730^{+0.037}_{-0.021}$	$0.606^{+0.022}_{-0.020}$	$0.555^{+0.001}_{-0.011}$
HIP 2851	$0.699^{+0.039}_{-0.037}$	$0.634^{+0.045}_{-0.042}$	$0.373^{+0.012}_{-0.011}$	$0.509^{+0.048}_{-0.023}$
HIP 27639	$0.732^{+0.007}_{-0.009}$	$0.597^{+0.010}_{-0.011}$	$0.490^{+0.006}_{-0.007}$	$0.499^{+0.008}_{-0.006}$
HIP 28232	$0.644^{+0.026}_{-0.022}$	$0.651^{+0.027}_{-0.022}$	$0.383^{+0.019}_{-0.015}$	$0.525^{+0.027}_{-0.022}$
HIP 31771	$0.417^{+0.009}_{-0.002}$	$0.547^{+0.011}_{-0.001}$	$0.239^{+0.008}_{-0.020}$	$0.424^{+0.010}_{-0.002}$
HIP 37023	$0.773^{+0.008}_{-0.008}$	$0.754^{+0.012}_{-0.010}$	$0.489^{+0.008}_{-0.010}$	$0.594^{+0.008}_{-0.010}$
HIP 37369	$0.638^{+0.005}_{-0.010}$	$0.533^{+0.007}_{-0.012}$	$0.384^{+0.005}_{-0.009}$	$0.431^{+0.007}_{-0.011}$
HIP 38016	$0.715^{+0.030}_{-0.019}$	$0.585^{+0.028}_{-0.019}$	$0.435^{+0.031}_{-0.014}$	$0.476^{+0.028}_{-0.020}$
HIP 20376	$0.500^{+0.011}_{-0.009}$	$0.470^{+0.013}_{-0.011}$	$0.322^{+0.011}_{-0.010}$	$0.401^{+0.013}_{-0.011}$
HIP 56211	$0.640^{+0.007}_{-0.006}$	$0.576^{+0.019}_{-0.024}$	$0.397^{+0.014}_{-0.019}$	$0.446^{+0.020}_{-0.024}$
Main-sequence stars				
GL 14	$0.240^{+0.006}_{-0.006}$	$2.077^{+0.041}_{-0.035}$	$0.161^{+0.008}_{-0.005}$	$1.517^{+0.060}_{-0.050}$
GL 212	$0.274^{+0.009}_{-0.008}$	$2.172^{+0.090}_{-0.086}$	$0.182^{+0.016}_{-0.015}$	$1.615^{+0.083}_{-0.081}$
GL 221	$0.225^{+0.010}_{-0.008}$	$1.836^{+0.039}_{-0.064}$	$0.157^{+0.010}_{-0.011}$	$1.295^{+0.070}_{-0.086}$
GL 289	$0.131^{+0.017}_{-0.016}$	$1.244^{+0.146}_{-0.116}$	—	$0.909^{+0.083}_{-0.154}$
GL 1114	$0.135^{+0.022}_{-0.024}$	$1.175^{+0.148}_{-0.144}$	—	$0.856^{+0.162}_{-0.137}$
GJ 3438	0.206 ± 0.010	$1.815^{+0.063}_{-0.074}$	$0.127^{+0.008}_{-0.009}$	$1.363^{+0.054}_{-0.066}$
GL 15 A	$0.209^{+0.012}_{-0.015}$	$1.755^{+0.132}_{-0.119}$	—	$1.219^{+0.099}_{-0.091}$
GL 382	$0.263^{+0.009}_{-0.004}$	$2.603^{+0.218}_{-0.201}$	$0.192^{+0.015}_{-0.031}$	$1.846^{+0.174}_{-0.179}$
GL 411	$0.164^{+0.018}_{-0.026}$	$1.404^{+0.250}_{-0.249}$	$0.130^{+0.039}_{-0.033}$	$1.107^{+0.214}_{-0.216}$
GJ 820B	$0.192^{+0.009}_{-0.025}$	$1.501^{+0.132}_{-0.145}$	$0.113^{+0.016}_{-0.017}$	$1.107^{+0.137}_{-0.142}$
WTTSs				
LkCa 14	0.234 ± 0.030	1.470 ± 0.050	—	$1.105^{+0.123}_{-0.128}$
V827 Tau	$0.382^{+0.004}_{-0.014}$	$2.030^{+0.331}_{-0.225}$	$0.345^{+0.021}_{-0.044}$	$1.530^{+0.250}_{-0.164}$
CTTSs				
DN Tau	$0.331^{+0.008}_{-0.002}$	$1.580^{+0.133}_{-0.168}$	$0.122^{+0.040}_{-0.000}$	$1.179^{+0.112}_{-0.119}$
IQ Tau	$0.170^{+0.011}_{-0.000}$	$0.888^{+0.152}_{-0.185}$	—	$0.668^{+0.121}_{-0.149}$

The lines unmeasured due to the low S/N and/or rapid rotation are expressed as "—".

Table 6: The age comparison of the PMS stars estimated from EWR and photometric method.

Name	EWR (This work)			Bertout et al. 2007	
	log g (g: cm/s^2)	log $(L/L_\odot)$[1]	Age (Myr)	log $(L/L_\odot)$	Age (Myr)
CTTSs					
DN Tau	$3.77^{+0.07}_{-0.11}$	$-0.20^{+0.12}_{-0.07}$	$1.71^{+0.53}_{-0.61}$	$-0.10^{+0.10}_{-0.10}$	$1.41^{+0.41}_{-0.31}$
IQ Tau	$3.91^{+0.19}_{-0.23}$	$-0.35^{+0.24}_{-0.19}$	$2.93^{+3.00}_{-1.73}$	$-0.28^{+0.27}_{-0.20}$	$1.91^{+1.18}_{-0.74}$
WTTSs					
V827 Tau	$3.94^{+0.15}_{-0.10}$	$-0.23^{+0.11}_{-0.18}$	$2.80^{+2.16}_{-0.88}$	$-0.06^{+0.18}_{-0.15}$	$2.14^{+1.02}_{-0.69}$
LkCa 14	$4.08^{+0.16}_{-0.18}$	$-0.52^{+0.19}_{-0.17}$	$5.13^{+4.67}_{-2.36}$	$-0.12^{+0.11}_{-0.09}$	$1.45^{+0.41}_{-0.33}$

[1] Estimated from the comparison of log g and Baraffe et al. (1998).

Table 7: The properties and the equivalent widths for each objects observed in the study of part II.

Name	Sp. type	$T_{\rm eff}$ (K)	EW $(\AA)$			
			Na (8183.3$\AA$)	Fe (8186.7$\AA$)	Na (8194.8$\AA$)	Fe (8204.9$\AA$)
CTTSs						
DL Tau	K7	4060	$0.326^{+0.018}_{-0.016}$	$0.048^{+0.003}_{-0.008}$	$0.350^{+0.017}_{-0.024}$	$0.047^{+0.004}_{-0.005}$
GI Tau	K6	4200	$0.731^{+0.023}_{-0.023}$	$0.082^{+0.012}_{-0.008}$	$0.913^{+0.005}_{-0.057}$	$0.086^{+0.007}_{-0.007}$
TD Objects						
LkCa 15	K5	4350	$0.528^{+0.027}_{-0.029}$	$0.078^{+0.013}_{-0.011}$	$0.692^{+0.037}_{-0.034}$	$0.069^{+0.009}_{-0.007}$
V819 Tau	K7	4060	$0.817^{+0.012}_{-0.027}$	$0.118^{+0.023}_{-0.008}$	$0.974^{+0.030}_{-0.022}$	$0.095^{+0.007}_{-0.008}$

Table 8: The estimated surface gravity and the age of the pre-main sequence stars. Age is determined by comparing the surface gravity with the evolution model of Baraffe et al. (1998) and Siess, Dufour, & Forestini (2000).

Name	log g	Baraffe et al. (1998)			Siess et al. 2000		
	(g: cm/s^2)	Mass	Age	Luminosity	Mass	Age	Luminosity
		($M/M_\odot$)	(Myr)	(log ($L/L_\odot$))	($M/M_\odot$)	(Myr)	(log ($L/L_\odot$))
CTTSs							
DL Tau	$3.56^{+0.13}_{-0.11}$	0.8	<1.00	> 0.06	0.7	$1.20^{+0.42}_{-0.27}$	$0.15^{+0.12}_{-0.13}$
DN Tau	$3.77^{+0.07}_{-0.11}$	0.7	$1.71^{+0.53}_{-0.61}$	$-0.20^{+0.12}_{-0.07}$	0.6	$1.90^{+0.42}_{-0.52}$	$-0.18^{+0.11}_{-0.07}$
GI Tau	$3.92^{+0.08}_{-0.10}$	0.9	$2.40^{+0.85}_{-0.86}$	$-0.09^{+0.11}_{-0.09}$	0.9	$2.62^{+0.82}_{-0.70}$	$0.15^{+0.12}_{-0.13}$
IQ Tau	$3.91^{+0.19}_{-0.23}$	0.7	$2.93^{+3.00}_{-1.73}$	$-0.35^{+0.24}_{-0.19}$	0.5	$3.10^{+2.46}_{-1.49}$	$-0.46^{+0.23}_{-0.18}$
TD objects							
LkCa 15	$3.79^{+0.12}_{-0.14}$	1.0	$1.41^{+0.81*}_{-0.81}$	$0.14^{+0.13*}_{-0.13}$	1.1	$1.69^{+0.75}_{-0.58}$	$0.24^{+0.15}_{-0.11}$
V819 Tau	$3.90^{+0.08}_{-0.08}$	0.8	$2.40^{+0.85}_{-0.63}$	$-0.18^{+0.09}_{-0.09}$	0.8	$2.51^{+0.84}_{-0.54}$	$-0.09^{+0.08}_{-0.09}$
WTTSs							
HBC 374	$3.94^{+0.13}_{-0.11}$	0.8	$2.80^{+1.80}_{-0.95}$	$-0.23^{+0.12}_{-0.15}$	0.8	$2.90^{+1.60}_{-0.87}$	$-0.13^{+0.11}_{-0.14}$
LkCa 14	$4.08^{+0.16}_{-0.18}$	0.7	$5.13^{+4.67}_{-2.36}$	$-0.52^{+0.19}_{-0.17}$	0.6	$4.92^{+3.20}_{-2.21}$	$-0.48^{+0.18}_{-0.15}$
V827 Tau	$3.94^{+0.15}_{-0.10}$	0.8	$2.80^{+2.16}_{-0.88}$	$-0.23^{+0.11}_{-0.18}$	0.8	$2.90^{+1.91}_{-0.80}$	$-0.13^{+0.10}_{-0.16}$

* Since the upper limit of the surface gravity of LkCa 15 is out of the range of Baraffe et al. (1998), the lower limit of age is estimated as the same amount as the upper limit. The same treatment was applied to the luminosity as well.

Table 9: The age, $K-L$ color, and the equivalent width of Hα emission feature.

Name	Age (Myr)			K-L (mag)[1]	EW $H\alpha$ ($\AA$)[2]
	EWR	BSC07[3]	KH95[1]		
CTTSs					
DL Tau	<1.00	—	1.05	1.21±0.34	105
DN Tau	$1.71^{+0.53}_{-0.61}$	$1.41^{+0.41}_{-0.32}$	<1.00	0.55±0.22	12
GI Tau	$2.40^{+0.85}_{-0.86}$	—	2.25	0.96±0.18	19
IQ Tau	$2.93^{+3.00}_{-1.73}$	$1.91^{+1.18}_{-0.73}$	1.66	0.96±0.13	7.8
TD objects					
LkCa 15	$1.41^{+0.81}_{-0.81}$	$5.01^{+2.23}_{-1.54}$	3.61	0.57±0.06	12.7
V819 Tau	$2.40^{+0.85}_{-0.63}$	$6.17^{+4.55}_{-2.62}$	1.76	0.21±0.00	1.7
WTTSs					
HBC 374	$2.80^{+1.80}_{-0.95}$	$5.25^{+3.26}_{-2.01}$	<1.00	0.01±0.16	3
LkCa 14	$5.13^{+4.67}_{-2.36}$	$1.45^{+0.42}_{-0.32}$	1.73	0.18±0.00	0.9
V827 Tau	$2.80^{+2.16}_{-0.88}$	$2.14^{+1.02}_{-0.69}$	1.53	0.10±0.18	1.8

[1]Kenyon & Hartmann (1995)

[2]Strom et al. (1989)

[3]Bertout, Siess, & Cabrit (2007)